STRUCTURAL STUDIES OF LARGE INTEGRAL MEMBRANE PROTEINS IN REVERSE MICELLES BY SOLUTION NUCLEAR MAGNETIC RESONANCE

Joseph M. Kielec

A DISSERTATION

in

Biochemistry and Molecular Biophysics

Presented to the Faculties of the University of Pennsylvania

in

Partial Fulfillment of the Requirements for the

Degree of Doctor of Philosophy

2009

Supervisor of Dissertation

_____
A. Joshua Wand
Benjamin Rush Professor of Biochemistry and Biophysics

Graduate Group Chairperson

_____
Kathryn M. Ferguson
Associate Professor of Physiology

Dissertation Committee
Bohdana M. Discher, Research Assistant Professor of Biochemistry and Biophysics
Walter Englander, Professor of Biochemistry and Biophysics
Roland G. Kallen, Professor of Biochemistry and Biophysics
Mark A. Lemmon, Professor of Biochemistry and Biophysics
Zhe Lu, Professor of Physiology
Jane Vanderkooi, Professor of Biochemistry and Biophysics

Structural studies of large integral membrane proteins in reverse micelles by solution nuclear magnetic resonance

ACKNOWLEDGEMENTS

I would like to thank Josh Wand for allowing me to join his lab, his attention in my training as a scientist, and his general patience. Special thanks to my committee members: Zhe Lu, for encouragement, support, and advice, both scientific and otherwise; Roland Kallen for useful discussion on membrane proteins and ion channels; Mark Lemmon for serving as chair of my committee, and for proving to be an excellent teacher; Walter Englander for being Walter Englander, and for scientific advice, guidance, and mentoring. I'd like to also thank additional committee members Bodana Discher and Jane Vanderkooi.

Thanks to Kathy Valentine for guiding me through the vagaries of nuclear magnetic resonance, and for intellectual, scientific, and technical advice. Thanks to Ron Peterson for NMR training, guidance, and advice in working with reverse micelles; and to Brian Lefebvre, for formative initial discussions on the technical aspects of reverse micelles and the application of membrane proteins to them.

I'd like to thank the staff at Penn and the graduate program in Biochemistry and Molecular Biophysics, including Ruth Keris, Angie Young, Nam Narain, Peggy Buckley, Susan Day, Regina Medlock, Mary Leonard, and Joanne Kuloszewski.

Thanks as well to past and present lab members (and friends of the Wand lab): Maxim Pometun, Tatiana Igumenova, Mike Marlow, Kevin Shi, John Gledhill, Kendra Frederick, Bruce Berry, Jakob Dogan, Sabrina Bédard, Anna Patrick, Dave Hindin, Sarah Chung, Robert Baigelman, Weixia Liu, Kristy Owens, Melissa Martinez, Vonni Morman, Kyle Harpole, Vignesh Kasinath, and Rob Culik. Thanks to Leland Mayne and Cecilia

Tommos for initial advice on circular dichroism, to Kathleen Howard for advice and assistance with EPR studies, James Lear with analytical ultracentrifugation, and Kate Ferguson and her lab for assistance with dynamic light scattering experiments.

I would especially like to thanks Kitty Wu for her advice, encouragement, and moral support. Also thanks to Mick Yoder for his advice and encouragement.

I'd like to also thank my parents and immediate family for their encouragement and patience; I promise I am almost finished growing proteins.

Thanks to my BMB colleagues Nathaniel V. Nucci and Bruce Lichtenstein for stimulating and occasionally useful discussions.

Thanks to Bruker and their excellent cryoprobes.

I would finally like to gratefully acknowledge funding from the National Science Foundation in the form of a Graduate Research Fellowship, the University of Pennsylvania's Cost of Education Allowance, and a National Institutes of Health predoctoral training grant.

Special thanks for gin and tonics.

ABSTRACT

STRUCTURAL STUDIES OF LARGE INTEGRAL MEMBRANE PROTEINS IN REVERSE MICELLES BY SOLUTION NUCLEAR MAGNETIC RESONANCE

Joseph M. Kielec

Supervisor: A. Joshua Wand

The structural characterization of integral membrane proteins represents one of the many challenges of the post-genomic era. While membrane proteins comprise approximately 50% of current and potential drug targets, their structural characterization lags far behind that of soluble proteins. Nuclear magnetic resonance (NMR) offers tremendous potential for the investigation of membrane proteins in aqueous environments with respect to structural characterization, relaxation properties, and the details of small ligand interactions. However, the size limitations of solution NMR due to the slow tumbling problem have restricted comprehensive structural characterization of membrane protein NMR structures to the relatively small β-barrel proteins or helical proteins of simple topology. Here we detail an approach for the encapsulation of integral membrane proteins in reverse micelles, allowing for their study in low viscosity solvents and thus limiting the slow tumbling issue. This approach obviates the traditional compromises in sample preparation for large proteins in NMR. Using a 54 kDa construct of the homotetrameric potassium channel KcsA, we present a hybrid surfactant screen to optimize NMR conditions and describe utilization of 3D NMR pulse sequences and backbone assignment strategies normally restricted to proteins of much smaller size. We

are able to confirm the helical structure of KcsA's transmembrane domains in reverse micelles, as well as proper quaternary arrangement of the monomers and preservation of potassium coordination in the selectivity filter. Additionally we show that the solvation properties of the channel in reverse micelles are analogous to a membrane protein solubilized by a traditional aqueous micelle. Relaxation studies of the channel are also presented.

TABLE OF CONTENTS

LIST OF TABLES

LIST OF FIGURES

LIST OF ABBREVIATIONS

AOT	Sodium bis(2-ethylhexyl)sulfosuccinate
B_o	Bulk magnetic field
$C_{12}E_4$	*n*-dodecyl tetra ethylene glycol
CD	Circular Dichroism
CSA (δ)	Chemical Shift Anisotropy
CTAB	Cetyltrimethylammonium bromide
DHAB	Dihexadecyldimethylammonium bromide
DM	n-decyl-β-D-maltopyranoside
DPC	Dodecylphosphocholine (foscholine)
DTAB	Dodecyltrimethylammonium bromide
FID	Free Induction Decay
γ	Gyromagnetic ratio of the given spin
GPCR	G protein-coupled receptor
$\hbar$	Plank constant divided by 2π ($\hbar = 1.055 \times 10^{-34}$ J s)
HSQC	Heteronuclear Single Quantum Coherence
$J(0)$	Normalized spectral density at zero frequency
$J(\omega^o)$	Spectral density at Larmor Frequency
$J(2\omega^o)$	Spectral density at twice the Larmor Frequency
k_B	Boltzman's constant (1.381×10^{-23} J K^{-1})
LDAO	Lauryldimethylamine oxide
MCD	Main Chain Directed
NAB	H_N-H_α-H_β

NMR	Nuclear Magnetic Resonance
NOE	Nuclear Overhauser Effect
NOESY	Nuclear Overhauser Effect Spectroscopy
η_w	Solvent viscosity
p	Dipole-dipole relaxation
PDB	Protein Data Bank
PPM	Parts Per Million
R_1	Spin-lattice or longitudinal relaxation rate
R_2	Spin-spin or transverse relaxation rate
R_{ex}	Chemical exchange
RM	Reverse micelle
S^2	The generalized order parameter
SAIL	Stereo-array isotope labeling
τ	Total motion
τ_m	Rotational correlation time (overall)
τ_e	Correlation time for internal motion
T	Temperature
T_1	Spin-lattice or longitudinal relaxation time
T_2	Spin-spin or transverse relaxation time
TALOS	Torsion Angle Likeness Obtained from Shift and Sequence Similarity
TM1	KcsA transmembrane helix 1
TM2	KcsA transmembrane helix 2
TOCSY	Total Correlation Spectroscopy

TROSY	Transverse Relaxation Optimized Spectroscopy
μ_0	Vacuum permeability (4π x 10^{-7} H m^{-1})
v/v	Volume / volume ratio

Chapter 1: Nuclear Magnetic Resonance of Membrane Proteins

1.1 The challenge of membrane proteins

Membrane proteins comprise 30-40% of the proteins expressed from open reading frames in the human genome (Watts, 2005). They play essential roles in nerve action potentials, homeostasis, signal transduction, tumor development, and are of key importance as drug targets. The crystal structure of the KcsA potassium channel (Doyle et al., 1998) heralded an explosion in the number of high resolution structures of integral membrane proteins over the past decade. Despite this progress, membrane proteins still present a significant challenge to structural studies. Of the 50,000-plus structures deposited in the Protein Data Bank (PDB), only a few hundred are of integral membrane proteins (White, 2009).

The difficulties in studying integral membrane proteins are numerous. The proteins typically express poorly in *in vitro* expression systems, can be difficult to isolate homogenously, and in many cases are inherently unstable. With its ability to rapidly screen different detergent or lipid conditions and potential to study protein structure and dynamics on multiple timescales in an aqueous environment, solution nuclear magnetic resonance (NMR) is both a promising yet flawed technique. The number of integral membrane protein structures solved by NMR is growing, but is still limited. Notable contributions include the bacterial β-barrel proteins OmpA and OmpX (Arora et al., 2001; Fernandez et al., 2004), the human mitochondrial β-barrel VDAC-1 (Hiller et al., 2008), and a handful of helical proteins: Mistic (Roosild et al., 2005), phospholamban (Oxenoid and Chou, 2005), and most recently the M2 channel (Schnell and Chou, 2008), DsbB (Zhou et al., 2008), and DAGK (Van Horn et al., 2009). Of these efforts only

phospholamban, DAGK, and VDAC-1 exceed 30 kDa in terms of protein size, and the structure of DAGK is based solely on the backbone fold and contains no assignment or structural information about sidechains.

Each of these structures were significant steps forward, but they also serve to highlight the major limitation of solution NMR, which is the slow molecular reorientation time of large marcromolecules in water. This has typically restricted comprehensive structural studies to proteins no larger than 30-35 kDa using traditional preparation techniques and pulse sequences. The limitation is due to the inverse relationship between molecular reorientation and transverse relaxation (T_2), which is an important component affecting both the quality and breadth of NMR experiments that can be performed. For membrane proteins this size limitation is exacerbated by the additional weight of detergents or lipids required to solubilize the hydrophobic domains of the protein; even a simple 18 kDa β-barrel protein such as OmpX has an overall size of nearly 60 kDa when its detergent micelle is taken into account.

The potential for solution NMR to address structural and dynamic studies of channels, G protein-coupled receptors (GPCRs), and other interesting but large integral membrane proteins is clearly limited by issues of size. Methodologies exist to combat size restrictions, but they are limited by compromises in terms of the quality of structural data, the breadth of a protein structure that can be analyzed, preparation techniques and, ultimately, practical issues in terms of time and resources for spectrometer usage, labeling costs, the patience of the researchers doing the work, and the pace of discovery relative to other, competing structural methods. Clearly there is room for new approaches to complement the existing methodologies.

1.2 The NMR slow tumbling problem

The slow tumbling problem in NMR is simple. The aforementioned transverse relaxation, or T_2, is a time constant describing the decay of a spin system as it returns to equilibrium. T_2 is essentially a measure of the time available for manipulation of spin states in an NMR pulse sequence and acquisition of the subsequent FID (free induction decay), which is the raw signal recorded by the NMR spectrometer. The T_2 is thus very important, and several factors play a role in its value.

The two major mechanisms that contribute to T_2 relaxation are chemical shift anisotropy (CSA) and dipole-dipole interactions (Cavanaugh et al., 2007). CSA is due to the induction of local magnetic fields of nuclear spins by the bulk magnetic field, B_o. These local magnetic fields are oriented with respect to B_o and, as a molecule reorients itself in solution, so too do these local fields. This leads to fluctuations that contribute to the relaxation of nearby nuclear spins. Since these fields are induced by the magnetic field, it follows that the CSA effect increases with field strength, shown by the following equation for spin S:

$$\delta_S = \frac{1}{3\sqrt{2}} \gamma_s B_0 \Delta\sigma_s \qquad (0.1)$$

where γ_s = the gyromagnetic ratio of spin S, B_o = the bulk magnetic field, and $\Delta\sigma_s$ = the difference between the axial and perpendicular components of the chemical shift tensor for spin S ($\Delta\sigma = \sigma_{\perp} - \sigma_{\parallel}$).

In the case of dipole-dipole interactions, nuclear spins generate a dipolar field that is proportional to the magnetic moment and the distance between the two nuclei. As with CSA, the interaction between these spins fluctuate as a molecule reorients itself. Dipole-dipole relaxation is given as:

$$p = \frac{1}{2\sqrt{2}} \gamma_I \gamma_S / r_{IS}^3 \tag{0.2}$$

where γ_I = the gyromagnetic ratio of spin I, γ_s = the gyromagnetic ratio of spin S, and r_{IS} = the distance between spin S and I.

The overall rate of transverse relaxation is given by:

$$\frac{1}{T_2} = \left(\frac{\hbar^2 \gamma_I^2 \gamma_S^2}{8 r_{IS}^6} \right) \left[4J(0) + J(\omega_I - \omega_S) + 3J(\omega_S) + 6J(\omega_I) + 6J(\omega_I + \omega_S) \right] + \frac{\omega_S^2 \Delta\sigma^2}{18} \left[4J(0) + 3J(\omega_S) \right] \tag{0.3}$$

where $J(0)$ = the spectral density at zero frequency, $J(\omega_I)$ = the spectral density at Larmor frequency for spin I, and $J(\omega_S)$ = the spectral density at Larmor frequency for spin S. The spectral density function describes the contribution of molecular motion to the relaxation mechanism. In the Lipari and Szabo model free expression for spectral density (Lipari and Szabo, 1982a, b), molecular motion is broken down into three parameters. The first parameter, τ_m, describes the overall rotation correlation time of a molecule, while the other two, S^2 and τ_e, describe internal motion. S^2, the generalized order parameter, describes the amplitude of motion between a value of 1 (rigid) and 0 (free), while τ_e describes the rate of this motion. The model free analysis does not account for the contribution of microscopic motion. It is described by the following equation:

$$J(\omega) = \frac{2}{5}\left[\frac{S^2\tau_m}{\left(1+\omega^2\tau_m^2\right)} + \frac{\left(1-S^2\right)\tau}{\left(1+\omega^2\tau^2\right)}\right]$$

(0.4)

The relationship between the rate of total motion, τ, rotational correlation time, τ_m, and internal motion, τ_e, is given as:

$$\frac{1}{\tau} = \frac{1}{\tau_m} + \frac{1}{\tau_e}$$

(0.5)

1.3 Solutions to the slow tumbling problem

As the T_2 decreases due to CSA and dipole-dipole interactions, the efficiency of coherence transfer decays. Coherence transfer describes the transfer of magnetization from one spin to another, and is essential for multidimensional NMR, particularly the more complex, 3D backbone pulse sequences. This ultimately limits the scope of experiments that can be run on a protein with a longer rotational correlation time. As coherence transfer decays, so too does the signal-to-noise of a typical Lorentzian line for a resonance peak, leading to flat, broadened peaks.

The development of Transverse Relaxation Optimized Spectroscopy (TROSY)-based pulse sequences and specific preparation and isotope labeling techniques (Pervushin et al., 1997) are able to address the issue of transverse relaxation in larger proteins, though they are not without their compromises. TROSY makes constructive use of the interference between dipole-dipole relaxation and CSA, selecting for the slowest-relaxing component of a nuclear spin system multiplet. This ultimately discards a great

deal of information leading to signal-to-noise loss, which is an issue for systems of only moderate to low solubility such as membrane proteins.

The most common labeling technique to limit the effects of transverse relaxation in larger proteins is perdeuteration, which replaces the aliphatic protons with deuterium. Deuterium (^{2}H) has a gyromagnetic ratio (γ) that is approximately 6.5-fold less than hydrogen (^{1}H), greatly reducing its contribution to dipole-dipole relaxation. Growth of cells is typically much slower in D_2O media and protein expression tends to be lower, which is already an issue for membrane proteins. Deuteration ultimately requires the back-exchange of the deuterium atom for a hydrogen at the amide position, which is essentially the entryway for the typical NMR out-and-back backbone experiments. This is complicated for amide positions in well-ordered regions of a protein with high protection factors that do not readily exchange their protons.

Deuteration additionally hinders the ability to collect structural information derived from ^{1}H-^{1}H interactions by Nuclear Overhauser Effect Spectroscopy (NOESY) experiments, where the same $1/r^6$ distance dependence on dipolar relaxation is used as the molecular ruler that has traditionally been the foundation of NMR structural restraints. A common technique to combat this is the use of "ILV" labeled proteins, which only have hydrogen-labeled methyl sidechains for the isoleucine, leucine, and valine amino acids, relying on amide to sidechain proton NOE information from these residues alone while other amino acids types are deuterated. This technique, which yielded success for the membrane protein structure of VDAC-1 and DsbB nevertheless excludes a great deal of potential structural information. The SAIL (stereo-array isotope labeling) method (Kainosho et al., 2006) is an isotope labeling technique that is more elegant than

perdeuteration, though it is also at this writing prohibitively expensive. Cell-free expression of proteins for NMR study offers a means of reducing the costs of labeling relative to protein yields, but is still in its infancy and presently lacks the ability to produce homogenously folded membrane proteins.

1.4 Reverse micelle NMR

An additional strategy to improve a protein's relaxation properties is to simply attempt to shorten its rotational correlation time, τ_m. τ_m is an important component of the spectral density function, and the relationship between rotational correlation time and T_2 is inverse; the relaxation mechanisms of both dipole-dipole interactions and the CSA are limited in smaller, faster-tumbling proteins. The most common method to improve τ_m times in solution NMR is to increase the sample temperature as much as a sample can reasonably withstand. This decreases the viscosity of water, but only to a certain extent, and is limited in terms of keeping a macromolecule within a reasonable temperature range.

A different approach is to replace water as the bulk solvent through the use of reverse micelles (Wand et al., 1998a), nanometer-sized droplets of water surrounded by a protective, single layer of surfactant. Alkane solvents, presently the most commonly utilized bulk solvent in reverse micelle NMR, can have viscosities an order of magnitude smaller than water in the case of ethane. This allows for a true physical manipulation the Stokes-Einstein relationship:

$$\tau_m = \frac{\eta V_h}{k_B T}$$

(0.6)

where V_h = the volume of the protein or complex, T = temperature, k_B = Boltzman's constant (1.381 x 10^{-23} J K^{-1}), and η_w = solvent viscosity. Even with the additional volume of a surfactant layer and a solubilizing shell of water, a large protein can tumble fast enough to lower its rotational correlation time to that of a much smaller protein. The use of reverse micelles for high resolution NMR structural studies has been validated previously (Babu et al., 2001), and they have been effective at studying cold denaturation (Pometun et al., 2006) and metastable proteins by NMR (Peterson et al., 2004). Recent efforts utilizing ethane and a novel preparation cell (Peterson and Wand, 2005) have shown improvement in T_2 relaxation times by nearly one-third from aqueous samples of ubiquitin (Peterson et al., 2005a).

Reverse micelles are an almost ideal solution to the slow tumbling problem for membrane proteins. The penalty incurred by the additional size of a reverse micelle around a soluble protein is almost negligible for a membrane protein, which is already accompanied by a bulky, solubilizing agent in aqueous samples. Additionally the improved relaxation properties of reverse micelles remove the necessity of deuteration. This eliminates the complication of back-exchanging deuterium from amide protons, a process that has proven difficult or even impossible in the studies of some membrane proteins (Chill et al., 2006b; Oxenoid et al., 2004). Furthermore without the necessity of deuteration one is able to make use of sidechain protons in the assignment of the protein backbone. Membrane proteins suffer from issues of relatively homogenous structure and

sequence redundancy, particularly for their transmembrane domains, making unambiguous i to i-1 connections through traditional backbone correlation experiments difficult. The use of sidechain protons in complementary TOCSY and through-space NOESY experiments assists greatly in these types of assignments.

1.5 Membrane protein reverse micelle studies

The inspiration for the encapsulation of membrane proteins in reverse micelles for their study by NMR developed from the investigations of rhodopsin-lipid complexes at microliter concentrations in organic solvents by Montal and colleagues (Darszon et al., 1979). Small angle X-ray scattering studies of these complexes revealed a dumbbell-like structure, described as a protein cross-link between two inverted phospholipid micelles in a pool of hexane (Ramakrishnan et al., 1983). Our initial efforts at adapting this approach to NMR was met with limited success; the transfer from aqueous-based micelle to organic-based reverse micelle either left membrane proteins unfolded or of insufficient concentration for study beyond basic 2D pulse sequences. Through the development and utilization of hybrid surfactants - detergents that are competent as both aqueous micelles and reverse micelles - in the sample preparation, we were able to attain promising samples amenable to 3D NMR experiments. The initial model of membrane protein encapsulation devised over 25 years ago carries forward to this present day, where the intra- and extra-cellular domains of a membrane protein are proposed to be solubilized by two reverse micelles whose lateral detergent acyl chains run parallel to the transmembrane domain in a manner analogous to a traditional micelle. This concept, which we have elegantly termed the ‘shower cap’ model, is illustrated in Figure 1.1.

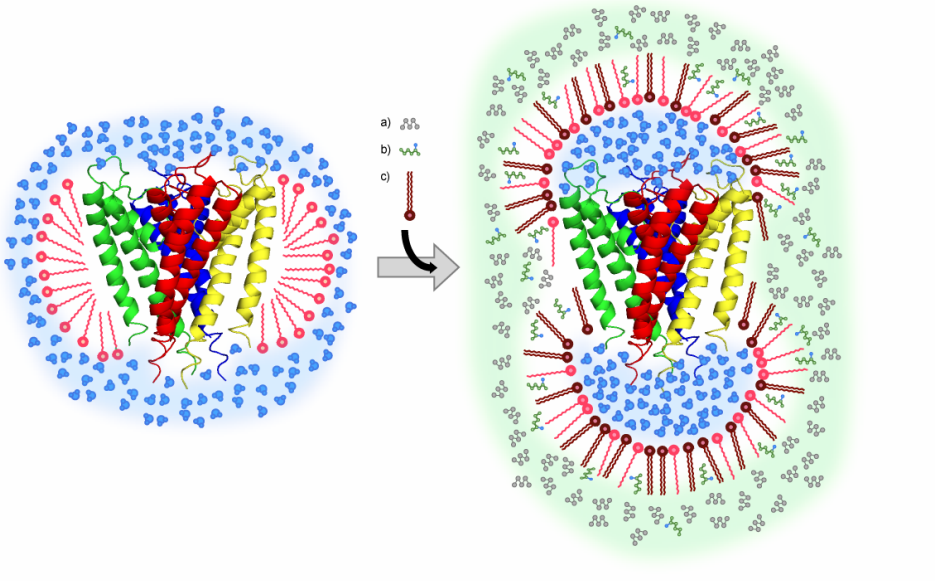

Figure 1.1 Conversion from aqueous micelle to reverse micelle solubilized membrane protein

In bulk water a hybrid surfactant such as CTAB solubilizes the hydrophobic transmembrane domains of a membrane protein. Upon insertion of the membrane protein into a bulk alkane solvent (a), the hybrid surfactant serves two purposes: the conventional solubilization of hydrophobic domains, as well as the formation of a water-filled pocket to solubilize and extra- and intracellular regions of the protein. The use of certain co-surfactants such as hexanol (b) is necessary for the transition of some detergents to this hybrid state. This condition promotes control over the process. In other cases additional co-surfactants (c) may be added for the role of charge-balancing of surfactant headgroups and/or different tail regions, such as the double-chained (DHAB). The ribbon representation of $KcsA_{\Delta C35}$ (Doyle et al., 1998) was generated using PyMol (DeLano, 2002)

Flynn and colleagues have developed their own approach for the NMR study of simple peptides in reverse micelles (Van Horn et al., 2008), but it is based on much simpler assumptions of membrane protein structure, topological complexity, and size.

Here we describe both the protocol for iterative screens to successfully encapsulate and study membrane proteins by reverse micelle NMR and the characterization of a membrane protein using this method, the KcsA potassium channel. A 68 kDa homotetramer from the soil bacteria *Streptomyces lividans* (Schrempf et al., 1995), KcsA contains the potassium channel signature sequence of TVGYG in the selectivity filter (Heginbotham et al., 1992), and is a prokaryotic ancestor to Shaker and other eukaryotic channels (Derst and Karschin, 1998). The three main segments of KcsA, an outer transmembrane helix (TM1), a pore region comprised of a pore helix and the selectivity filter, and an inner transmembrane helix (TM2) are homologous to regions S5, H5, and S6 in voltage gated potassium channels such as KvAP. Like many other bacterial potassium channels, KcsA is structurally very similar to eukaryotic channels (MacKinnon et al., 1998; Ruta et al., 2003), and has been proven a robust experimental system for the study of channels from these organisms (LeMasurier et al., 2001).

KcsA expresses well in *Escherichia coli* minimal media expression systems, is stable, and is well-characterized by other structural, physiological, and biochemical efforts. Here we utilize a 125 residue construct of the channel, which lacks the soluble, 35 residue C-terminal domain ($KcsA_{\Delta C35}$). This is the same version utilized in the initial crystallographic studies of KcsA, and is a stable homotetramer of 54 kDa (Doyle et al., 1998; LeMasurier et al., 2001). NMR studies of varying degrees of structural and functional inquiry have been conducted on KcsA in solution detergent micelles (Baker et al., 2007a; Chill et al., 2006; Takeuchi et al., 2007), in bilayers by solid-state NMR (Schneider et al., 2008). These efforts and others form the basis of comparisons used to validate our results.

Presently approximately 68% of the amide residues in our KcsA construct in reverse micelles ($^{RM}KcsA_{\Delta C35}$) are assigned. In terms of confirmation of the channel's fold, secondary chemical shift patterns show helical content of transmembrane domains and the N-terminal helix. Additionally, solvent exposure of KcsA's transmembrane, intracellular, and extracellular domains in reverse micelles determined from amide-water NOEs and deuterium exchange experiments are analogous to that of a membrane protein solubilized in traditional aqueous micelles. Notably, the N-terminal helix shows amphipathic and mobile properties, consistent with studies of KcsA in liposomes (Cortes et al., 2001). The functional integrity and quaternary structure of the channel are confirmed by the ability of the selectivity filter, which is comprised of backbone carbonyls from each of KcsA's monomers, to exhibit specific structural changes in response to potassium ions. Initial relaxation experiments on the channel have also been conducted and are described, validating the use of these experiments for in-depth studies of the dynamic properties of the channel. This work not only opens new possibilities for further structural and dynamic studies of KcsA in an aqueous environment, but lays the foundation for the study of other integral membrane proteins in reversemicelles.

Chapter 2: The Nuts and Bolts of Reverse Micelle NMR

2.1 Introduction

Reverse micelles are composed of four components: the protein or protein complex of interest, the surfactant system, the aqueous buffer, and the bulk solvent (Ekwall et al., 1969). Each protein occupies a single, nanometer-sized droplet of buffered aqueous solution. Surrounding the droplet are the hydrophilic headgroups of the surfactant molecules. The tails of the surfactant molecules are assembled as a curving, hydrophobic monolayer extending into the bulk organic solvent. In optimal conditions up to 300 uM of protein can be incorporated into a reverse micelle solution (Babu et al., 2001). With an NMR spectrometer equipped with a modern-generation cryoprobe, complex 3D experiments are possible with protein concentrations as low as 0.1 mM.

Although protein concentrations in a reverse micelle NMR sample may be lower than that of a traditional aqueous sample, the utilization of a cryoprobe can overcome this disadvantage. The low dielectric of the alkane solvent allows for the full realization of four-fold sensitivity improvement over a conventional probe, an advantage that is normally mitigated by the high dielectric of traditional aqueous NMR samples (Flynn et al., 2000). Another benefit of reverse micelle NMR is the reduced water signal; the water volume in a typical reverse micelle can be one-twentieth of that of an aqueous NMR sample. Water suppression pulses in most NMR experiments, including the critical 3D backbone experiments work very well with reverse micelles samples.

2.2 Reverse micelle bulk solvents

The traditional bulk solvents of choice for reverse micelle NMR studies have typically been low-viscosity alkanes (Table 2.1). This includes pentane which, as a liquid at room temperature and pressure, is suitable for initial screening, optimization of conditions, and most experimental studies on smaller proteins. Structural investigations of larger proteins will typically require the use of lower viscosity, pressurized solvents, such as butane, propane (Wand et al., 1998), and ethane (Peterson et al., 2005a). These solvents are capable of significantly improving (lowering) the rotational correlation times (τ_m) of a protein and, by extension, transverse relaxation (T_2) properties (Wand et al., 1998).

For pentane samples a screw cap tube (Wilmad Labglass) is sufficient to contain the sample and prevent evaporation. For butane samples a pressure tube can be used (Wilmad Labglass). Likewise, pentane samples can be pressurized with the use of N_2 and run at elevated temperatures to improve relaxation properties. 50 psi is sufficient to run samples at 50° C. Reverse micelles encapsulated in ethane require a high pressure NMR

Table 2.1: Viscosities of short-chain alkanes

Solvent (Pressure)	Water (15 psi)	Pentane (30 psi)	Butane (50 psi)	Propane (400 psi)	Ethane (4500 psi)
Temperature			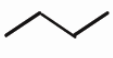		
0° C	1790.9	272.79	203.14	130	95.478
5° C	1517.6	260.36	193.09	123.51	91.977
15° C	1137.2	237.93	174.83	111.49	85.488
25° C	**889.88**	**218.21**	**158.62**	**100.56**	**79.612**
35° C	719.17	200.66	144.11	90.478	-
45° C	595.96	184.89	131.27*	81.033	-

cell and mixing chamber (Daedalus Innovations, LLC) to maintain pressures as high as 6000 psi (Peterson et al., 2005a; Peterson and Wand, 2005). Generally, once sample conditions are optimized in pentane, they are easily translated to lower viscosity solvents.

Sample ^{2}H locking in the NMR spectrometer can be achieved with a D_2O-filled capillary inserted into a sample tube. Given the relatively low protein loading of reverse micelle samples, deuterated solvents are recommended: d_{12}-pentane, d_{10}-butane, d_8-propane or d_6-ethane (Cambridge Isotope Laboratories, Isotec Sigma-Aldrich). A steady lock can be achieved with as little as 33% deuterated solvent. For low-sensitivity 3D experiments, the use of 100% deuterated bulk solvent is recommended to minimize proton signals originating from the solvent.

2.3 Buffers and water loading

Most buffer conditions are compatible in a reverse micelle system. Additionally, due to the confined space in a reverse micelle, hydrogen exchange rates are slower than in bulk water and higher pH values will not adversely affect NMR signal sensitivity. However, the experimental pH and its relation to the protein of study's pKa are important factors in reverse micelle encapsulation efficiency. The surface charge of a protein at a given pH is a consideration in the selection of surfactants (Peterson et al., 2005b), and a survey of pH levels for a given protein is advised as a refinement step.

A low salt concentration in the range of 10 to 40 mM, should be used as a starting point for encapsulation, as this limits the effects of charge-charge interactions between the protein surface and the surfactant headgroups. The amount of salt that is tolerated varies from system to system. Ubiquitin in AOT reverse micelles in pentane only shows

a decrease in protein with salt concentrations over 500 mM NaCl (Babu et al., 2003). For flavodoxin in CTAB reverse micelles in pentane, the concentration of encapsulated protein decreases above salt levels of 400 mM NaCl, while in eGFP, greater than 25 mM NaCl leads to a sharp decline in encapsulation efficiency (literature from Daedalus Innovations, LLC). Not all systems have a simple, linear correlation between salt concentration and encapsulation. The encapsulation of cytochrome c increases with increasing salt, reaching a maximum efficiency at approximately 200 mM before declining (Literature from Daedalus Innovations, LLC).

Water loading (w_o) is a measure of the molar ratio of water to surfactant in the reverse micelle solution:

$$w_o = \frac{\text{mM } H_2O}{\text{mM surfactant}} \tag{1.1}$$

For example, a sample with 150 mM of surfactant and a target water loading value of 20 would require 3,000 mM H_2O to satisfy the water loading ratio. If the total sample volume of the bulk alkane solvent in a typical 5 mm diameter NMR tube is 600 uL, this results in the requirements of 32.4 uL of buffer in the sample to achieve the water loading of 20. The water loading can be quantified by integrating the water and detergent peaks in the 1D ^{1}H NMR spectrum (Babu et al., 2003). Testing the maximal water loading of a surfactant system is important. AOT, for example, has a maximal water loading value of 40-45, whereas CTAB and DTAB both have a maximal value in the range of 20-25 (Lefebvre et al., 2005). In the interest of minimizing the overall size of the reverse micelle particle to optimize the transverse relaxation properties of a system, it is typical

to use the smallest water loading possible for a given protein-surfactant system that provides reproducible, native-like HSQCs.

The ^{1}H chemical shift of reverse micelle encapsulated water differs from that of bulk water. In terms of sample referencing in the NMR spectrometer, the use of an internal reference compound is recommended. The methyl resonance of sodium 4,4-dimethyl-4-silapentane-1-sulfonate (DSS) is sufficient for the purpose of providing a reference to 0.0 ppm (Babu et al., 2003). The use of 50 mM DSS in the reverse micelle aqueous buffer gives a final concentration of ~1 mM in the reverse micelle sample, depending on the water loading, which is sufficient signal for reference in 1D NMR experiments.

2.4 Surfactants and surfactant selection

A variety of reverse micelle surfactants have been used successfully to accommodate different proteins for NMR studies. Typical surfactants include the anionic, di-acyl chain bis(2-ethylhexyl) sodium succinate (AOT) (Wand et al., 1998), the mono-acyl chain, cationic cetyltrimethylammonium bromide (CTAB) (Lefebvre et al., 2005), the non-ionic tetraethyleneglycol monododecylether ($C_{12}E_4$) and the (C_nE_m) family of surfactants (Peterson et al., 2005b), and the zwitterionic, mono-acyl chain lauryldimethylamine oxide (LDAO) (Valentine et al., 2006) (Figure 2.1).

When encapsulating a protein for the first time it is important to test a variety of surfactants. Matching the surface charge of the protein to the charge of the headgroup will minimize protein-surfactant interactions and typically give the most native-like ^{15}N HSQC spectra. In general, anionic surfactants (AOT) work best with proteins that have a

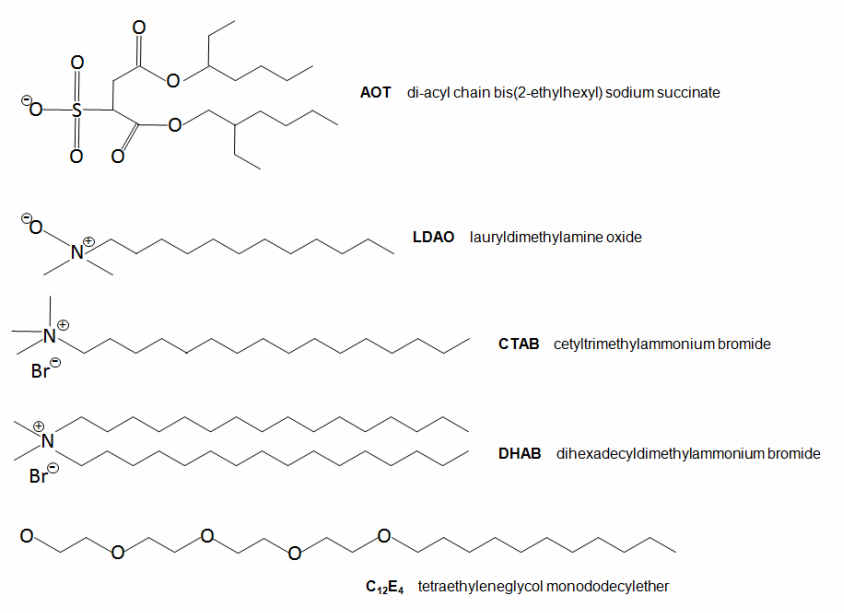

Figure 2.1: A menagerie of reverse micelle surfactants

A mixture if anionic, cationic, zwitterionic, and non-ionic reverse micelle surfactants are shown. Many can form reverse micelles individually, though some (DHAB and $C_{12}E_4$) work best in mixtures with other surfactants.

net negative charge, while cationic surfactants (CTAB, DTAB) work well with proteins that have a net positive charge. The zwitterionic surfactant, LDAO was found to encapsulate proteins with either negative, positive, or zero net charge. A mixture of surfactants may also be used to reduce electrostatic interactions between the surface of the protein and the surfactant headgroups of the reverse micelle. For example, a composition of 70:30 AOT:$C_{12}E_4$ was found to be optimal for flavodoxin encapsulation. For the very basic cytochrome c the optimal native like HSQC spectrum is obtained by balancing the net charge at pH 5 with a mixture of DTAB:AOT:$C_{12}E_4$ in the ratio of 5:25:70 (Peterson et al., 2005b).

Some surfactants work best in a mixture. For instance, the cationic, di-acyl chain surfactant dihexadecyldimethylammonium bromide (DHAB) forms reverse micelles that are unstable for extended periods as a homogeneous surfactant, while the mixture of 1:1 DHAB:CTAB gives better HSQC spectra with extended stability for KcsA.

Hexanol can also be considered a co-surfactant and is required for the formation of reverse micelles in alkane solvents for most mono-acyl chain surfactants, which have the shape of an inverted cone compared to the cylindrical DHAB and the conical AOT. The percent volume of hexanol in the bulk solvent depends on the length of the acyl chain and the properties of the headgroup. For example, 100 mM of the the 16 carbon CTAB will require 8% v/v hexanol in the bulk solvent. The shorter 12 carbon, zwitterionic LDAO requires 4% v/v in bulk solvent for 100 mM. Mixing surfactants of different chain types will also affect the amount of hexanol required. Dihexadecyldimethylammonium bromide (DHAB) is a 16 carbon di-acyl chain analogue of CTAB that, although unstable as a reverse micelle surfactant alone and unable to produce a structured protein when used to make flavodoxin reverse micelles, mixes well with CTAB to form stable reverse micelles able to provide structured HSQCs of flavodoxin. Due to the increased volume of DHAB's tail region, these mixtures require less hexanol than would be required of a CTAB mixture alone. With the tighter curvature the geometries that di-acyl chain surfactants are capable of, it is hypothesized that they may allow for smaller reverse micelles.

The expanded hydrophobic volume of a surfactant such as DHAB is more analogous to a di-acyl lipid tail than a mono-acyl chain surfactant such as CTAB or LDAO. This property may assist in more accurately providing a membrane mimetic for

membrane proteins encapsulated in reverse micelles, a point that will be described in greater detail later. A chart of the hexanol and stability survey of CTAB and DHAB mixtures are shown in Table 2.2. To highlight the differences in NMR spectra and, in turn protein structures that result from even subtle differences in surfactant concentration, a comparison of HSQCs of flavodoxin in reverse micelles comprised of 100% DHAB mixture and 1:3 CTAB:DHAB (molar ratio) is shown in Figure 2.2. The sample prepared with DHAB alone is clearly unfolded, while the same protein made up with a 1:3 CTAB:DHAB mixture gives excellent spectra of flavodoxin. This may be due to the potentially tighter curvature of the 100% DHAB reverse micelle, which may not allow for the accommodation of proteins within the reverse micelle that is enabled by the inclusion of mono-acyl CTAB to a preparation mixture. As a side note, flavodoxin, along with ubiquitin and a few other select proteins, is commonly used as a test protein for novel surfactant mixtures. This is due in part to flavodoxin's yellow color in the visible spectrum from the presence of the flavin mononucleotide (Knight and Hardy, 1967). Additionally flavodoxin can conveniently be concentrated on the order of 6-7 mM, making its usage suitable for the injection method. This is the simplest and fastest technique for reverse micelle preparation, and is discussed in the next section.

Table 2.2: CTAB and DHAB hexanol requirements

Mixture	% CTAB	% DHAB	Total mM	% Hexanol	Initial Stability	Overnight Stability
1	0	100	200	0.5	Yes	No*
2	25	75	150	0.5	Yes	Yes
3	50	50	150	0.5	Yes	Yes
4	75	25	150	2.0	Yes	Yes

*100% DHAB mixtures showed a propensity to 'leak' water to the bottom of the vial over time, perhaps due to the fact that they cannot support larger micelles. 100% DHAB mixtures were also unable to produce folded HSQC spectra of flaxodoxin in reverse micelles.

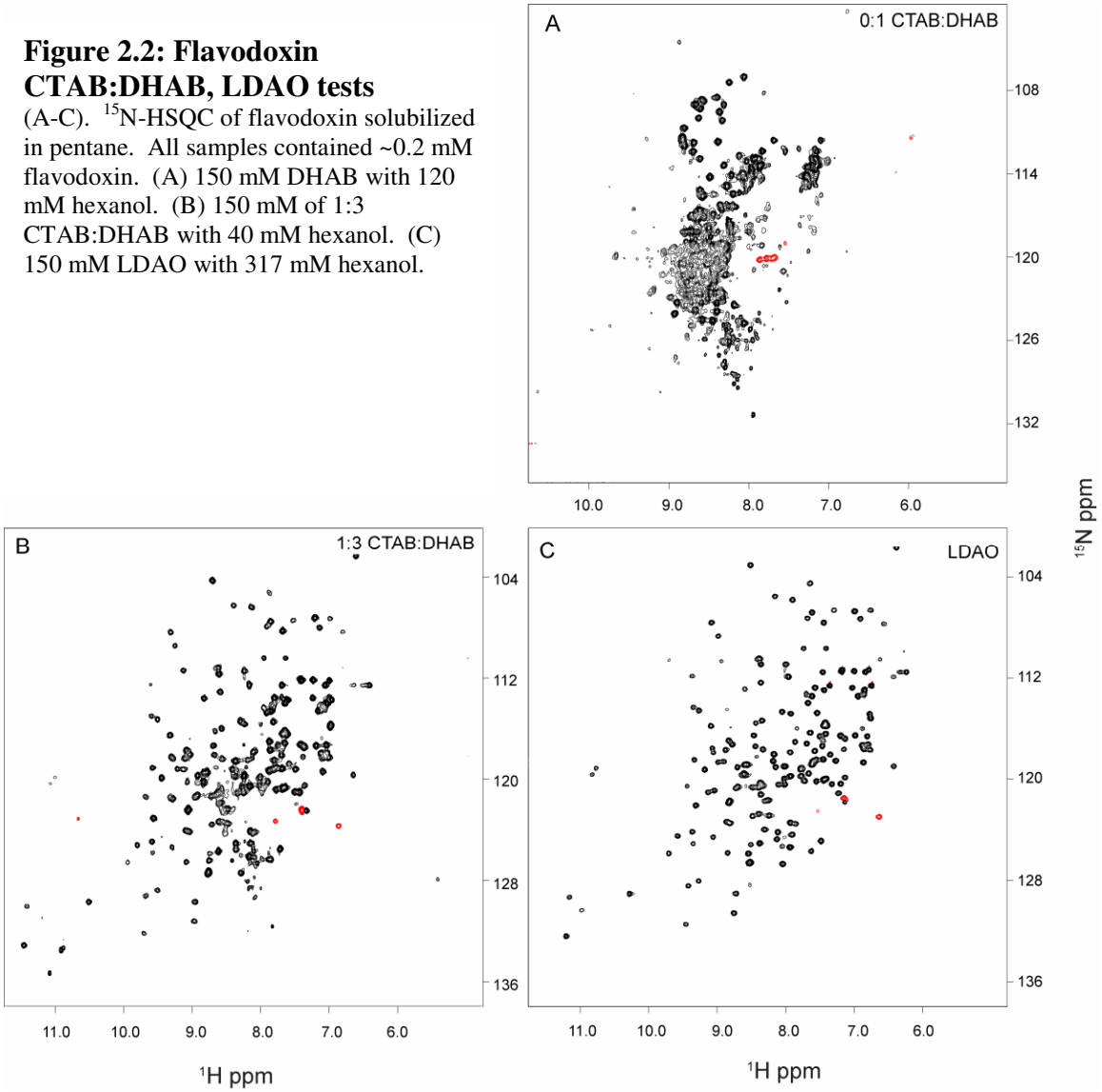

Figure 2.2: Flavodoxin CTAB:DHAB, LDAO tests
(A-C). ^{15}N-HSQC of flavodoxin solubilized in pentane. All samples contained ~0.2 mM flavodoxin. (A) 150 mM DHAB with 120 mM hexanol. (B) 150 mM of 1:3 CTAB:DHAB with 40 mM hexanol. (C) 150 mM LDAO with 317 mM hexanol.

The investigation of new surfactant mixtures is a common practice in reverse micelle NMR. The simplest test of whether or not a detergent or surfactant makes reverse micelles is to make up a mixture at a typical NMR concentration (75-150 mM) in a glass vial using pentane as the bulk solvent. Using suitable salt and buffer concentrations, an important tip is to use a dye such as bromophenol blue in the buffer. If the surfactant is able to properly form reverse micelles then the entire solution should

turn blue, otherwise the dye will accumulate at the bottom of the tube. In many cases it is necessary to titrate hexanol in increments of 1% v/v into the bulk solvent, up to about 10-12%, to determine the amount of the alcohol required as a co-surfactant for a given surfactant or mixture. Testing the maximal water loading of a surfactant system is important as well, as is the extended stability of a surfactant system. Test samples should be evaluated over several days and checked for beads of water or excessive surfactant aggregation at the bottom of the tube. After successfully passing this stage, a colored protein such as green fluorescent protein (GFP) or flavodoxin may be used to test how the mixture accommodates proteins, extending the same principle of bromophenol blue. As illustrated by Figure 2.2 however, it is of course important to test new creations on the NMR spectrometer as well.

2.5 Transferring proteins into reverse micelles

There are three techniques for the encapsulation of a protein into reverse micelles: phase transfer, the injection method, and lyophilizaton (Babu et al., 2003). Each technique has its advantages and disadvantages, and selection depends both on the compatibility of the protein to the technique and the experimental goals. For NMR studies this is typically the smallest reverse micelle assembly possible.

Using the phase transfer scheme, reverse micelles are pre-formed in an alkane solvent with just enough buffer to form empty bags. The protein is introduced in a concentrated aqueous state and the two phases, aqueous and organic, are allowed to mix. This method will generate samples of up to 0.3 mM protein concentration (Babu et al., 2001), though it does not allow for control of water loading. If a low initial concentration

of surfactant is used during the phase transfer step, additional surfactant can be added to reduce the water loading.

The injection method involves the addition of a highly concentrated protein to a mixture of organic solvent and surfactant (Lefebvre et al., 2005). The addition of the aqueous buffered protein solution will induce reverse micelle formation and protein encapsulation. Though simple, this technique requires a very soluble protein that can tolerate high concentrations for a short time. For example, typical reverse micelle preparations of 18.5 kDa flavodoxin require a water loading of at least 12.5. In 200 mM LDAO surfactant, this allows for the addition of 24.8 ul of aqueous buffered protein stock solution. To achieve a protein concentration of 300 uM, the protein stock solution would have to be at 7 mM. This concentration range may be problematic for proteins of higher molecular weight, low solubility, or membrane proteins and their required detergent accompaniment.

Lyophilization, another alternative method of encapsulation, allows for more precise control of both protein concentration and water loading. However, it requires that a protein and, in the case of membrane proteins their solubilizing detergents, be amenable to dialysis into water, freezing, and lyophilization. In all, the protein must be able to go through these processes without unfolding or, at the very least, have the ability to refold in the experimental milieu of reverse micelles. Our initial membrane protein model system of KcsA, which will only refold in a lipid environment (Valiyaveetil et al., 2002) or after specific denaturing conditions in a detergent environment (Barrera et al., 2005), successfully undergoes both the dialysis and lyophilization steps with its native tetrameric fold intact, as verified by reverse micelle studies discussed in this work and by

other groups working with KcsA in aqueous solution NMR(Chill et al., 2006). Prior to testing a protein directly in reverse micelle conditions, the consecutive steps of dialysis, lyophilization and resuspension into buffer should be assessed by a structure or activity based assay, or simply the comparison of pre- and post-lyophilization-resuspension HSQCs. Once the integrity of the sample is verified, conditions for reverse micelle encapsulation can be explored and optimized.

Chapter 3: Optimization of Membrane Proteins in Reverse Micelles

3.1 Introduction

The initial attempts at KcsA encapsulation into reverse micelles involved the use of the membrane protein solubilized in aqueous lipid and/or detergent mixtures. These preparations were screened first as aqueous preparations for peak count and dispersion by ^{15}N-HSQC experiments. The best detergent-protein candidates in terms of spectral dispersion and peak count were then exposed to separate reverse micelle preparations of CTAB, DTAB, and AOT in pentane by the phase transfer method. These attempts often resulted in visible aggregations of lipid and detergent. Resulting ^{15}N-HSQC spectra often showed extremely crowded spectra of insufficient peak counts indicative of aggregated and unfolded protein. The few detergent-lipid-reverse micelle mixtures that gave promising spectra were of such low signal-to-noise as to preclude detailed investigation beyond the most rudimentary NMR pulse sequences.

It had been assumed that reverse micelle surfactants would shield both the membrane protein and the solubilizing detergent from the alkane solvent, and that, further, the solubilizing detergents would remain soluble as co-surfactants with reverse micelle surfactants. After the first round of encapsulation tests these assumptions proved to be incorrect. Indeed, further experimental exploration of the list of typical membrane protein solubilizing detergents yielded no successes. The poor encapsulation results were attributed to two factors: the inability of some detergents and lipids to form reverse micelles in alkane solvents and the incompatibility of these detergents with reverse micelle surfactants. It became apparent that a strategy to avoid the potential aggregation

was to use a more homogeneous mixture of detergent, removing this incompatibility from the list of variables.

The use of a single surfactant or surfactant family (i.e. of the same or similar headgroup composition but varying in the hydrocarbon chain length or number of chains) was postulated to be advantageous for consistent sample preparations with improved signal-to-noise spectra. Thus, instead of attempting to employ a mixture of traditional aqueous lipids or detergents and reverse micelle surfactants, we attempted to find a single detergent surfactant that could perform these dual duties:

1) The solubilization of the hydrophobic transmembrane domains of a membrane protein.

2) The maintenance of the proper fold of both the extra- an intracellular domains of a membrane protein in the aqueous cavity of the reverse micelle.

These dual-duty surfactants are more suitably termed hybrid surfactants, and formed the foundation of the reverse micelle encapsulation strategy for membrane proteins that we have employed.

3.2 Reverse micelle hybrid surfactant system

A two-part survey was undertaken: determining which traditional reverse micelle surfactants would be suitable as aqueous micelles, and expanding the list of typical aqueous detergents capable of forming reverse micelles. In summary, surfactants such as CTAB and DTAB proved useful in the aqueous solubilization of membrane proteins, while AOT, due to its relatively low solubility in water, did not support membrane protein concentrations suitable for NMR studies. The aqueous detergent LDAO, shown to solubilize KcsA in x-ray crystallography studies (Doyle et al., 1998), functions well as

a reverse micelle surfactant, though it proved more suitable for water soluble proteins (Valentine et al., 2006) than for KcsA, as evidenced by the low amide peak count in the HSQC spectrum and the absence of tryptophan indole sidechain peaks (Figure 3.1).

The basic premise of hybrid surfactants is the ability to transition from solubilizing a membrane protein in water to solubilizing the same protein in an alkane solvent. In this sense the hybrid surfactant works as a carrier detergent, keeping the protein properly folded as it transitions from an aqueous to an organic bulk solvent. By method, the surfactant solubilizing the hydrophobic domain will flip out to form reverse micelle pockets around the extra- and intracellular domains of the membrane protein. This was shown in Figure 1.1.

3.3 Detergent screens for membrane proteins in reverse micelles

The screen to determine the optimal reverse micelle surfactant or mixture of surfactants must be viewed in the same way as the detergent and lipid screens for aqueous micelle membrane protein NMR samples (Krueger-Koplin et al., 2004; Sanders and Oxenoid, 2000). Traditional reverse micelle surfactants are first tested with a membrane protein in solution to see if they give reasonable HSQC spectra. These micelle samples are then transferred into reverse micelles and the HSQC spectra screened for dispersion and proper peak count. Further optimization involves variables such as water loading, detergent levels, and addition or use of co-surfactants or lipids. The key is to find the set of conditions that allow the protein and all of its domains to assume a single, natively folded conformation. It is equally important that these conditions be stable and consistent from sample to sample, and the folded protein is able to exist with a high

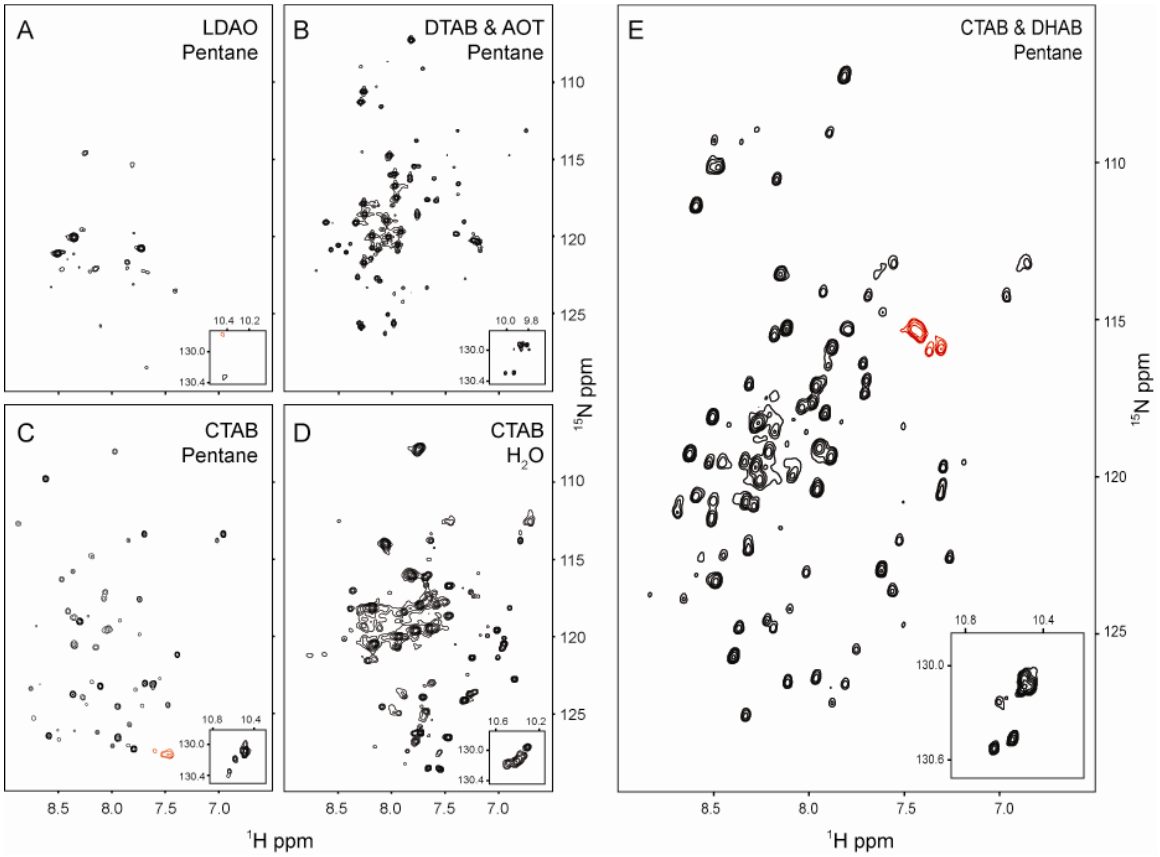

Figure 3.1: Surfactant optimization

^{15}N-HSQC spectra of $KcsA_{\Delta C35}$ solubilized in aqueous and reverse micelle surfactant systems. Detergents were tested as aqueous samples first before preparation as reverse micelles. All samples were ~0.15 mM in $KcsA_{\Delta C35}$ solubilized in pentane, and run at 25 ^{o}C. Panel (A) 200 mM LDAO reverse micelles in pentane with 320 mM hexanol. (B) 195 mM AOT and 195 mM DTAB. (C) 200 mM CTAB reverse micelles in pentane with 800 mM hexanol. (D) 125 mM CTAB and 125 mM DHAB with 390 mM hexanol. Insets show the spectral region containing the tryptophan indole N-H correlations.

enough free energy barrier that minor perturbations, variations, or incursions into the system (such as the addition of a ligand) not skew or alter the population of properly folded states.

Additionally, native lipids can be added to preparations if deemed necessary. In some KcsA reverse micelle preparations this included phosphatidylglycerol (PG) (Avanti Polar Lipids) at 5% of the total molar amount of CTAB and DHAB. PG is co-purified with KcsA and is believed to be important for the proper gating of the channel (Valiyaveetil et al., 2002). Addition of PG did not appreciably change HSCQ spectra of KcsA in reverse micelles.

3.4 Circular Dichrosim as a screening method for reverse micelle studies

It is important to also consider other spectroscopic techniques as screening methods for membrane proteins and reverse micelles in general. Circular dichroism (CD) has been used in other studies as a probe of KcsA secondary structure – both to verify the proper helical structure of SDS detergent-solubilized KcsA (Chill et al., 2006) or a water-soluble analogue (Slovic et al., 2004), and as a probe of KcsA unfolding by the small alcohol TFE (Barrera et al., 2005; van den Brink-van der Laan et al., 2004). CD is a relatively quick way of screening membrane proteins for their proper secondary structure – alpha helix or beta sheet; they are typically one or the other. The drawback to using CD in this manner is its incompatibility with some buffers and with achiral detergents, such as CTAB and DHAB, which lack a handedness and absorb too much signal at lower wavelengths. Examples of chiral detergents are LDAO and DM. The limitation on the absorption of signal monitored by the dynode in CD is concentration dependent, thus at limited concentrations even achiral detergents can be utilized. In the case of full length KcsA, aqueous samples in CTAB were accurate until roughly 214 nm. This was sufficient to compare the mean residue ellipticity trace of the membrane protein in this

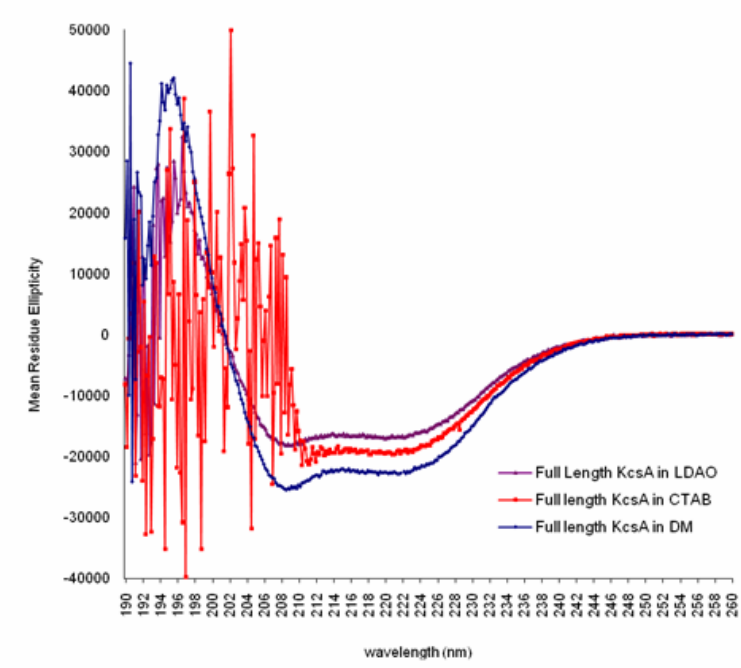

Figure 3.2: Circular dichroism of aqueous KcsA samples

Circular dichroism trace of aqueous KcsA solubilized in three different detergents: LDAO (purple), CTAB (red), and DM (blue). The disruption of signal in the CTAB sample is apparent beginning at 214 nm, due to this detergent's achiral character.

detergent to other samples run in DM and LDAO (Figure 3.2). DM is a common extraction detergent for KcsA, and LDAO was the solubilizing detergent for both the original and subsequent x-ray crystallography studies of KcsA (Doyle et al., 1998). Other than having slightly different values of mean residue ellipticity (MRE), due to slightly different structures of the channel in these different detergents or simply due to errors in the concentration measurements of the protein, the traces are nearly identical. As calculated from the amplitude of the signal at wavelength 222 nm, the helical contents of the three preparations are 53% in DM, 47% in CTAB, and 41% in LDAO. These values of helical content and of the amplitudes of the CD trace minima and maxima are comparable to CD traces of KcsA in other detergents (Chill et al., 2006).

The combination of DHAB and CTAB proved to be prohibitively absorptive for circular dichroism studies of KcsA in reverse micelles. And while LDAO is a more accommodating detergent for CD studies in general, it failed to show any signal for KcsA in reverse micelles. This result is consistent with the poor HSQC spectra for KcsA in LDAO reverse micelles, and showed that despite its adequate support of KcsA's aqueous structure, LDAO is not sufficient as a reverse micelle detergent for the protein. It should be noted that when these studies were done the wealth of backbone assignments and other NMR data discussed later in this work were not available to us. Although the CD reverse micelle efforts with CTAB and DHAB proved inconclusive, it was nevertheless important to show that the secondary structure of KcsA in aqueous CTAB preparations was comparable to that of other, more commonly used detergents.

A more successful application of circular dichroism to screen for reverse micelle surfactants was shown with the combination of flavodoxin and LDAO (Figure 3.3). Here the circular dichroism spectra of flavodoxin matched the trace seen for aqueous flavodoxin. LDAO's successful encapsulation of flavodoxin was confirmed by NMR, as shown previously by Figure 2.2. It should be emphasized that even if a sample exhibits proper secondary structure in circular dichroism, one cannot necessarily equate that with proper tertiary or quaternary structure, or even stable secondary structure. Appendix A contains more detailed results on circular dichroism studies done of individual system components: buffers, detergents, and both aqueous and organic preparations.

3.5 Optimization of membrane protein sample conditions for reverse micelle NMR

After the successful encapsulation of a membrane protein in a reverse micelle and subsequent approximation of a reasonable peak count by 2D HSQC or 3D HNCO spectra, further optimization of sample conditions may be required to perform the full suite of NMR structural studies. Two of these variables are water loading and the use of co-surfactants, if they have not already been surveyed to achieve initial encapsulation success.

For soluble proteins in reverse micelles, a greater ratio of water to surfactant is required for larger proteins than for smaller ones. The typical water loading for a small protein such as ubiquitin (8.5 kDa) is 10, while water loading required for medium to large-sized proteins such as flavodoxin (18.5 kDa) or GFP (54 kDa) may be 15 or even greater. In the case of membrane proteins, the extra- and intracellular domains of the protein are the only regions that require solubilization. Thus the water loading requirement may be thought to reflect that required for two small proteins, representing

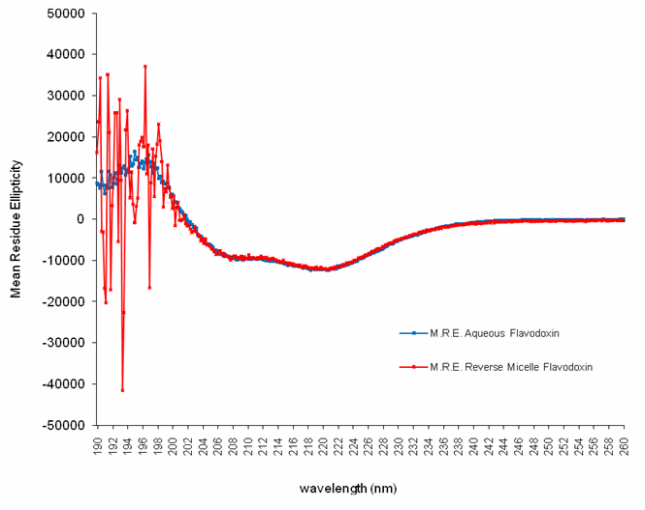

Figure 3.3: Circular dichroism of aqueous and reverse micelle flavodoxin

Circular dichoism trace of aqueous (blue) and reverse micelle (red) flavodoxin. The effects of LDAO detergent are seen beginning in the trace signal for the reverse micelle sample at around 204 nm.

the extent of the extra- and intracellular domains of a given membrane protein. A smaller water loading was shown to be optimal for membrane proteins in reverse micelles by Waks and colleagues (Binks et al., 1989). This was also true for studies of $^{RM}KcsA_{\Delta C35}$, where the HSQC spectra were examined over a range of water loadings from 3 to 30, and it was found that a water loading in the range of 7-8 gave optimal HSQC spectra. Figure 3.4 shows a sample of HSQCs from this water loading experiment. While most peaks in the spectra had consistent chemical shifts as the amount of water in the reverse micelles increased, the red circle on the spectra highlights an area where chemical shift changes were observed. Downfield (higher) shifts in the nitrogen dimension are sometimes indicative of unfolded structure, and this is observed with increasing frequency in spectra from boxes B, C, and D in Figure 3.4. In the case of KcsA, the appearance of these shifts at higher water loadings led to the decision to go forward with lower water loading values.

The impetus for using the smallest water loading possible is two-fold. First, smaller water loadings will result in smaller reverse micelle particles, and subsequently lower rotational correlation times and longer T_2 times; secondly, the confined space of a smaller water pocket may induce some unfolded regions of the protein to fold, as has been observed previously in reverse micelle studies of a metastable protein (Peterson et al., 2004). The other aspect of this latter point to consider is the potential undesirable interaction of headgroups with the protein's surface if the water shell separating these two components is too small. In the case of KcsA where most of the spectra seemed unaffected by changes of water loading in the range of 6-20, it appears that this undesirable interaction is not present.

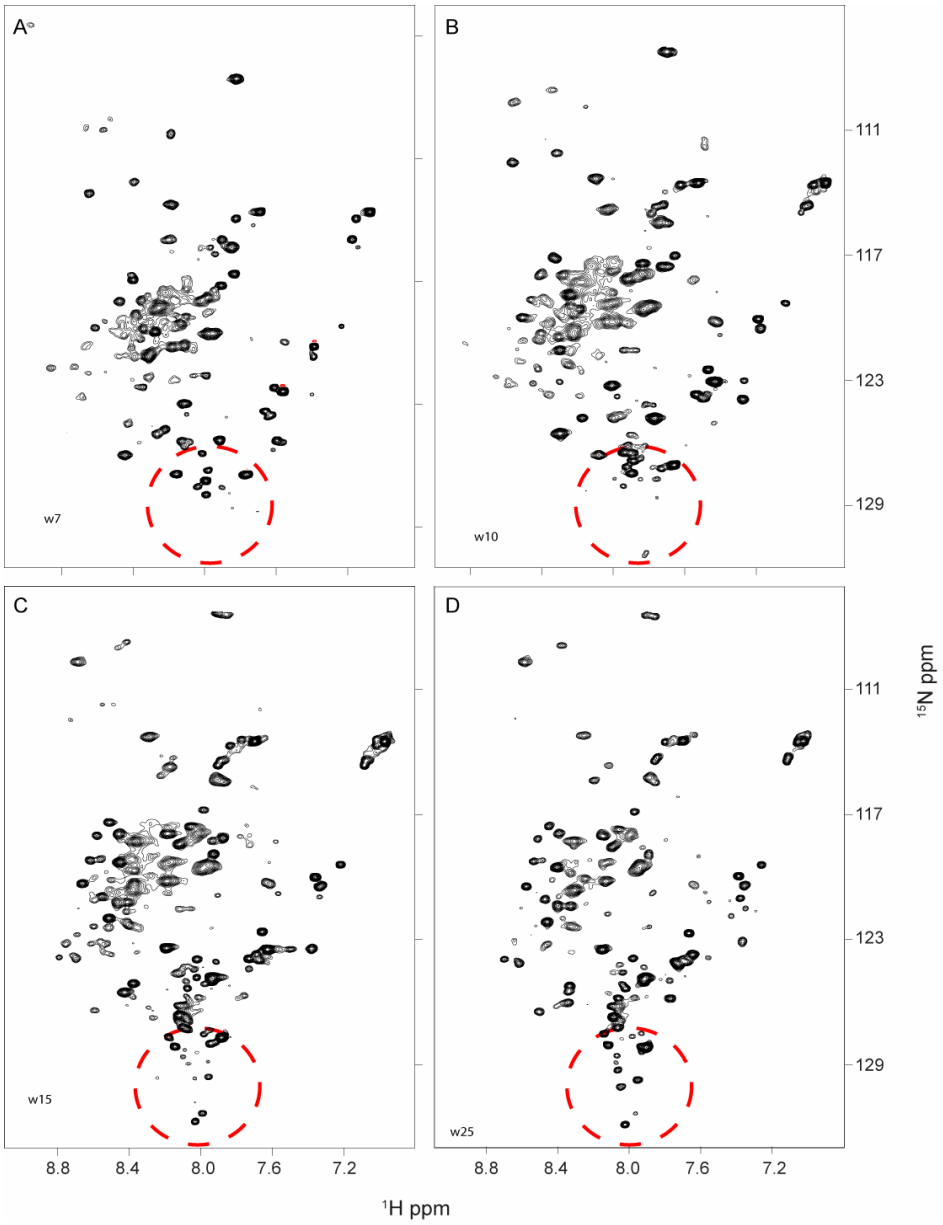

Figure 3.4: KcsA$_{\Delta C35}$ reverse micelle water loading survey

(A-D). ^{15}N-HSQC of a single KcsA$_{\Delta C35}$ sample solubilized in pentane with 323 mM of 1:1 CTAB:DHAB, 396 mM hexanol, at 15^{o} C. (A) Sample as originally formulated with a water loading of 7.3. (B) Sample with additional buffered water added to bring total measured water loading to 11.0. (C) Water loading of 12.9. (D) Water loading of 19.4.

The use of a co-surfactant, particularly for reverse micelle studies involving membrane proteins, is an additional optimization step that may improve spectral quality. KcsA gave promising spectra in the mono-acyl chained CTAB, though in light of literature correlating membrane lateral pressure on a protein with stability (Barrera et al., 2005; van den Brink-van der Laan et al., 2004), a di-acyl chain CTAB analogue, DHAB, was added as co-surfactant, intuiting that the expanded volume of the surfactant tail would further stabilize KcsA. A series of $^{RM}KcsA_{\Delta C35}$ samples were made with varying ratios of CTAB and DHAB to test if the addition of DHAB had any effect on KcsA's structure and, if so, if they resulted in better HSQCs. The results of this survey are shown in Figure 3.5. The 1:1 ratio of CTAB:DHAB seems to give narrower linewidths than CTAB alone, indicating the potential of both a lower correlation time and the removal of intermediate exchange for some residues. The effects of intermediate exchange on NMR performance are discussed in more detail later. The broadened quagmire of peaks seen in the 1:3 CTAB:DHAB sample is indicative of some sort of aggregation; if the di-acyl DHAB surfactants are acting as hypothesized and exerting some degree of lateral pressure on the KcsA transmembrane region, this may be a case of too much lateral pressure. Alternatively, as was seen in the case for flavodoxin DHAB reverse micelles, there may not be enough CTAB surfactant this system to adequately support proteins in the reverse micelle.

3.6 Sample Consistency

Achieving consistent NMR spectra is problematic for membrane proteins. This is partially due to the experimental compromises that must be made for their study.

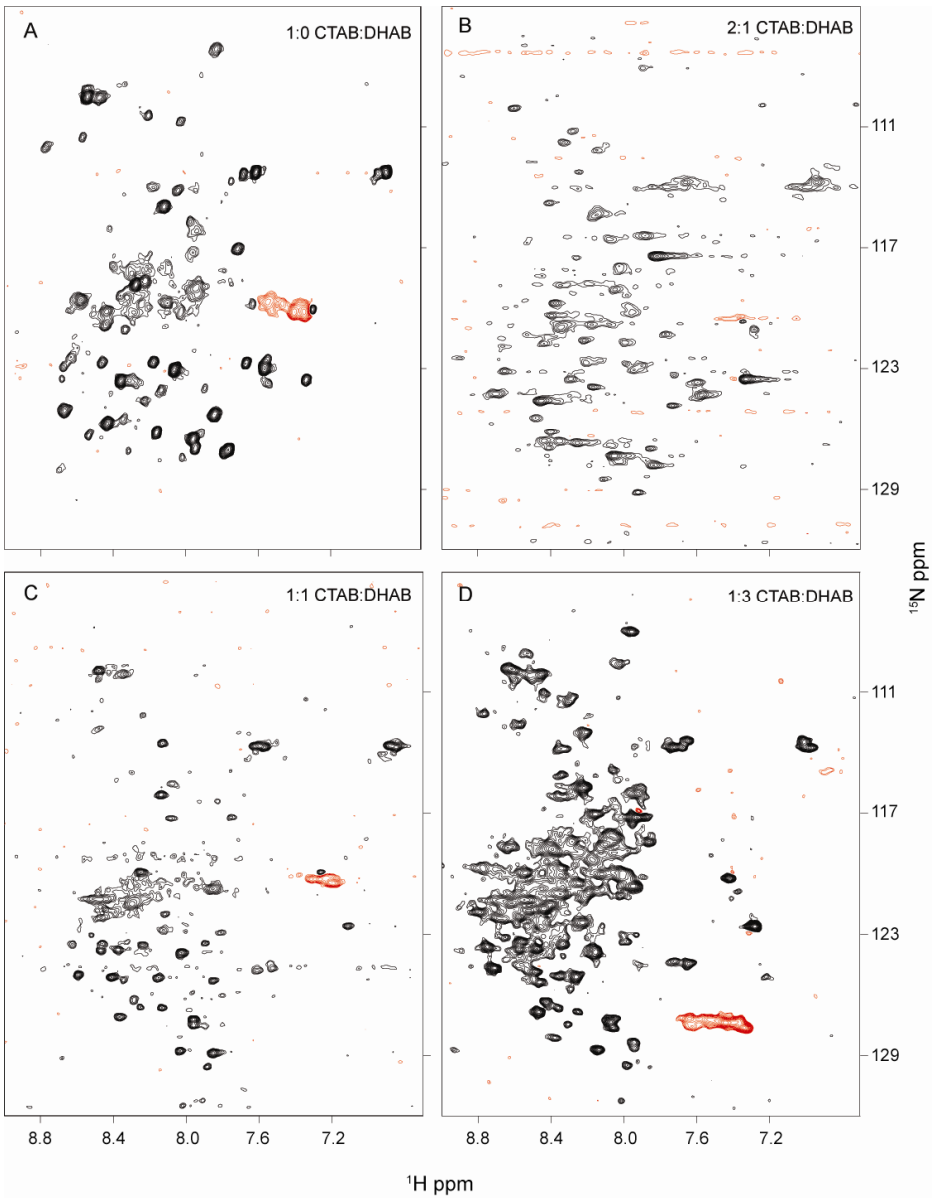

Figure 3.5: CTAB:DHAB survey of $^{RM}KcsA_{\Delta C35}$

(A-D) In what will never be call a handsome lineup of NMR HSQCs, the efforts shown here eventually led to better overall NMR spectra of KcsA in reverse micelles. All samples were ~0.15 mM $KcsA_{\Delta C35}$ monomer, equivalent water loadings, and solubilized in pentane. (A) 200 mM CTAB with 793 mM hexanol. (B) 100 mM CTAB and 50 mM DHAB with 238 mM hexanol. (C) 150 mM CTAB and 150 mM DHAB with 159 mM hexanol. (D) 50 CTAB and 150 mM DHAB with 79 mM hexanol.

Detergent micelles provide an imperfect mimetic for the native bilayer, but they are nevertheless a necessity in the size-critical world of solution NMR. Finding the correct detergent is important, as the same protein can have vastly different spectra depending on the detergent or lipid solubilizing it (Krueger-Koplin et al., 2004). These differences can reasonably assumed to be due to the length, number, and volume of acyl chains, as well as the vast plethora of different headgroups, which may be positive (cationic), negative (anionic), neutral (nonionic), or both positive and negatively (zwitterionic) charged, and can potentially interact with the intra- and extracellular loops and domains of a membrane protein. For this reason once a detergent or lipid system that gives optimal performance is decided upon it is important that the membrane proteins of study is cleanly exchanged from the extraction detergent to the experimental detergent to provide consistent, homogenous samples.

In the case of KcsA it became apparent that while samples made from the same protein cell growth and initial purification from said growth were consistent with one another in terms of proton and nitrogen chemical shifts, samples from different cell growths and preps were not. In these initial preps, the exchange from the extraction detergent n-decyl-β-D-maltopyranoside (DM) to the experimental NMR detergent CTAB were carried out over an 85 mL volume Superdex-200 column. Due to differences in spectra from prep to prep, it became apparent that this detergent exchange was not always consistent, perhaps owing to different relative ratios of extraction detergent (DM, in this case) to protein from prep to prep. This effect was remedied by performing the detergent exchange during the initial purification steps of the prep, when KcsA was still bound to TALON resin via its His-tag, allowing for a much more thorough exchange step.

The basic purification involved harvesting and lysis of the cells, extraction using DM, ultracentrifugation, and then binding the His-tag protein to a TALON column. After high salt and low imidazole washes containing DM, the protein is washed extensively in-place on the column with buffer containing CTAB. An additional overnight wash using a 10-fold excess of CTAB-containing buffer was also used with the loose resin, which was removed from the column and placed into 50 mL conical tubes (5 mL of resin per tube). The resin was then repacked into a column, washed with additional CTAB-containing buffer, and finally eluted with a high concentration imidazole solution containing CTAB. It should be noted that extraction of the membrane protein with the milder DM gave a better protein yield than extraction using CTAB alone. This technique of in-place detergent exchange works well with numerous detergents, and has been reported elsewhere in the literature for the preparation of membrane proteins for study by NMR (Baker et al., 2007a). Initial test screenings of different detergents can also be used in this same manner to ensure complete detergent exchange. After loading and binding a protein onto an affinity column and initial wash steps are performed, the column may be split into several fractions, with each then washed with a separate detergent. These smaller column volumes, by extension, facilitate the use of smaller detergent-buffer wash volumes. This is an important consideration when the high cost of some detergents or lipids are taken into account.

Other factors that play a role in sample consistency of membrane proteins and reverse micelles include the molar ratio of detergent to protein, the relative molar ratios of the different detergents in a system, pH, water loading and, particularly in KcsA's case, potassium concentration. This latter difference was noted in preliminary studies of

$^{RM}KcsA_{\Delta C35}$, and additional studies of these changes are discussed later in this work. Another consideration for membrane protein studies in reverse micelles is the bulk solvent. This latter factor may be due to differing relaxation properties in parts of the same protein and the effect of changing viscosities. There also exists the possibility that the common short chain alkanes presently employed in reverse micelle NMR (pentane, propane, and ethane) may intercalate amongst the transmembrane domains of a membrane protein in a reverse micelle, interacting with residues in these regions. In the present model of membrane protein reverse micelle encapsulation, the transmembrane domains of the protein are more intimately associated with the bulk solvent than for that of a soluble protein in a reverse micelle shielded completely by the bulk solvent. In the case of KcsA, there are very minor shift differences in the nitrogen and proton dimensions of some peaks between ethane and pentane samples. In the comparison of pentane and ethane backbone assignments, the nitrogen and carbon chemical shifts of the two types of samples are nearly identical for KcsA's selectivity filter region residues (Figure 3.6), N-terminal helix residues (Figure 3.7), and the turret and loop residues (Figure 3.8).

The maintenance of sample consistency is easier in theory than in practice. The quantification of reverse micelle samples by 1D NMR to determine the proper ratio of different detergents (if there is more than one) and water loading, and then the tracking of these values over a sample's lifetime, is important. By adhering to these protocols, we have generally been able to achieve consistent, reproducible spectra, as shown by reverse micelle preparations of KcsA in the bulk solvent ethane (Figure 3.9).

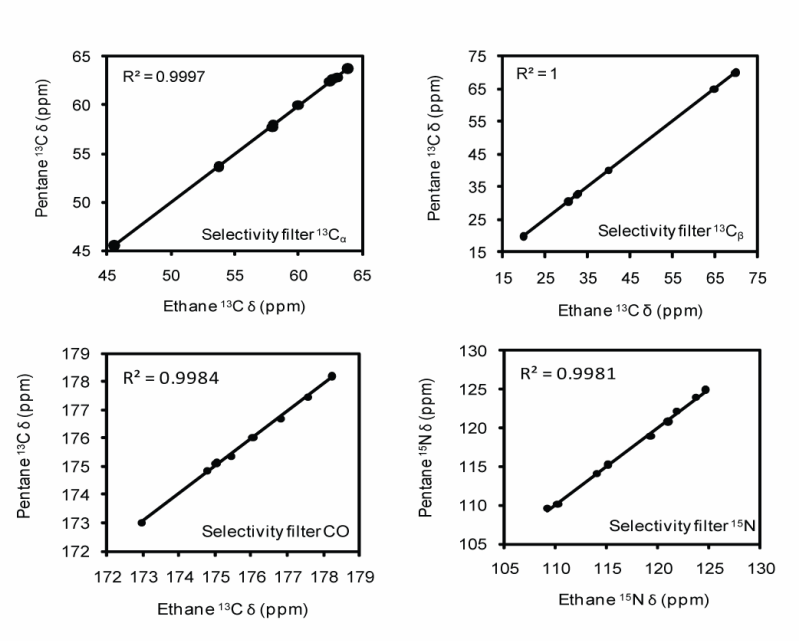

Figure 3.6: Selectivity filter ethane and pentane differences

Comparison of chemical shift differences for $^{13}C_{\alpha}$, $^{13}C_{\beta}$, ^{13}CO, and ^{15}N atoms in $^{RM}KcsA_{\Delta C35}$. Other than the bulk solvent, samples were prepared similarly in terms of detergent selection and water loading.

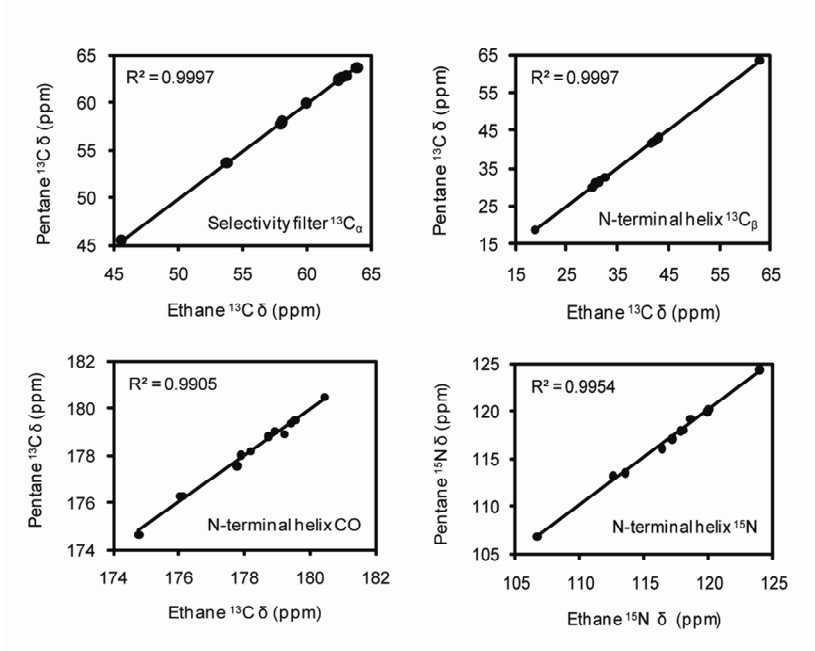

Figure 3.7: N-terminal helix ethane and pentane differences.

Comparison of chemical shift differences for $^{13}C_{\alpha}$, $^{13}C_{\beta}$, ^{13}CO, and ^{15}N atoms in $^{RM}KcsA_{\Delta C35}$.

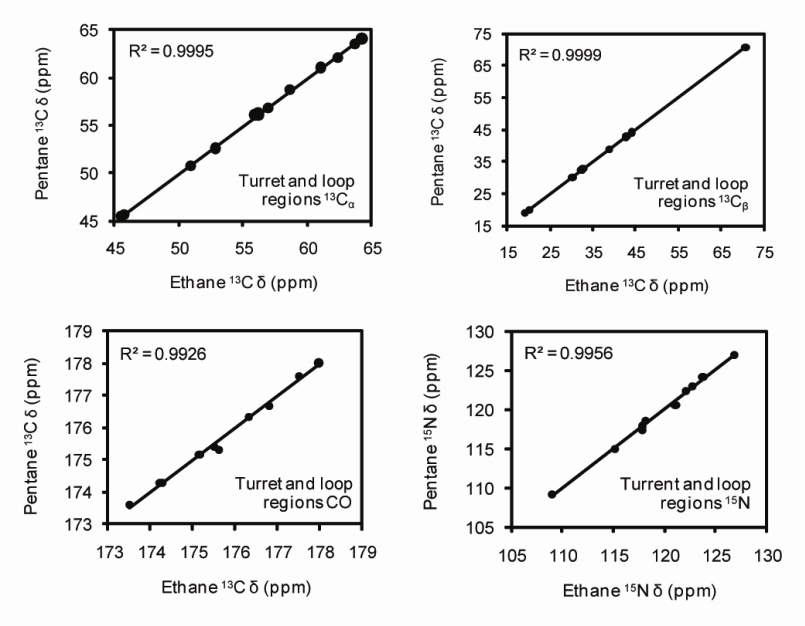

Figure 3.8: Turret and loop region ethane and pentane differences

Comparison of chemical shift differences for $^{13}C_{\alpha}$, $^{13}C_{\beta}$, ^{13}CO, and ^{15}N atoms in $^{RM}KcsA_{\Delta C35}$.

3.7 Optimization of transverse relaxation properties

Improved spectral resolution is often achieved by raising the temperature of an aqueous protein solution just to the point of denaturing or beyond with selected mutants (Chill et al., 2006). The same reasoning extends to reverse micelle solutions, as evidenced by improved T_2 relaxation properties of KcsA in pentane reverse micelles at 15°, 25°, and 35° C. The spectra were acquired in a sealed butane tube (Wilmad Labglass) and pressurized to 50 psi to keep the solution below the boiling temperature of pentane (Figure 3.10). Based on the Stokes-Einstein equation, these results are expected. However, it should be noted that the improvement in relaxation properties due to an increase in sample temperature in an organic solvent is much less relative to an aqueous

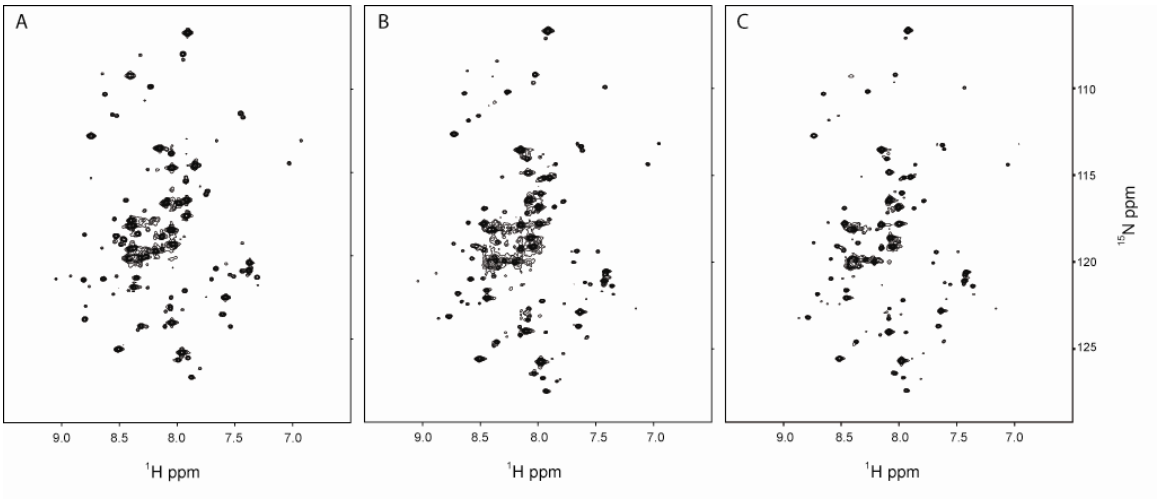

Figure 3.9: Reproducibility of reverse micelle $KcsA_{\Delta C35}$ preparations

^{15}N-labeled $KcsA_{\Delta C35}$ (A), $^{13}C^{15}$N-labeled $KcsA_{\Delta C35}$ (B), and $^{13}C^{15}$N-labeled $KcsA_{\Delta C35}$ (C) in ethane bulk solvent, all from different growth preparations. Each sample contains ~ 200 mM of 1:1 CTAB:DHAB. and 0.225 mM $KcsA_{\Delta C35}$ monomer concentration. The bulk solvent is ethane at 4,000-4,500 psi, with an additional 5% v/v of pentane, and 800 mM hexanol. The theoretical viscosity of the sample at 4,500 psi is 86.9 uPa-s, calculated from the molar fractions of ethane and pentane at 4,500 psi and taking into account the compressibility of pentane at pressure.

NMR sample, as shown by the comparison of viscosities of water, pentane, and ethane at different temperatures in Figure 3.11. As noted previously, membrane proteins are fickle customers in the stability department. This is true in terms of a sample's half-life as well as the exchange properties of individual residues. When the effect of temperature on a sample's viscosity is mitigated, one is no longer beholden to running samples only at high temperatures to achieve necessary relaxation properties to run 3D NMR experiments. Temperature thus becomes a variable that can be adjusted in a wider range to improve sample stability and spectral properties. In the case of KcsA reverse micelles

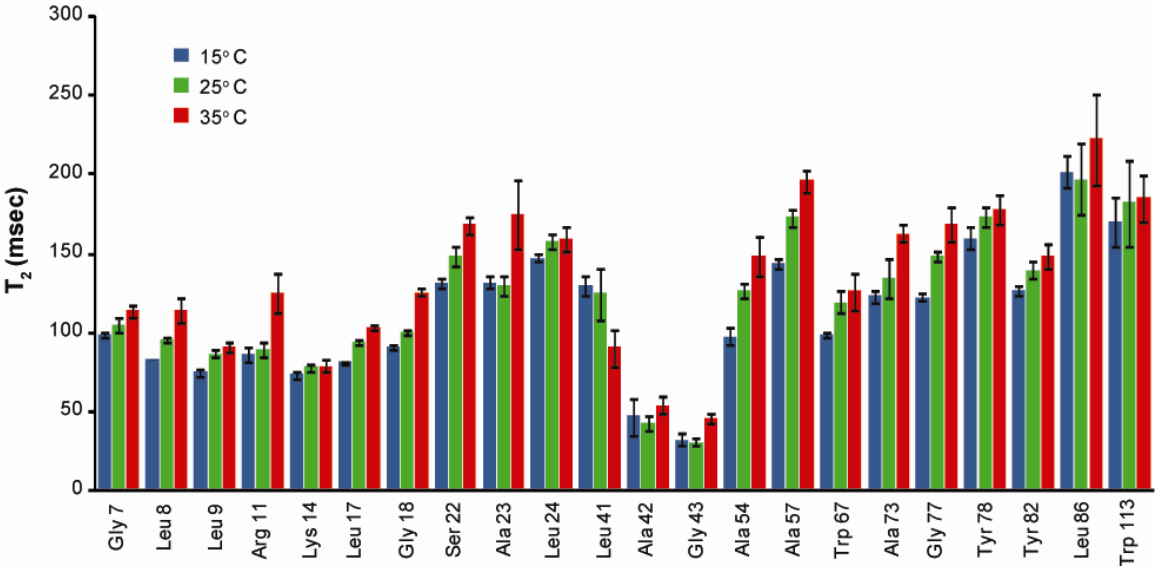

Figure 3.10: Effect of temperature on $^{RM}KcsA_{\Delta C35}$ T_2 relaxation in pentane

A comparison of amide ^{15}N T_2 relaxation times for $KcsA_{\Delta C35}$ reverse micelle samples in bulk solvent pentane at 15, 25, and 35 ^{o}C. The sample contained 194 mM total surfactant of a 1:1 molar ration of CTAB:DHAB and 340 mM hexahol. ^{15}N T_2 relaxation was measured using the pulse sequence of Farrow et al. (Farrow et al., 1994) and collected at 500 MHz (1H) on a Varian Inova NMR spectrometer.

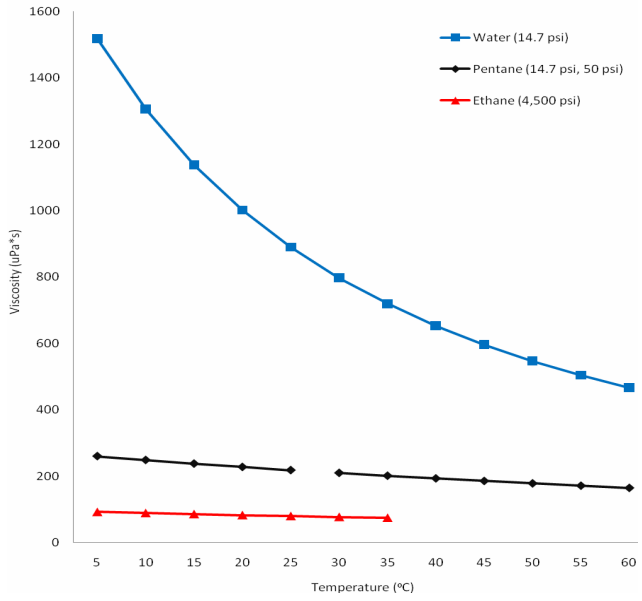

Figure 3.11: Viscosity of water, pentane, and ethane by temperature

Unpressurized pentane viscosity is shown from 5-25^{o} C. From 30-60^{o} C, pentane viscosity is for 50 psi pressurization.

in ethane, samples were eventually run at 25^{o} C. This choice was largely made to extend the lifetime of the sample as long as possible, as the gains in viscosity at a higher temperature in this solvent are near-negligible.

A major objective in any optimization process is to identify the variables that are the greatest contributing factors to a given outcome. In terms of sample consistency this turned out to be the clean exchange from protein prep extraction detergents into experimental detergents. In terms of sample viscosity, which in reverse micelle NMR can be considered the penultimate experimental variable, it was shown that temperature had a relatively minor contribution. It was discovered, however, that the amount of detergent in a system had a major effect on viscosity.

The surfactants in a reverse micelle solution are continuously exchanging between reverse micelle assemblies, just as detergents exchange among micelles in an aqueous solution. In both cases an excess of both empty detergent micelles and empty reverse micelles are necessary for the long-term stability of the sample. It follows that the increase in the number of macromolecular particles in either system will result in an adverse increase in overall viscosity and an increase in the rotational correlation time of protein-detergent particles in the system (Seigneuret et al., 1991). Higher levels of surfactant will support higher protein concentrations, ideally with one protein molecule occupying a single micelle or reverse micelle. However, once the maximal protein loading is reached any excess surfactant contributes unnecessarily to viscosity. The extent of this contribution is an important consideration as illustrated in Figure 3.12.

The improved T_2 relaxation times of KcsA with a low surfactant concentration are striking. Similar results were seen previously for reverse micelle samples prepared with

the surfactant AOT (Babu et al., 2003). From these studies it became apparent that for the successful application of 3D backbone experiments to KcsA in reverse micelles it would be necessary to sacrifice the protein loading of a sample for the sake of improved relaxation properties. This sacrifice in protein concentration for the sake of improvement in viscosity also plays a role in the selection of a bulk solvent for 3D backbone experiments and, by extension, the amount of sample that can be placed within the NMR coil because of solvent constraints, since the high pressure ethane NMR tubes contain approximately 20-33% less sample than a traditional glass NMR tube (Ron Peterson, personal communication).

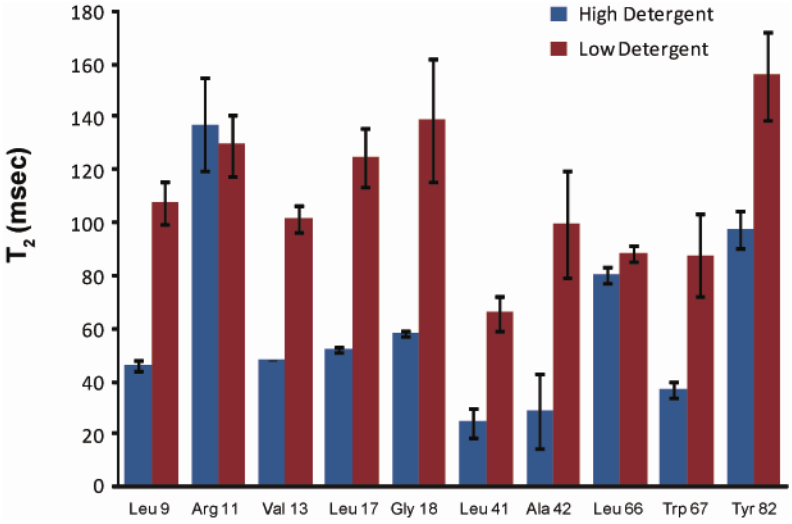

Figure 3.12: Effect of surfactant concentration on T_2 times for $^{RM}KcsA_{\Delta C35}$

A comparison of amide ^{15}N T_2 relaxation times for $KcsA_{\Delta C35}$ reverse micelle samples in pentane at 25° C. The high detergent sample contained 390 mM total surfactant of a 1:1 molar ratio of CTAB:DHAB, and 560 mM hexanol. The low detergent sample contained 150 mM total surfactant of a 1:1 molar ratio of CTAB:DHAB and 400 mM hexanol. ^{15}N T_2 relaxation was measured using the pulse sequence of Farrow et al. (Farrow et al., 1994) and collected at 600 MHz (^1H) on a Varian Inova NMR spectrometer.

The optimized conditions of reverse micelle KcsA in pentane allowed for a the backbone assignments of nearly 60% of the amide cross peaks for $KcsA_{\Delta C35}$. However, the assignments were sharply skewed towards the sharper (longer T_2) resonances in the spectra. Of the unassigned residues, 69% resided in the more rigid, and thus faster-relaxing, transmembrane regions of the protein. Due to the sparse nature of assignments for the transmembrane residues, the use of high pressure ethane (Peterson et al., 2005b) was employed in the encapsulation of KcsA to improve the correlation time of the assembly, with the goal of achieving a more uniform distribution of backbone assignments by mitigating the limitations of T_2 relaxation. Figure 3.13 shows the scope

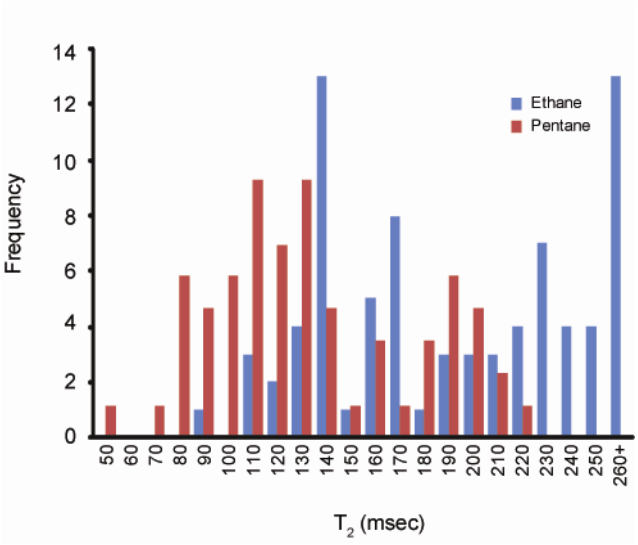

Figure 3.13: Comparison of NMR relaxation properties of $KcsA_{\Delta C35}$ in reverse micelles dissolved in pentane and ethane

A comparison of the distributions of amide ^{15}N T_2 relaxation times for $KcsA_{\Delta C35}$ reverse micelles in pentane (red) and ethane (blue) at 600 MHz (^1H). The distribution clearly shows an improvement in transverse relaxation properties of residues in ethane. Higher T_2 values in both samples (>150 msec) are attributed to

residues in more mobile regions of KcsA, such as loop regions and the N-terminal helix. The pentane sample contained 150 mM total surfactant at a 1:1 molar ratio of CTAB:DHAB with 400 mM hexanol. The ethane sample contained 180 mM total surfactant at a 1:1 molar ratio of CTAB:DHAB with 800 mM hexanol and included 5% v/v of pentane. The sample was pressurized to 4,500 psi (300 bar).

of the improvement achieved for $^{RM}KcsA_{\Delta C35}$ by moving from pentane to ethane as the bulk solvent.

In relatively simple NMR experiments such as the HSQC the payoff of greater T_2 times may in some cases only be apparent as a subtle narrowing of linewidths. However given the improvement in transfer efficiency relative to T_2 times in NMR spectroscopy, the full effects of encapsulation in ethane over pentane are realized in 3D backbone and sidechain experiments. The improvement in performance in these experiments more than compensates for lower protein concentrations. Figure 3.14 shows an experimental comparison of two backbone through-bond correlation experiments, the HNCACB and the CBCACONH, in both pentane and ethane, for the selectivity filter of $^{RM}KcsA_{\Delta C35}$. The most notable difference between the two bulk solvents can be seen by studying the weakest of the four peaks given by the HNCACB, the C_β(i-1), which is circled in red here. The marked difference is due to both the improved lineshape and the transfer efficiency resulting from improved transverse relaxation properties (T_2) due to the fast molecular reorientation time of the reverse micelle particles in ethane relative to pentane. It should be noted that these data sets were performed on two different fields and different cryogenic probes (750 Mhz with a current-generation probe for the ethane sample and 600 Mhz with a first-generation probe for the pentane sample), though these factors alone cannot account for the improvement seen in the ethane data set.

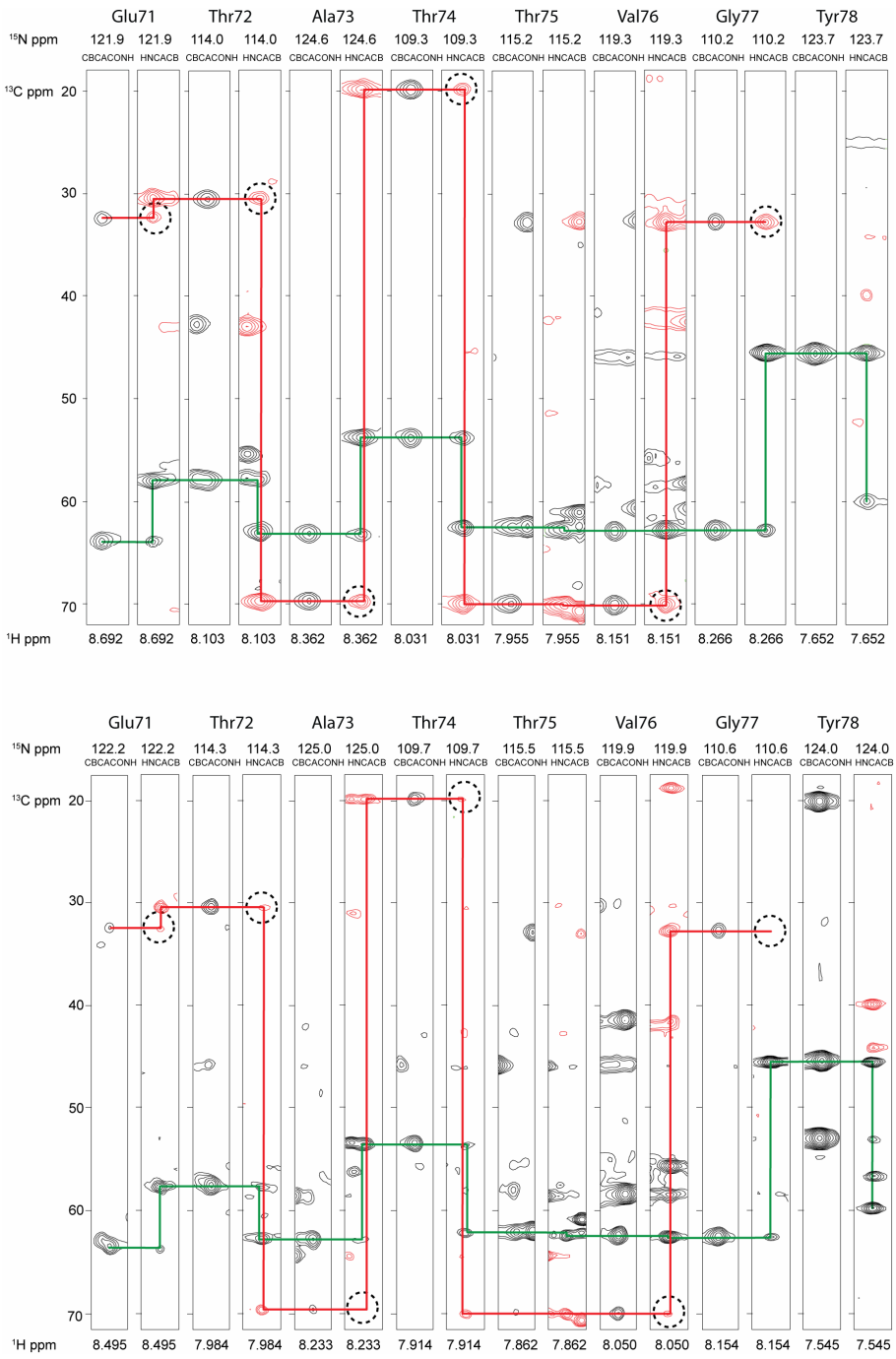

Figure 3.14: Comparison of HNCACB & CBCACONH triple resonance experiments of $^{RM}KcsA_{\Delta C35}$ solubilized in pentane and ethane

Strips are from the KcsA selectivity filter. Green and red lines show C_α and C_β connectivity, respectively.

3.8 Discussion

The most important step for the structural study of by a membrane protein by traditional aqueous methods is the selection of a detergent. The case is no different for studies of membrane proteins in reverse micelles, and the same goes for the study of soluble proteins in reverse micelles. Indeed, the selection of a suitable hybrid surfactant must preserve functional integrity for both soluble and insoluble domains for a membrane protein. It should be emphasized that the steps to select a suitable surfactant is an iterative process and required no prior knowledge of KcsA's structure. Thus the techniques and strategies employed here should be easily applied to the study of other integral membrane proteins.

Where we have been able to prioritize the variables that lead to better NMR performance in reverse micelles in terms of limitation of overall surfactant concentrations over variation of temperature, the most crucial optimization step is the selection of a suitable detergent. This issue of stability and correctly matching a membrane protein to a correct detergent or mixture of detergents is the first step in the structural characterization of a membrane protein. The concept here that lateral forces can have an effect on a membrane protein's structure, stability, and subsequent NMR spectra is not unique. Other studies of membrane proteins have shown that lipid composition and bilayer forces can have an effect on a protein's stability, both for beta barrel (Hong and Tamm, 2003) and alpha helical (Allen et al., 2004a) membrane proteins. And just as there are examples in the literature of helical transmembrane domains 'kinking' due to too thin of a bilayer (Tiburu et al., 2009), there also exists the possibility of a membrane protein having too

much room in a lipid bilayer mimetic (Columbus et al., 2009), resulting in – at least in terms of NMR spectroscopy – residues that enter into intermediate exchange, the most common result of which is broadened spectral linewidths.

It should also be noted here that native-like does not necessarily equate to success in structural characterization. Most membrane proteins are simply not stable. From cysteine substitution studies of the homotrimer diacylglycerol kinase (DAGK), it was found that 1 in 10 mutations in a transmembrane-spanning region improved both catalytic activity and thermodynamic stability (Lau et al., 1999). Beyond just catalytic and denaturation assays, the exploration of these mutants led to the later success of structural studies of DAGK by NMR (Blois and Bowie, 2009; Oxenoid et al., 2004). However, the details of this improved stability are that although a trio of mutations led to a super-stable mutant, s-DAGK, that had a longer lifetime and assisted in the assignment process, this was not without complications. The 100 kDa protein-micelle complex of DAGK necessitates 100% perdeuteration for study by convention solution NMR. This typically requires some sort of exchange protocol for the backbone amides of the protein, particularly for the non-solvent exposed transmembrane domains. Whereas an unfolding-refolding protocol allowed for complete back-exchange of all amides in wt-DAGK, this protocol did not work for about 20 transmembrane residues of s-DAGK due to the high stability of this construct. This example, along with that of the solution studies of KcsA (Chill et al., 2006), emphasize the importance of being able to avoid deuteration as a preparation step, particularly for membrane proteins.

Chapter 4: Backbone Assignments of KcsA in Reverse Micelles

4.1 Introduction

Assignment of backbone and sidechain resonances for a protein encapsulated in a reverse micelle follow the same processes as for an aqueous protein sample. The previous chapter outlined the pathway taken to improve KcsA spectral quality in reverse micelles. The samples used to obtain the bulk of the $^{RM}KcsA_{\Delta C35}$ backbone assignments described here were from the fifth major generation of KcsA reverse micelles. Each iteration typically represents some sort of major improvement over previous versions, and a summary of KcsA reverse micelle efforts are shown in Table 4.1

Briefly, although sample relaxation properties were improved in pentane at 45°C, the relatively short, four to five week lifetime of these samples forced a compromise to

Table 4.1: Major experimental advances in KcsA reverse micelle solubilization

Sample Generation: Major Advancement	Viscosity* (uPa*s)	Notes
1st: First alkane (pentane) solubulization	217.9	Initial efforts. Suffered from low S/N and sample to sample inconsistency
2nd: Pentane consistency	217.9	
3rd: Pentane signal-to-noise improvement	217.9↑↑**	Optimized S/N to get 30' HSQC
4th: Pentane with low detergent (<300 mM total surfactant)	217.9	Optimized detergent levels for balance of S/N and T_2 relaxation
5th: Heated pentane (35° C / 45° C)	201 / 185	Warm pentane at 50 psi showed improved T_2 times
5th: Ethane (with 5% pentane at 4,500 psi)	86.9	Improved T_2 times

*Viscosity values are from the NIST Chemistry Webbook (NIST, 2009). Pentane values are for room temperature and pressure unless otherwise noted. The ethane/pentane mixture is calculated from the molar fractions of the two solvents at 4,500 psi, taking the compressibility of pentane into account. A more detailed study of this is covered in the Materials and Methods chapter of this work.

**The third generation of KcsA samples had higher viscosities than those typical of other samples in the same bulk solvent due to excessive detergent concentrations.

run samples at 35°C, a temperature that showed generally the same longevity as samples run at 25° C, which are stable for up to two months. As mentioned previously, higher temperatures did indeed improve transverse relaxation properties of samples, but to a much lesser extent than they would have in water. Thus the interest in preservation of a good sample trumped a slight improvement in T_2 times. The present use of ethane and its roughly 2.5-fold improvement in sample viscosity over pentane allowed for the use of 25° C as a conservative temperature for running samples, particularly considering the larger amounts of protein required for the high pressure mixing cell, which has a volume of 1.82 mL compared to the 0.650 mL typical of a pentane reverse micelle sample. The sample lifetimes of $^{RM}KcsA_{\Delta C35}$ in ethane have been approximately six weeks before significant degradation is apparent.

The bulk of the experiments used for the backbone assignments of $^{RM}KcsA_{\Delta C35}$ in ethane were run on a current generation Bruker cryoprobe on a 750 Mhz NMR spectrometer. A comparison of backbone assignments for the KcsA selectivity filter collected on a current ethane sample with the experimental setup described herein versus $^{RM}KcsA_{\Delta C35}$ in pentane on a cryoprobe-equipped 600 Mhz NMR spectrometer was shown previously in Figure 3.14. The improvements in performance are most notable when comparing i-1 peaks of C_β resonances in the HNCACB experiments, most of which is due to the improved transverse relaxation properties of KcsA in ethane over pentane. The 750 Mhz field is somewhat penalized by the greater chemical shift anisotropy (CSA) relative to 600 Mhz. This is a problem for large proteins at all large magnetic fields, though the superior resolution offered at such fields is nearly a prerequisite for untangling the cases of spectral crowding and overlap inherent to membrane proteins.

4.2 Addressing issues of membrane proteins

In addition to issues of spectral crowding, some residues of $^{RM}KcsA_{\Delta C35}$ showed instances of multiple conformers. It should be noted that this is an issue not uncommon for membrane proteins, and most of the conformers of KcsA are located where they would be expected: in turns and loops (Figure 4.1). Some instances are more extreme than others. A23, lying at the turn between the N-terminal helix and TM1 has two conformers, while L86, laying at the top of TM2, has up to five conformers, depending on the sample preparation. Some conformers share equal intensity, while most are dominated by a single resonance. As $^{RM}KcsA_{\Delta C35}$ samples age and degrade, the number of residues displaying minor conformers increases. Many of these are of very low signal-to-noise and would otherwise be unnoticeable in a well-behaved NMR. The increasing presence of these minor conformers may give some clue as to how $^{RM}KcsA_{\Delta C35}$ degrades.

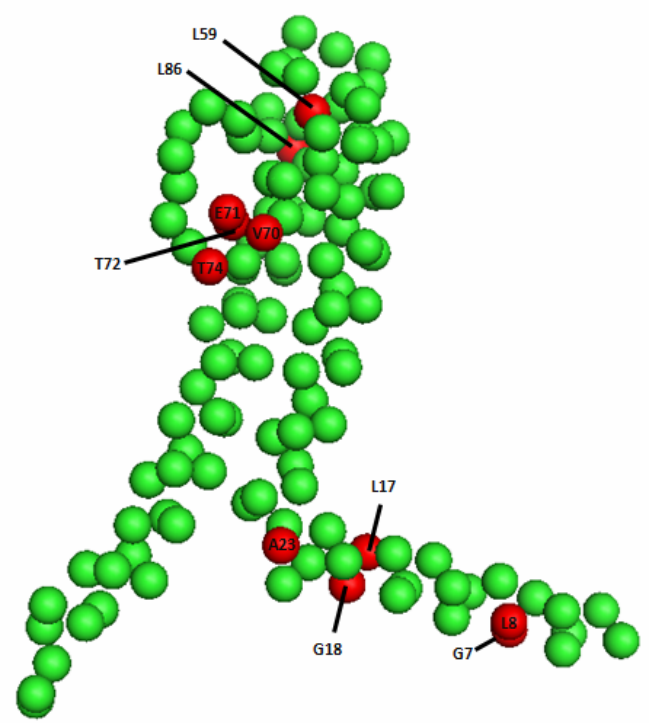

Figure 4.1: $^{RM}KcsA_{\Delta C35}$ multiple conformer residues

A single monomer of KcsA is shown. Residues that had multiple conformers are shown in red, while other residues are green. Illustration based on 1FG6 from Perozo and colleagues (Cortes et al., 2001).

The extra peaks for a given residue represent a unique environment from the dominant peak, or what may naively be termed the native fold. As the sample ages these explorations into local minima become common and more pervasive, spreading from turn and loop residues to transmembrane residues, until entire sections of the protein move into alternative conformations. At this stage evidence of protein aggregation becomes apparent. In aging samples of $^{RM}KcsA_{\Delta C35,}$ the population of amide shifts in an HSQC generally migrate downfield in the nitrogen dimension and upfield in the proton dimension to form a crowded mass of peaks. Spectra from degraded samples are reminiscent of $^{RM}KcsA_{\Delta C35}$ sample preparations that are simply not properly folded to begin with.

With their mixture of transmembrane and soluble domains, membrane proteins have a high degree of overall heterogeneity. In NMR this is oftentimes reflected experimentally by significant overall signal-to-noise differences between regions of the protein. Whereas a typical, well-behaved soluble protein may have a near-horizontal line across a plot of signal-to-noise by residue, this line may be angled downward for a membrane protein. A plot of the signal-to-noise ratios of assigned $^{RM}KcsA_{\Delta C35}$ HSQC and HNCO in ethane ordered from largest to smallest in Figure 4.2 illustrates this point. These differences in signal may be due to faster transverse relaxation times of the generally more rigid transmembrane regions affecting the signal for these residues. This may also be due to residues in transmembrane regions are in unfavorable exchange regimes. The result of both of these instances is broader linewidths and lower overall signal-to-noise. When the above data is organized along KcsA's sequence, the lowest peak signals from both HSQC and HNCO peaks correspond to the transmembrane

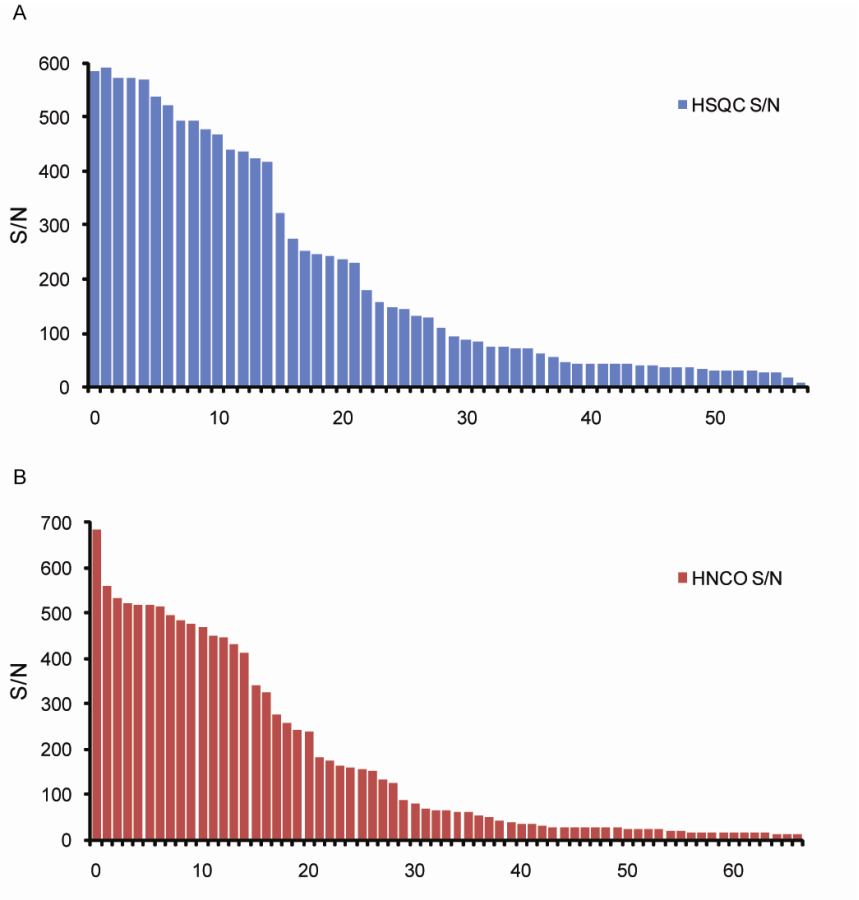

Figure 4.2: Signal-to-noise of assigned $^{RM}KcsA_{\Delta C35}$ HSQC and HNCO peaks

Plot of highest to lowest signal-to-noise ratios for assigned peaks in a 2D HSQC experiment (A) and a 3D HNCO experiment (B) collected on an $^{RM}KcsA_{\Delta C35}$ sample in bulk solvent ethane.

regions of KcsA, accounting for the generally lower success rate in gathering backbone resonance assignments for these peaks (Figure 4.3). The signal-to-noise trends in the chart stand out very strongly, with drop-offs in signal-to-noise coming as residues approach a turn, as in the case of the turn leading from the N-terminal helix to TM1. As the residues move closer into TM1 and in what a traditional micelle or lipid system would be the hydrophobic core of the bilayer – and what we assume to be the case here in reverse micelle KcsA – the signal-to-noise drops considerably. Moving further along

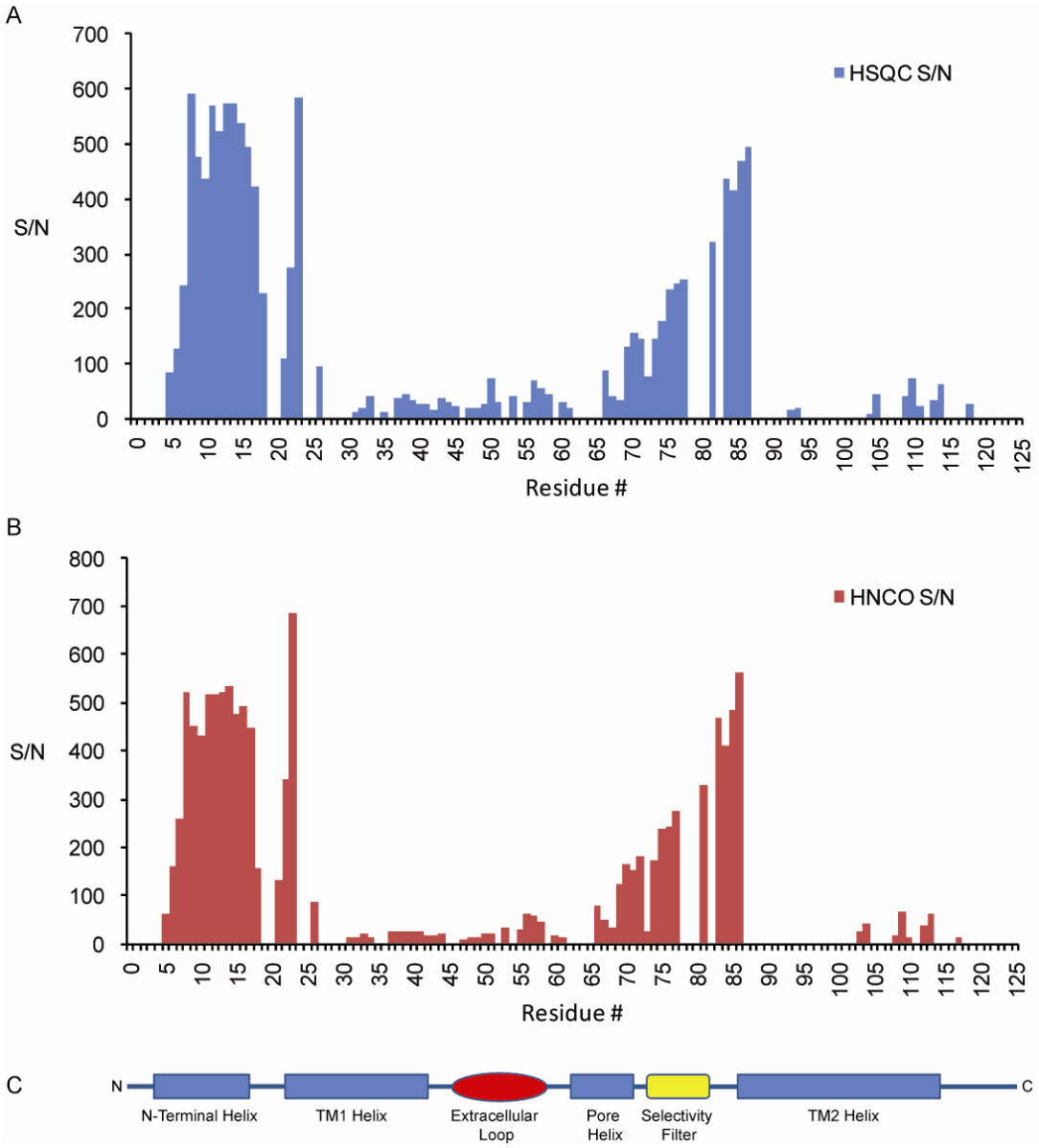

Figure 4.3: Relative signal-to-noise comparisons across the sequence of $^{RM}KcsA_{\Delta C35}$

(A-C) Signal-to-noise ratios of assigned peaks of reverse micelle KcsA in both 2D HSQC (A) and 3D HNCO experiments (B). (C) KcsA's secondary structure as determined by the original crystal structure (1BL8) (Doyle et al., 1998) helices are represented by rectangles, turns by straight lines, major loops by ovals, and the selectivity filter by a curved rectangle. TM1 and TM2 are the two transmembrane helices of the channel.

KcsA's sequence, the resonance signals are much stronger in the extracellular loop and selectivity filter regions compared to peaks from transmembrane domains. The signal-to-noise ratio drops once again in the second transmembrane domain of the channel, TM2, which has been by far the most difficult region of the protein to assign. Although a neutral buffer at pH 7.0 was used in the preparations of $^{RM}KcsA_{\Delta C35}$, the generally poor results for assigning TM2 in KcsA may be due to the inherent flexibility of this section of the protein, which undergoes conformational changes in the mechanism of KcsA gating at low pH values (Baker et al., 2007a; Perozo et al., 1999).

It should be emphasized that the difficulties in the characterization of $^{RM}KcsA_{\Delta C35}$ are potentially faced in the study of any membrane protein. A common culprit and the most likely cause for the low signal-to-noise ratio's in KcsA's transmembrane domains is chemical exchange, specifically intermediate exchange. Chemical exchange is caused by the sampling of two or more conformations of unique electronic environments by a residue or individual atoms within a residue. The timescale of chemical exchange is wide, ranging from nanoseconds to several seconds (Levitt, 2001). The manifestations of chemical exchange on spectral lineshape are dependent on both the rate of exchange, k_{ex}, and the difference in resonance frequency between the two peaks, $\Delta\omega$. For peaks in slow exchange where k_{ex} is much less than $\Delta\omega$, distinct signals are observed. This is observed for the residues of $^{RM}KcsA_{\Delta C35}$ shown previously in Figure 4.1 that have multiple conformers. In general, k_{ex} for slow exchange is on the order of 20 to 0 s^{-1}. For peaks in fast exchange, k_{ex} is much greater than $\Delta\omega$, on the order of 10,000 s^{-1}. A residue in this fast exchange regime averages out to a single resonance.

Cases where $\Delta\omega$ is approximate to k_{ex} are residues in the regime of intermediate. Here peaks fall into a gray area, neither at home as a single peak or as double peaks in data sets, but peaks of very low signal-to-noise, if they are distinguishable from the noise at all. At the nuclear spin level, a well-behaved spin from a single conformation will experience a smooth precession and, subsequently, a smooth decay. If a nuclear spin is exploring different states or conformations, the frequency of the precession changes. This mixture of precession frequencies for the same nuclear spin leads to phase differences and ultimate acceleration of the transverse relaxation, lowering T_2 times.

4.3 $^{RM}KcsA_{\Delta C35}$ backbone assignment strategy

A strategy of through-bond and through-space connectivity experiments was used in a complementary fashion to arrive at a majority of KcsA's backbone assignments. The standard suite of experiments were utilized, including HNCACB (Farrow et al., 1994; Wittekind and Mueller, 1993), CBCACONH (Farrow et al., 1994; Grzesiek and Bax, 1993), HNCA (Grzesiek and Bax, 1992; Kay et al., 1994; Schleucher et al., 1993), HN(CO)CA (Grzesiek and Bax, 1992; Kay et al., 1994), and HNCO (Grzesiek and Bax, 1992; Kay et al., 1994; Schleucher et al., 1993). Although $^{RM}KcsA_{\Delta C35}$ in ethane gave reasonable sensitivity in 3D experiments for most residues, the triple resonance sequential backbone walk was not sufficient for complete backbone assignments. The combination of the high helical content, sequence redundancy, low signal-to-noise for some regions, and the general homogeneity of the transmembrane domains in KcsA all contribute to spectral crowding and overlap of carbon chemical shifts for many residues.

These factors contributed to the difficulty of making sequential connections based on traditional through-bond correlation experiments alone.

To resolve the assignment ambiguities and to ensure fidelity of the backbone assignments, a 3D ^{15}N-NOESY-HSQC (Kay et al., 1992; Palmer et al., 1991; Schleucher et al., 1994; Zhang et al., 1994) was utilized to confirm assignments based on helical amide-amide connectivities of i to i+1 and i to i-1 sequence residues where possible. A 3D HC(CCO)NH-TOCSY (Carlomagno et al., 1996; Clowes et al., 1993; Grzesiek et al., 1993; Logan et al., 1993; Lyons and Montelione, 1993; Montelione et al., 1992) was used in a complementary fashion by matching the resonances of aliphatic protons to that of the NOESY experiment. More commonly known as the main chain directed (MCD)

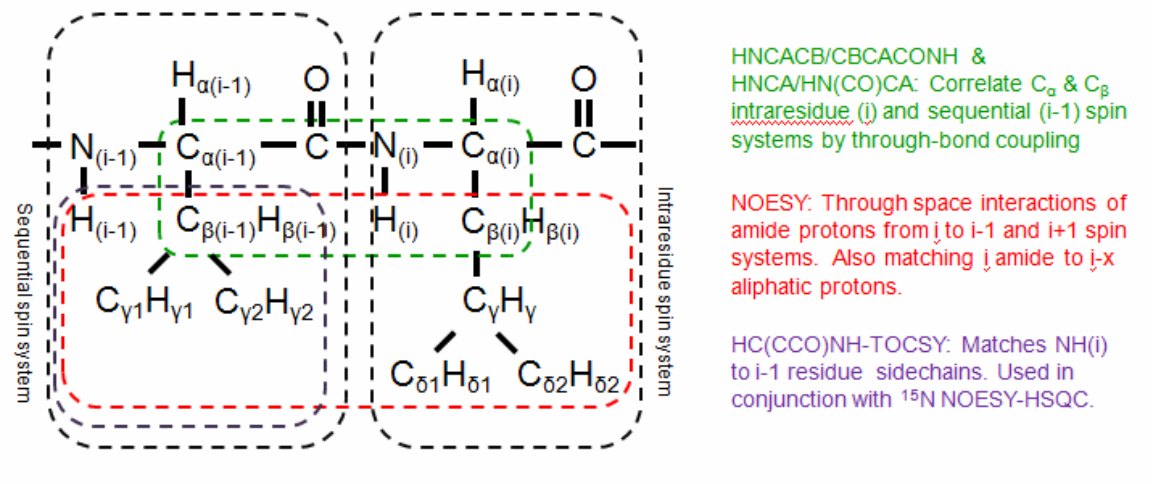

Figure 4.4: Backbone assignment strategy for reverse micelle KcsA

General schematic of the combination of both through-bond 3D backbone experiments and through-space interactions that formed the foundation of the backbone assignments for KcsA. Both NOESY and TOCSY experiments took advantage of the protonation of sidechain residues, which would typically be deuterated in a protein of this size.

assignment strategy, this approach relies upon the recognition of intra-residue H_N-H_α-H_β (NAB) sets (Wand and Nelson, 1991) and was developed prior to the advent of the 3D backbone correlation experiments that are relied upon today. More recently, a similar approach to the MCD strategy was invoked as a complement to contemporary backbone assignment pulse sequence methodologies (Xu et al., 2006). This is essentially the same strategy utilized here. A summary is shown in Figure 4.4.

4.4 $^{RM}KcsA_{\Delta C35}$ backbone assignment results

The backbone assignment efforts on $^{RM}KcsA_{\Delta C35}$ have, as of this writing, yielded ~68% assignment of amide crosspeaks (Table 4.2). The breakdown of KcsA amide assignments are shown in Table 4.3.

A major area of weakness has been the assignments of KcsA's second transmembrane domain. This gap in information is potentially due to intermediate exchange, as discussed earlier. The majority of backbone assignments were completed in ethane, though some of the amide and other backbone atoms accounted for are from KcsA samples made in pentane. As shown by earlier figures of assignments from different regions of the protein (Figures 3.6, 3.7, and 3.8), there is little difference in KcsA ^{15}N, ^{13}CO, $^{13}C_\alpha$, and $^{13}C_\beta$ chemical shifts due to bulk solvent or temperature differences. Continuation of assignment strings using complementary ethane and pentane data sets, as was the case here, are faithful in their i to i-1

Table 4.2: $^{RM}KcsA_{\Delta C35}$ backbone and H_α assignments

Atom(s)	Percent
Amide (HN & N)	68%
CO	64%
Cα	77%
Cβ	68%
Hα	52%
Any Assignment	78%

Table 4.3: $^{RM}KcsA_{\Delta C35}$ amide assignments by domain

Domain	Residues	Percent Complete
N-terminal Helix	A2 to L24	86%
TM1	H25 to L46	86%
Turret Loop	A47 to P63	87%
Pore Helix	R64 to A73	70%
Selectivity Filter	T74 to D80	86%
Filter to TM2 Loop	L81 to L86	100%
TM2	W87 to F125	33%

connectivities. $^{RM}KcsA_{\Delta C35}$ backbone chemical shift assignments are shown in Table 4.4.

The bulk of available reverse micelle KcsA assignments are from ethane samples. As shown previously (Figure 3.14), using ethane as the bulk solvent typically has given better performance for 3D backbone assignment experiments. This was particularly the case for transmembrane residues, which dramatically improved in terms of amide assignments in ethane. Gaps in ethane assignments for which data were available in pentane data sets are typically from turn and loop regions in KcsA. The reasons for this discrepancy may be due to a difference in the amount of spectral overlap for some of these residues, or possibly to dynamic effects from the difference of the rotational correlation time between pentane and ethane. Signal-to-noise may also play a role. While shorter rotational correlation times in ethane lead to longer T_2 values, there is still roughly 20-33% less protein sample in an ethane tube relative to a traditional glass NMR tube. As nearly all of the assignment gaps in ethane that can be filled in with complementary data from pentane are in loop regions that have reasonable T_2 relaxation times regardless of the bulk solvent, the raw signal-to-noise of a given residue in a pentane sample relative to the smaller ethane NMR tube may play a role.

Table 4.4: $^{RM}KcsA_{\Delta C35}$ assignments

Residue	^{1}HN	^{15}N	^{13}CO	$^{13}C\alpha$	$^{13}C\beta$	$^{1}H\alpha$	Source
M1							
A2							
P3							
M4							
L5			181.432	59.347	43.293	4.076	ethane 25°
S6	8.603	111.844	176.108	61.469	62.804	4.03	ethane 25°
G7	8.639	111.576	176.036	47.004		4.148	ethane 25°
L8	8.109	123.967	178.908	58.575	42.263	4.177	ethane 25°
L9	8.47	117.797	178.732	58.549	41.596	4.105	ethane 25°
A10	8.199	119.976	180.437	55.816	18.83	4.041	ethane 25°
R11	8	117.171	179.412	59.451	30.067	4.127	ethane 25°
L12	8.373	119.918	178.719	58.414	42.005	4.174	ethane 25°
V13	8.393	118.1	177.902	67.803	31.559	3.573	ethane 25°
K14	8.064	118.615	179.537	60.558	32.629	3.968	ethane 25°
L15	8.064	118.615	179.227	58.136	42.587	4.253	ethane 25°
L16	8.078	116.438	177.771	57.771	42.756	4.191	ethane 25°
L17	8.429	113.531	178.197	55.354	43.031	4.458	ethane 25°
G18	7.915	106.691	174.776	46.129		4.118	ethane 25°
R19	8.408	120.01	176.435	56.259	30.664		ethane 25°
H20	8.546	119.178	175.160	56.287	30.062		pentane 45°
G21	8.45	109.758	174.275	46.004		4.044	pentane 45°
S22	8.087	114.854	174.547	58.619	64.544	3.995	ethane 25°
A23	8.505	125.572	176.569	53.313	20.265	4.397	ethane 25°
L24	7.636	122.875		56.695	44.319		ethane 25°
H25							
W26			176.964	57.17	30.438		pentane 35°
R27	8.305	120.47	176.425	56.595	30.69		pentane 35°
A28	8.21	124.265	177.023	53.327	20.076		pentane 35°
A29	8.48	122.844	177.911	53.439	19.829		pentane 45°
G30	8.37	108.898	174.536	46.606			pentane 45°
A31	8.574	124.156	179.369	55.903	19.011	4.057	ethane 25°
A32	8.727	118.106	179.198	55.781	18.353	4.051	ethane 25°
T33	7.915	114.51	176.37	68.123		3.853	ethane 25°
V34	8.077	120.039	178.436	67.887	31.540	3.543	ethane 25°
L35	8.307	117.972		58.657	41.501	N/A	ethane 25°
L36	7.984	123.540		58.576			ethane 25°
V37			178.022	67.942	31.515	3.617	ethane 25°
I38	8.397	118.689	178.051	66.467	37.439	3.728	ethane 25°
V39	8.563	119.071	178.488	67.783	31.335	3.656	ethane 25°
L40	8.652	119.355	180.633	58.539	41.977	4.211	ethane 25°
L41	8.883	120.651	179.251	58.529	42.229	4.176	ethane 25°
A42	9.04	121.102	180.211	55.723	18.291	4.193	ethane 25°
G43	9.093	106.191	175.605	47.616		3.851	ethane 25°
S44	8.289	117.117	176.108	63.203		4.234	ethane 25°
Y45	8.234	121.527		61.635	38.824	4.257	ethane 25°
L46	8.324	117.44		54.496			ethane 25°
A47			179.17	54.973	19.28	4.168	ethane 25°
V48	7.714	113.356	177.253	64.508	32.732	4.117	ethane 25°

Table 4.4: $^{RM}KcsA_{\Delta C35}$ assignments (cont.)

Residue	^{1}HN	^{15}N	^{13}CO	$^{13}C\alpha$	$^{13}C\beta$	$^{1}H\alpha$	Source
L49	7.827	118.551	177.6	56.158	42.817	4.252	ethane 25°
A50	7.709	119.401	177.528	53.042	19.974	4.266	ethane 25°
E51	8.017	118.728	176.09	56.857	31.222	4.322	ethane 25°
R52	7.878	125.58		57.805			ethane 25°
G53	8.405	109.153	173.497	45.54		N/A	pentane 35°
A54	8.16	123.735		50.942	19.128		ethane 25°
P55			177.984	64.22	32.356	4.522	ethane 25°
G56	8.612	108.988	174.235	45.783		4.026	ethane 25°
A57	8.081	122.688	177.514	52.886	20.163	4.446	ethane 25°
Q58	8.246	118.105	175.162	55.904	30.204	4.434	ethane 25°
L59	7.837	126.868		56.96	44.02		ethane 25°
I60			175.602	61.891	39.078	4.253	ethane 25°
T61	7.98	113.948	174.124	61.437	70.433	4.284	ethane 25°
Y62	8.276	122.237		56.659			ethane 25°
P63							
R64							
A65							
L66			176.434	56.116	42.531	4.222	ethane 25°
W67	7.858	116.818	174.839	57.144	30.223	N/A	ethane 25°
W68	7.575	124.322	175.773	59.19	30.435	4.807	ethane 25°
S69	8.311	115.096	175.039	58.042	64.809	4.113	ethane 25°
V70	8.584	120.984	176.812	63.88	32.41	4.134	ethane 25°
E71	8.693	121.811	177.578	57.974	30.474	4.343	ethane 25°
T72	8.096	114.039	175.448	63.041	69.725	4.375	ethane 25°
A73	8.357	124.612	178.251	53.766	19.915	4.379	ethane 25°
T74	8.025	109.202	175.025	62.441	69.981	4.42	ethane 25°
T75	7.897	115.124	174.782	62.692	70.111	4.319	ethane 25°
V76	8.152	119.268	176.038	62.726	32.793	4.242	ethane 25°
G77	8.266	110.2	172.97	45.569		4.046 & 3.877	ethane 25°
Y78	7.652	123.693		59.945	39.972		ethane 25°
G79			174.33	45.939			pentane 35°
D80	8.06	119.762	176.481	55.206	42.273		pentane 35°
L81	8.399	120.151	176.337	56.16	42.774	4.303	pentane 35°
Y82	7.992	117.787		56.161	38.779		ethane 25°
P83			176.809	63.659	32.52	4.616	ethane 25°
V84	8.149	117.868	175.513	62.36	32.707	4.255	ethane 25°
T85	7.897	115.124	174.279	61.044	70.699	4.325	ethane 25°
L86	8.445	122.069	175.629	56.161	42.958	4.272	ethane 25°
W87	7.427	121.085		58.643	30.539		ethane 25°
G88			173.46	45.9			pentane 35°
R89	7.871	124.249		57.436	32.2		pentane 35°
L90							
V91							
A92				55.262	18.937	NA	ethane 25°
V93	115.721	7.798	178.116	65.446	32.321	NA	ethane 25°
V94	7.988	119.425		65.157		NA	ethane 25°
V95	8.944	120.328		64.008			ethane 25°
M96							

Table 4.4: $^{RM}KcsA_{\Delta C35}$ assignments (cont.)

Residue	^{1}HN	^{15}N	^{13}CO	$^{13}C\alpha$	$^{13}C\beta$	$^{1}H\alpha$	Source
V97							
A98							
G99							
I100							
T101							
S102							
F103			178.197	62.053		4.008	ethane 25°
G104	8.861	111.751	173.629	46.193		4.103	ethane 25°
L105	7.932	124.045		57.205			ethane 25°
V106							
T107							
A108			177.618	55.693	21.951	NA	ethane 25°
A109	8.384	120.815	176.444	55.721	20.672	NA	ethane 25°
L110	8.532	119.093	176.331	54.888	42.761	NA	ethane 25°
A111	7.689	121.282		52.414	20.721		ethane 25°
T112			174.926	62.038	70.291	4.541	ethane 25°
W113	8.862	123.245	175.015	58.235	30.098	4.552	ethane 25°
F114	7.594	121.178		59.252	41.62		ethane 25°
V115							
G116							
R117			178.01			3.83	ethane 25°
E118	7.976	125.75		58.391	30.68		ethane 25°
Q119							
E120							
R121							
R122							
G123							
H124							
F125							

Also of note is the fact that most of the pentane data was collected at temperatures of 35° or 45° C, whereas the ethane data was collected at 25° C to preserve the lifetime of the sample. While the ethane data sets gave overall better results owing to their improved T_2 relaxation properties, it may be noted that in regions with a propensity for intermediate exchange, higher temperatures may increase the k_{ex} of a given residue or region, pushing the interconversion rate into fast exchange. This may be the case seen for H20 and G21, which were only seen in pentane reverse micelle samples run at 45° C, or G53, which was only seen at 35° C and 45° C samples. All three of these residues are from the ends of

helices; H20 and G21 for the N-terminal helix, and G53 at the top of TM2 and the beginning of the turret loop. Figure 4.5 shows the amide assignments for $^{RM}KcsA_{\Delta C35}$ mapped onto the EPR-determined fold of the channel (PDB: 1FG6) (Cortes et al., 2001), while Figure 4.6 shows an ^{15}N-HSQC labeled with assignments.

Owing to the availability of i-1 resonances from backbone correlation experiments, the percentage of KcsA residues with chemical shift information is 78%. Although the possession of amide resonance assignments contain greater potential for structural information (i.e. from NOESY experiments), the collection of any assignment for a given residue can prove useful for the determination of protein secondary structure. Algorithms such as TALOS (Torsion Angle Likeness Obtained from Shift and Sequence Similarity) can utilize incomplete chemical shift assignments for the calculation of phi and psi angles. This is discussed later in this chapter.

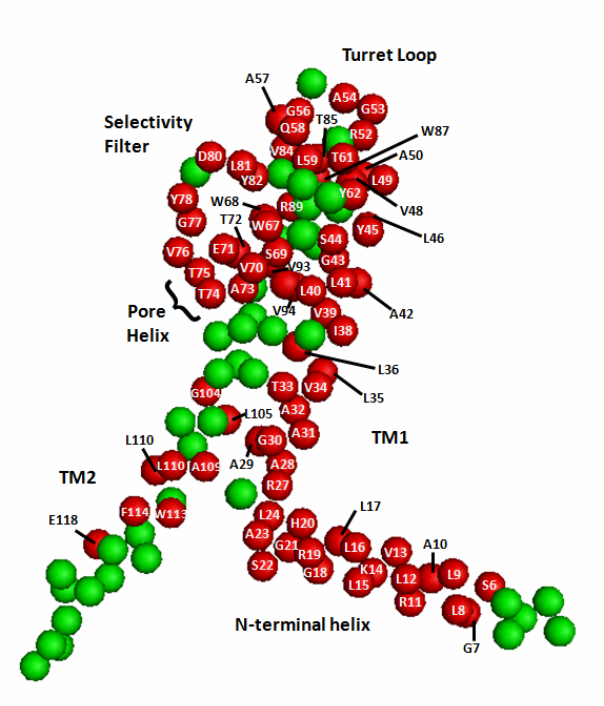

Figure 4.5: Amide assignments of $^{RM}KcsA_{\Delta C35}$

Structure of KcsA monmoner (Cortes et al., 2001). Assigned residues are colored red and labeled. Data is from KcsA samples encapsulated in both bulk solvent pentane and ethane. Note that only residues with amide (^{1}H-^{15}N) assignments are colored red.

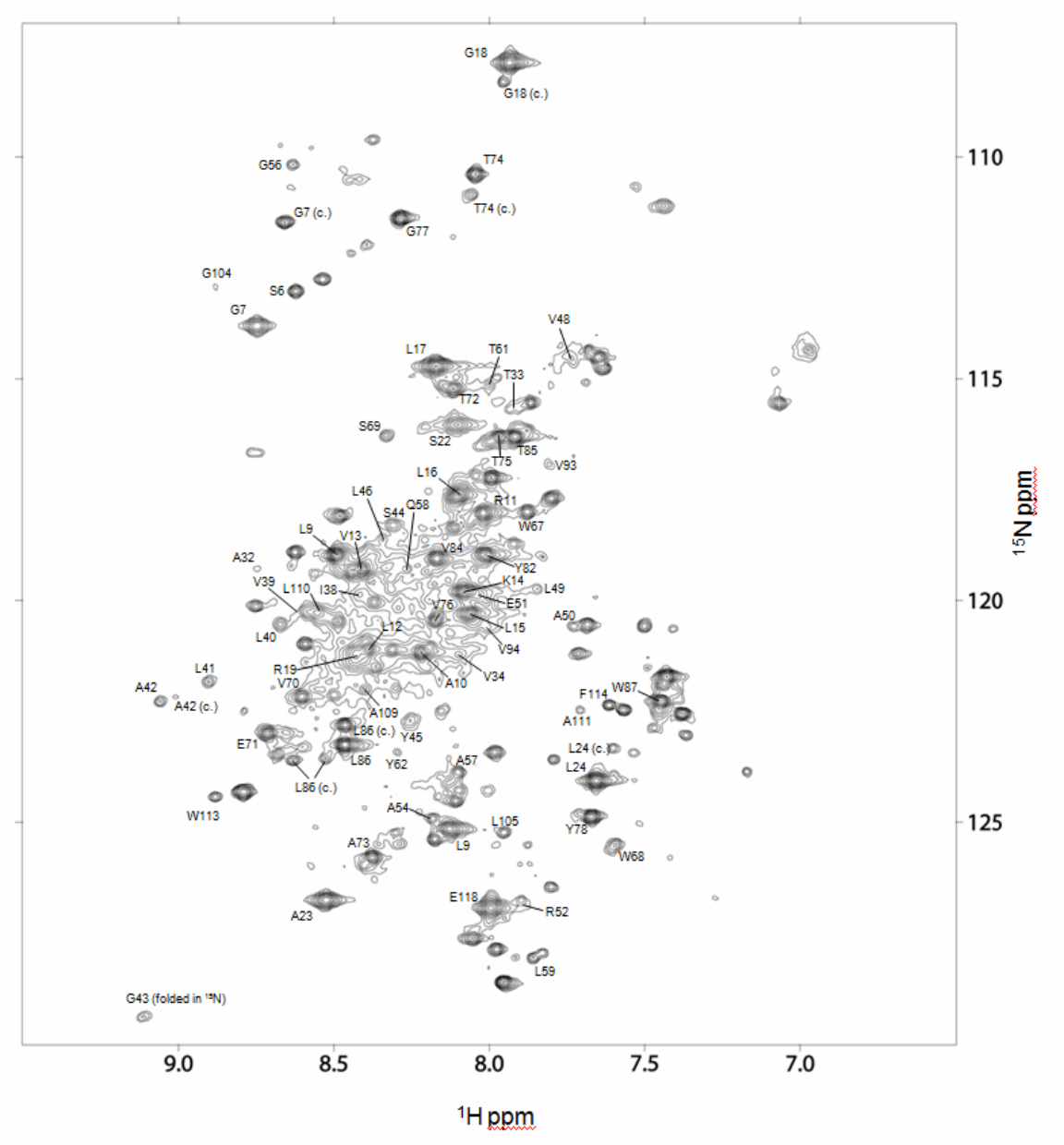

Figure 4.6: ^{15}N HSQC of ^{RM}KcsA$_{\Delta C35}$ in ethane

Amide resonance assignments collected from ^{RM}KcsA$_{\Delta C35}$ samples solubilized in ethane.

4.5 Secondary chemical shift analysis

The chemical shift of an atom in a protein is dependent upon its electronic environment – its type of amino acid, the primary sequence of the surrounding residues, and local structure. The influence of secondary structure on an atom's chemical shift value is properly referred to as its secondary chemical shift. This empirical relationship between protein chemical shifts and protein secondary structure in NMR was first explored by Spera and Bax (Spera and Bax, 1991), who showed the strong correlation that existed between a residue's $^{13}C_{\alpha}$ and $^{13}C_{\beta}$ chemical shift deviations from average values and the distribution of a residue's phi and psi angles on a Ramachandran map from the high resolution crystal structure of that same protein. In short, for residues in regular alpha-helical secondary structure, their $^{13}C_{\alpha}$ shifts will tend to be positive relative to the average shift for that amino acid type, and their $^{13}C_{\beta}$ shifts will tend to be negative. The opposite is true for residues in regular beta-sheet secondary structure. Correlations exist between chemical shift deviations and secondary structure for ^{1}HN, ^{15}N, $^{13}C_{\alpha}$, $^{13}C_{\beta}$, ^{13}CO, and $^{1}H_{\alpha}$ chemical shifts (Zhang et al., 2003). Appendix D of this work contains a list of average $^{13}C_{\alpha}$ and $^{13}C_{\beta}$ chemical shifts for amino acids in random coil, alpha-helical, or beta-sheet secondary structure, and their composite averages.

Secondary $^{13}C_{\alpha}$ and $^{13}C_{\beta}$ chemical shifts for $^{RM}KcsA_{\Delta C35}$ are shown in Figure 4.7. If chemical shifts for both atoms are available, typical utilization of this information involves the subtraction of the $^{13}C_{\beta}$ deviation from the $^{13}C_{\alpha}$ deviation to achieve the graph in 4.6.C, which removes any effects from improper chemical shift referencing. $^{RM}KcsA_{\Delta C35}$ secondary shifts match well with KcsA's overall structure as determined by x-ray crystallography (Doyle et al., 1998; Zhou et al., 2001). The N-terminal helix,

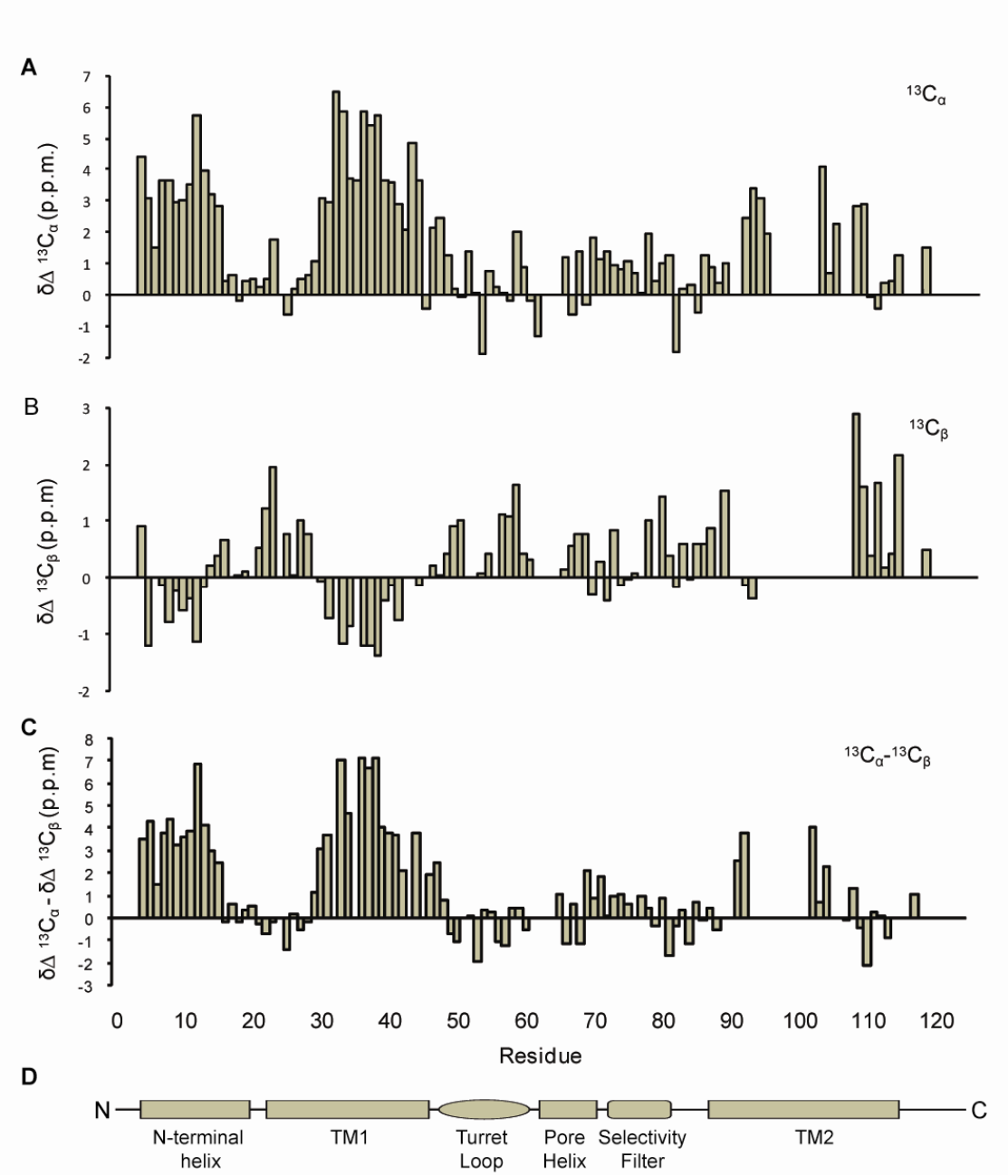

Figure 4.7: $^{RM}KcsA_{\Delta C35}$ $^{13}C_\alpha$ and $^{13}C_\beta$ secondary chemical shifts

(A) Experimental $^{13}C_\alpha$ chemical shift deviations from average random coil values for a given amino acid type. Positive values indicate helical secondary structure. (B) Experimental $^{13}C_\beta$ chemical shift deviations from average random coil values. Positive values indicate beta sheet secondary structure. (C) Difference between $^{13}C_\alpha$ and $^{13}C_\beta$ secondary shift deviations. (D) Secondary structure of $KcsA_{\Delta C35}$.

absent from the crystal structure but determined to be helical from EPR studies on full-length KcsA (Cortes et al., 2001), is helical for KcsA in reverse micelles. The turn leading into TM1, approximately comprising residues 19-25, is represented as a drop towards average random coil values in the data here. This is consistent with secondary chemical shifts for solution NMR studies of full-length KcsA in foscholine micelles (Baker et al., 2007a). Both Chill (Chill et al., 2006) and Baker's KcsA solution NMR efforts possess secondary shifts indicative of a TM1 helix, as do the solid state NMR studies of KcsA-Kv1.3 in liposomes (Schneider et al., 2008). $^{RM}KcsA_{\Delta C35}$ results are consistent with these other findings, as well as the coil and beta-sheet values from the turret loop region of KcsA. $^{RM}KcsA_{\Delta C35}$ results from the pore helix are sparse in terms of assignments. The collected shifts for the pore helix represent the turn leading into the selectivity filter, which is consistent with other NMR results in both solution, solid state, and the crystal structures of KcsA (Doyle et al., 1998).

The differences in $^{13}C_{\alpha}$ secondary shifts of KcsA's selectivity filter between $^{RM}KcsA_{\Delta C35}$ and other efforts are shown in Figure 4.8. $^{RM}KcsA_{\Delta C35}$ appears slightly less helical relative to other structural efforts except for the water soluble KcsA construct (WS KcsA) (Ma et al., 2008). The only residues in which the $^{RM}KcsA_{\Delta C35}$ $^{13}C_{\alpha}$ chemical shift difference is greater than 1.5 ppm in both aqueous SDS micelles and liposomes are V70, T72, V76, and G77. V70 and T72 are both at the end of the pore helix, leading into the selectivity filter, and differences here may be due to how far the pore helix extends into the KcsA vestibule. The shift differences of V76 and G77 occur at the heart of the selectivity filter. Proper coordination of potassium ions has been shown both for aqueous

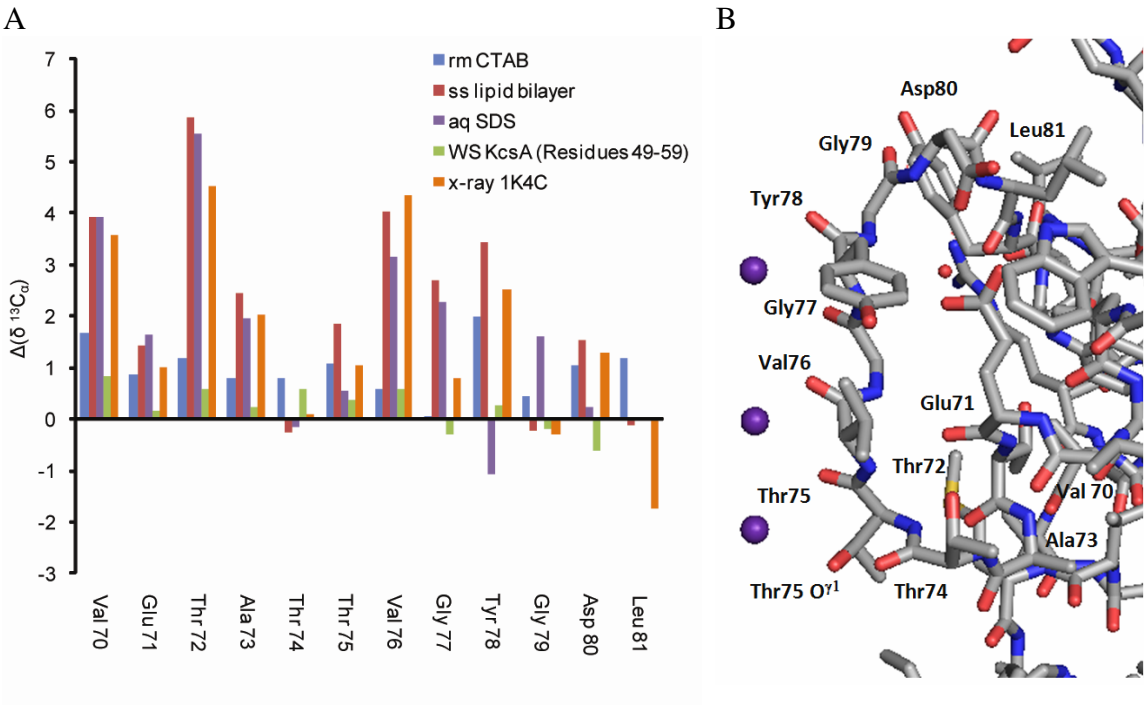

Figure 4.8: KcsA Selectivity filter C_α Secondary Shift comparison

Comparison of KcsA selectivity filter secondary chemical shifts: (A) $^{13}C_\alpha$ chemical shift deviations of the KcsA selectivity filter (T75, V76, G77, and Y78), and surrounding residues for $KcsA_{\Delta C35}$ reverse micelle solution NMR studies in CTAB & DHAB (blue), KcsA-Kv1.3 solid state NMR studies in liposomes (red), $KcsA_{\Delta N15}$ solution NMR studies in SDS micelles (purple), water soluble KcsA solution NMR studies (green), and generated from the high resolution, high potassium concentration crystal structure of KcsA (1K4C) (Zhou et al., 2001) using the program SHIFTX (Neal et al., 2003) (orange). (B) Swiss-PDB-generated structure of the KcsA selectivity filter showing the location of the residues described in A (Geux and Peitsch, 1997).

KcsA in SDS micelles (Chill et al., 2006) and for KcsA encapsulated in reverse micelles (Kielec et al., 2009b) with approximately the same dissociation constants. Thus the apparent minor structural differences between the two efforts do not appear relevant to functional comparisons between the two preparation strategies. Other notable differences

occur at L81, though as with the pore helix, this may be due to differences of the length of the loop leading from the selectivity filter.

The TM2 data are sparsest of all of the $^{RM}KcsA_{\Delta C35}$ domains. The stretch of valines (V93, 94, and 95) all show helical structure comparable to other published NMR results (Baker et al., 2007a; Chill et al., 2006; Schneider et al., 2008). The end of TM2's helical propensity seems to occur around residue 115 in NMR solution studies in both foscholine and SDS micelles (Baker et al., 2007a; Chill et al., 2006). This is consistent the findings for $^{RM}KcsA_{\Delta C35}$ which show evidence of a turn or kink around this same region.

4.6 TALOS analysis

The TALOS program attempts to predict phi and psi backbone torsion angles for a given set of input chemical shifts (Cornilescu et al., 1999). TALOS essentially divides the residues of an input data series into tripeptide sets (i, i-1, and i+1) and compares them to the ten best tripeptides (j, j-1, and j+1) in its database for matches in terms of chemical shift and residue type. The proteins in the TALOS tripeptide chemical shift database are all drawn from those with high resolution crystal structures, which serves as the source of the phi and psi angles for these tripeptides. When psi and psi angles for nine of the ten matched tripeptides fall within the same cluster of a Ramachandran map, TALOS can make an accurate prediction of the torsion angles for a residue from an input data set. The original TALOS program had a 20-protein database, while TALOS+ has a 200 protein database (Shen et al., 2009).

TALOS+ phi and psi angle predictions for $^{RM}KcsA_{\Delta C35}$, based on inputs of ^{1}HN, ^{15}N, $^{13}C_{\alpha}$, $^{13}C_{\beta}$, ^{13}CO, and $^{1}H_{\alpha}$ chemical shifts, are shown in Table 4.5. The phi and psi angle predictions for KcsA in reverse micelles are in line with the known secondary structure elements of the channel, particularly the N-terminal helix and transmembrane helices one and two. For all of these sections of continuous chemical shift assignment information, we are able to see repeating values of phi and psi indicative of right hand alpha helices. Areas where TALOS+ cannot give good predictions tend to be in loop regions or turns, such as H19 and H20 in the N-terminal helix to TM1 turn, or A57 and R52 in the turret loop region. R52 lies at the top of TM1, and gives phi and psi angles more indicative of a beta sheet structure. Its torsion angle is a bad match in TALOS+ and the predicted phi and psi values do not match the original KcsA crystal structure (1BL8) (Doyle et al., 1998), though they do match the torsion angles for the high resolution crystal structure of KcsA (1K4C) (Zhou et al., 2001). TALOS+ allows for a direct comparison of torsion angle predictions to a crystal structure. The results of this are shown in Figure 4.9, where green colored residues indicate good torsion angle matches and red colored residues indicate poor or bad matches. A Warn indication for the TALOS+ prediction

The most notable regions of poor matches are TM2, the pore helix, and selectivity filter residues T75 and Y78. It should be noted from the secondary chemical shift analysis of $^{RM}KcsA_{\Delta C35}$ that both of these residues had $^{13}C_{\alpha}$ chemical shifts that were very close (<0.5 ppm), and the two selectivity filter residues that differed the most from KcsA crystal structure 1K4C were V76 and G77. In terms of thoroughness and accuracy, the TALOS+ analysis, composed torsion angle predictions based on the secondary chemical

Table 4.5: TALOS+ phi and psi predictions for $^{RM}KcsA_{\Delta C35}$

Residue	Torsion angles Phi, φ	Psi, ψ	Std. Dev. φ +/-	ψ +/-	TALOS+ Matches	TALOS+ Prediction
M1						
A2						
P3						
M4						
L5	-61	-42	4	7	10	Good
S6	-64	-42	4	6	10	Good
G7	-67	-39	7	5	10	Good
L8	-65	-43	3	6	10	Good
L9	-63	-42	5	5	10	Good
A10	-63	-40	5	4	10	Good
R11	-65	-44	4	8	10	Good
L12	-64	-45	4	4	10	Good
V13	-64	-42	5	4	10	Good
K14	-59	-41	6	3	10	Good
L15	-64	-44	5	4	10	Good
L16	-72	-38	11	15	10	Good
L17	-85	-26	19	16	8	Good
G18	87	6	11	13	8	Good
R19	-85	111	10	34	5	Warn
H20	-67	146	14	11	6	Warn
G21	85	5	12	17	10	Good
S22	-87	140	14	30	9	Good
A23	-88	-12	21	27	10	Good
L24	-84	123	25	20	10	Good
H25						
W26	-94	-16	19	18	9	Good
R27	-89	-5	27	33	7	Warn
A28	-77	-22	25	29	7	Good
A29	-78	-22	26	27	8	Good
G30	-60	-43	6	5	9	Good
A31	-58	-41	6	10	10	Good
A32	-61	-41	4	7	10	Good
T33	-64	-44	3	5	10	Good
V34	-63	-40	7	11	10	Good
L35	-62	-41	5	6	10	Good
L36	-66	-45	2	6	10	Good
V37	-67	-42	6	8	10	Good
I38	-66	-42	4	6	10	Good
V39	-61	-43	7	4	10	Good
L40	-62	-40	5	4	10	Good
L41	-66	-41	4	6	10	Good
A42	-63	-42	5	5	10	Good
G43	-63	-43	4	5	10	Good
S44	-65	-43	5	9	10	Good
Y45	-63	-39	10	4	10	Good
L46	-85	-20	22	19	10	Good
A47	-64	-34	6	7	10	Good
V48	-73	-33	8	7	10	Good
L49	-73	-30	22	21	9	Good
A50	-94	-11	13	12	10	Good
E51	-94	-6	10	21	8	Good
R52	-80	145	33	13	10	Bad
G53	85	-4	11	13	8	Good
A54	-84	132	21	24	10	Good
P55	-60	144	7	12	8	Good
G56	76	6	21	31	7	Good
A57	-88	117	21	38	6	Warn
Q58	-92	134	24	25	8	Good
L59	-93	132	26	13	10	Good
I60	-99	-25	15	16	9	Good
T61	-126	151	30	13	10	Good
Y62	-81	144	8	19	8	Good
P63						
R64						
A65						
L66	-76	-22	16	18	10	Good
W67	-104	1	7	16	10	Good
W68	-94	147	35	13	9	Good
S69	-99	141	29	28	9	Good
V70	-59	-33	5	9	10	Good
E71	-65	-35	8	16	10	Good
T72	-64	-40	7	13	10	Good
A73	-70	-36	11	12	10	Good
T74	-80	-16	20	19	9	Good
T75	-84	-21	17	22	9	Good
V76	-94	-6	12	19	9	Good
G77	90	3	7	9	7	Good
Y78	-75	124	11	29	10	Good
G79	84	-1	9	14	8	Good
D80	-66	-32	11	14	8	Good
L81	-98	-15	15	21	9	Good
Y82	-112	106	27	38	6	Warn
P83	-67	153	6	10	10	Good
V84	-101	148	32	18	5	Warn
T85	-108	159	23	13	10	Good
L86	-77	-25	19	13	7	Warn
W87	-71	131	15	25	10	Good
G88	-83	144	28	10	4	Bad
R89	-66	-39	4	8	10	Good
L90						
V91						
A92						

Table 4.5: TALOS+ phi and psi predictions for $^{RM}KcsA_{\Delta C35}$ (cont.)

Residue	Torsion angles Phi, φ	Psi, ψ	Std. Dev. φ +/-	ψ +/-	TALOS+ Matches	TALOS+ Prediction
V93	-66	-39	4	8	10	Good
V94	-66	-41	7	12	10	Good
V95	-74	-29	14	16	9	Good
M96						
V97						
A98						
G99						
I100						
T101						
S102						
F103	-63	-39	5	10	10	Good
G104	-67	-43	6	8	10	Good
L105	-74	108	15	27	6	Warn
V106						
T107						
A108	-64	-41	3	8	10	Good
A109	-73	-33	13	11	9	Good

Residue	Torsion angles Phi, φ	Psi, ψ	Std. Dev. φ +/-	ψ +/-	TALOS+ Matches	TALOS+ Prediction
L110	-93	-4	18	17	10	Good
A111	-114	138	38	29	9	Warn
T112	-89	146	25	9	9	Warn
W113	-102	-4	14	23	9	Good
F114	-94	136	28	28	9	Warn
V115						
G116						
R117						
E118						
Q119						
E120						
R121						
R122						
G123						
H124						
F125						

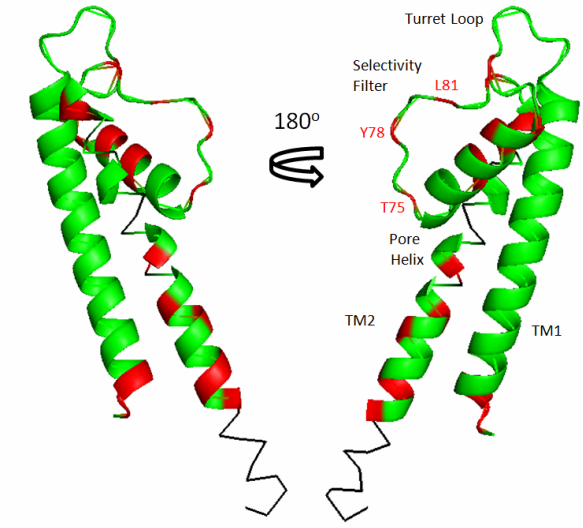

Figure 4.9: Comparison of torsion angles between $^{RM}KcsA_{\Delta C35}$ TALOS+ prediction and high resolution KcsA crystal structure

TALOS+ predicted phi and psi angles are compared to the high resolution, high potassium KcsA crystal structure 1K4C (Zhou et al., 2001). Residues whose average TALOS+ phi/psi angle cluster with the value from 1K4C are green. Residues that do not are red. Residues for which there are no TALOS+ torsion angle predictions are black.

shifts of six residues, is likely closer to a true prediction of structure than $^{13}C_{\alpha}$ secondary shift analysis alone.

4.7 NOESY-HSQC results and analysis

Proteins in molten globule states are capable of exhibiting secondary structure by common spectroscopic techniques such as circular dichroism or NMR. True structure is better determined by collection of restraints from NOE (Nuclear Overhauser Effect) experiments. For helical membrane proteins, the amide i to i-1 and i+1 connectivity of transmembrane helices is a good test of proper structure for these domains. Table 4.6 shows the amide-amide connectivity of $^{RM}KcsA_{\Delta C35}$ in ethane, as well as the amide-sidechain connectivity, for residues that had distinguishable amide crosspeaks from a 3D ^{15}N-NOESY-HSQC experiment. The use of both amide-amide connectivities and amide-sidechain connectivities assisted immensely in the backbone assignment process of $^{RM}KcsA_{\Delta C35}$, particularly in cases of ambiguity arising from chemical shift degeneracy from the backbone correlation experiments. The combination of both through-bond correlation experiments and through-space experiments that allow for collection of NOEs highlights the utility of reverse micelles for structural studies of membrane proteins. The use of sidechain assignments would not have been possible for a deuterated protein.

The two main assigned helices in $^{RM}KcsA_{\Delta C35}$, the N-terminal helix and TM1, both show amide connectivity. Residues in this experiment that don't show this connectivity, or at least reciprocal connectivity are typically located in turns or loops. This is the case for a few residues in the turn leading into the selectivity filter, for example: A73 and T74. Residues G104 and L105 in TM2 represents a case where there

Table 4.6: Amide-amide and amide-sidechain NOEs

Residue	Amide-amide connectivity i-1	Amide-amide connectivity i+1	Amide-sidechain NOEs*	Residue	Amide-amide connectivity i-1	Amide-amide connectivity i+1	Amide-sidechain NOEs
M1				A47			
A2				V48	NA	Yes	Yes
P3				L49	Yes	Yes	Yes
M4				A50	Yes	Yes	Yes
L5				E51	Yes	Yes	Yes
S6	NA	Yes	Yes	R52	Yes	NA	Yes
G7	No	Yes	Yes	G53			
L8	Yes	Yes	Yes	A54	NA	NA	No
L9	Yes	Yes	Yes	P55			
A10	Yes	Yes	Yes	G56	No	No	No
R11	Yes	Yes	Yes	A57	No	No	No
L12	Yes	Overlap	Yes	Q58	No	No	Yes
V13	Overlap	Yes	Yes	L59	No	No	Yes
K14	Yes	Overlap	Yes	I60			
L15	Overlap		Yes	T61	No	No	Yes
L16	Yes	Yes	Yes	Y62	No	No	No
L17	Yes	Yes	Yes	P63			
G18	Yes	Yes	Yes	R64			
R19	No	NA	Yes	A65			
H20				L66			
G21				W67	NA	Yes	Yes
S22	No	No	Yes	W68	No	No	No
A23	No	Yes	Yes	S69	No	No	No
L24	Yes	NA	Yes	V70	No	Yes	Yes
H25				E71	Yes	NA	Yes
W26				T72			
R27	NA	NA	Yes	A73	No	No	Yes
A28				T74	No	No	Yes
A29				T75	No	Yes	Yes
G30				V76	Yes	Yes	Yes
A31				G77	Yes	Yes	Yes
A32	NA	No	Yes	Y78	Yes	NA	Yes
T33	Yes	Yes	Yes	G79			
V34	Yes	No	Yes	D80			
L35	No	No	Yes	L81			
L36	No	No	No	Y82	NA	NA	Yes
V37				P83			
I38	NA	Yes	Yes	V84	NA	Yes	Yes
V39	Yes	Yes	Yes	T85	Yes	Yes	Yes
L40	Yes	Yes	Yes	L86	Yes	Yes	Yes
L41	Yes	Yes	Yes	W87	Yes	NA	Yes
A42	Yes	Yes	Yes	G88			
G43	Yes	Yes	Yes	R89			
S44	Yes	Yes	Yes	L90			
Y45	Yes	Yes	Yes	V91			
L46	Yes	NA	Yes	A92			

Table 4.6: Amide-amide and amide-sidechain NOEs (cont.)

Residue	Amide-amide connectivity i-1	Amide-amide connectivity i+1	Amide-sidechain NOEs*	Residue	Amide-amide connectivity i-1	Amide-amide connectivity i+1	Amide-sidechain NOEs
V93	NA	Yes	No	L110	Yes	Yes	Yes
V94	Yes	NA	No	A111	Yes	NA	No
V95				T112			
M96				W113	NA	No	No
V97				F114	No	NA	No
A98				V115			
G99				G116			
I100				R117			
T101				E118	NA	NA	Yes
S102				Q119			
F103				E120			
G104	NA	No	No	R121			
L105	No	NA	Yes	R122			
V106				G123			
T107				H124			
A108				F125			
A109	NA	Yes	No				

*A positive Amide-sidechain NOE is indicative of at least one NOE to a sidechain proton. A 90 millisecond mixing time was used in this experiment.

is no amide connectivity, despite helical content as determined by secondary chemical shift analysis and predicted alpha-helix phi and psi angles as determined by TALOS. It should be noted that G104 also lacks any amide-sidechain NOEs. Along with the lack of amide-amide connectivity this may indicate that this residue or region may be disordered or in intermediate exchange. Either explanation would contribute to the difficulty in attaining backbone assignments for residues in this domain.

The 3D ^{15}N-NOESY-HSQC experiment also provides information about a protein's interactions with other elements in an experimental system. Figure 4.10 shows NOE connections between $^{RM}KcsA_{\Delta C35}$ amides and water. There are two water signals in reverse micelle KcsA: the main signal at around 4.5 ppm, and a smaller downfield signal

at approximately 4.6 ppm (at 25^{o} C). Most amide peaks in reverse micelle KcsA have NOEs to both signals. Because of this it is unlikely that the extra water signal represents water from empty reverse micelles. The amide-water NOEs that are seen represent what would be expected for KcsA's tertiary structure based on crystallography (Doyle et al., 1998), EPR (Perozo et al., 1998), and other solution NMR studies (Baker et al., 2007a; Chill et al., 2006): TM1 and TM2 are not exposed to water, while most turret and nearly all selectivity filter residues are. All of the N-terminal helix, including the turn leading into TM1, have water NOE contacts, save the cluster of residues K14, L15, L16, L17, and R19. These residues may be buried deeper into the hydrophobic region of the surfactant, reflecting the angle of insertion of the N-terminal helix as predicted by EPR studies (Cortes et al., 2001) V13 is close to this cluster, though it does have an NOE to water, albeit a rather weak one. This may be due to the fact that this residue, or at least its amide, lays closer to water than is depicted by the representation of the N-terminal helix fold from EPR. On the side of the cluster, residues that are close in to the turn such as G18 and S22 also have water contacts, and perhaps this region of the turn is exposed to water; the H25 located in this turn is purported to be involved in pH sensing for KcsA's gating mechanism (Takeuchi et al., 2007), which would explain the water NOEs of its neighboring residues.

A

Residue	Amide-Water Upfield NOE	Amide-Water Downfield NOE
M1		
A2		
P3		
M4		
L5		
S6	Yes	Yes
G7	Yes	Yes
L8	Yes	Yes
L9	Yes	Yes
A10	Yes	Yes
R11	Yes	Yes
L12	Yes	Yes
V13	Yes	Yes
K14	No	No
L15	No	No
L16	No	No
L17	No	No
G18	Yes	Yes
R19	No	No
H20		
G21		
S22	Yes	Yes
A23	Yes	Yes
L24	Yes	Yes
H25		
W26		
R27	Yes	Yes
A28		
A29		
G30		
A31		
A32	Yes	No
T33	No	No
V34	No	No
L35	No	No
L36	No	No
V37		
I38	No	No
V39	No	No
L40	No	No
L41	No	No
A42	No	No
G43	No	No
S44	No	No
Y45	Yes	No
L46	No	No
A47		
V48	No	No
L49	No	No
A50	Yes	Yes
E51	Yes	Yes
R52	No	No
G53		
A54		
P55		
G56	Yes	Yes
A57	No	No
Q58	Yes	Yes
L59	No	No
I60		
T61	Yes	Yes
Y62	Yes	Yes
P63		

Residue	Amide-Water Upfield NOE	Amide-Water Downfield NOE
R64		
A65		
L66		
W67	Yes	Yes
W68	No	No
S69	Yes	Yes
V70	Yes	Yes
E71	Yes	Yes
T72		
A73	Yes	Yes
T74	Yes	Yes
T75	Yes	Yes
V76	Yes	Yes
G77	Yes	Yes
Y78	Yes	Yes
G79		
D80		
L81		
Y82	Yes	Yes
P83		
V84	Yes	Yes
T85	Yes	Yes
L86	Yes	Yes
W87	Yes	Yes
G88		
R89		
L90		
V91		
A92		
V93	No	No
V94	No	No
V95		
M96		
V97		
A98		
G99		
I100		
T101		
S102		
F103		
G104	No	No
L105	Yes	No
V106		
T107		
A108		
A109	No	No
L110	No	No
A111	No	No
T112		
W113	No	No
F114	No	No
V115		
G116		
R117		
E118	Yes	Yes
Q119		
E120		
R121		
R122		
G123		
H124		
F125		

B

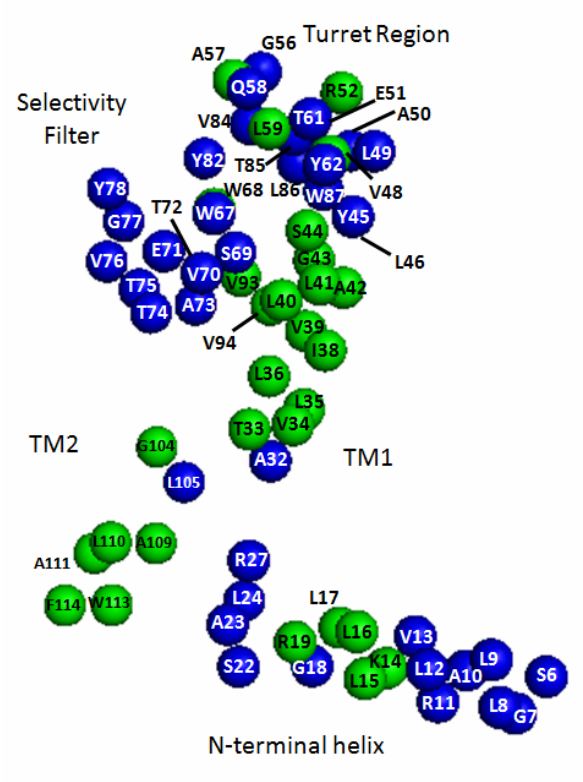

Figure 4.10: Amide-Water NOEs

(A) Chart of amide-water NOE contacts in a KcsA sample dissolved in ethane. There are two water signals in $^{RM}KcsA_{\Delta C35}$ samples: at 25° C the larger, upfield signal is at 4.5 ppm, and the smaller, downfield signal is at 4.7 ppm. Most residues with an amide to water NOE connection will 'see' both of these waters. Structure of KcsA monomer (B) (Cortes et al., 2001): Residues with amide-water NOEs are blue, while ones that do not have NOEs to water are green. Unassigned residues or residues for which data is not available are not shown.

4.8 KcsA N-terminal helix properties in reverse micelles

The strategy outlined above has allowed for near-complete backbone and sidechain assignments of KcsA's N-terminal helix, filling in a region of the protein that was disordered in the crystal structure (Doyle et al., 1998). Strip plots of HNCACB and CBCACONH from KcsA's N-terminal helix are shown in Figure 4.11. As highlighted by the box around their labels, there are two resonances for G7, illustrating an occurance of conformational exchange. One of the resonances for G7 extends from L8, and though it is clearly a gly(i)-serine(i-1), it does not match to the lone serine(i)–leucine(i-1) resonance in KcsA. Instead, a nearby glycine resonance matches cleanly to the resonance

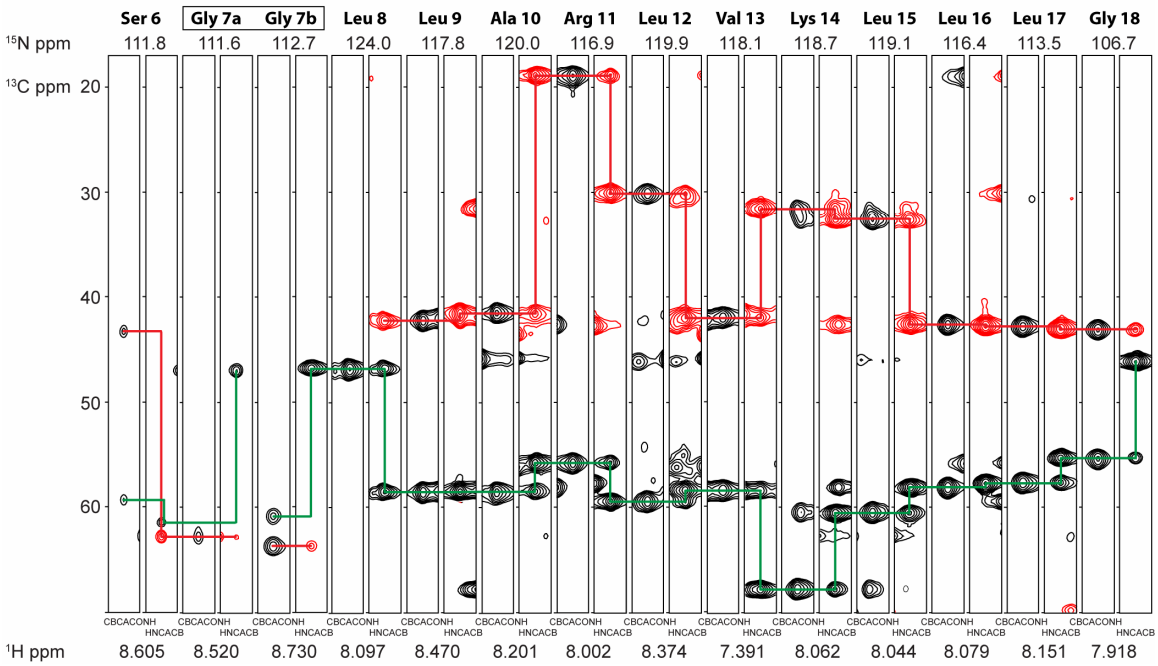

Figure 4.11: N-terminal helix 3D HNCACB & CBCACONH slices

Slices of the HNCACB and CBCACONH spectra of $^{RM}KcsA_{\Delta C35}$ dissolved in ethane showing the connectivities for N-terminal helix from G18 to S6. The opposite sign HNCACB peaks are shown in red. The C_α connectivity is shown by a solid green line and C_β connectivity is shown by a solid red line.

for S6, continuing the string of assignments. Of additional note from the strip plot shown is the increase in helical content from L18 to L17 and L16, reflected in the slight increase and decrease in C_α and C_β chemical shifts, respectively, as the residues get further away from the turn leading into KcsA's first transmembrane helix.

These assignments for the bulk of the N-terminal helix were confirmed by the use of amide-amide connectivities from the ^{15}N-NOESY-HSQC. Figure 4.12 illustrates the use of amide-amide connectivity in a helix. The wave-like pattern of the connectivities between the amide proton chemical shifts is indicative of an amphipathic helix laying along a water-membrane interface. This result is consistent with EPR studies of KcsA in liposomes (Cortes et al., 2001), and the residue by residue pattern of upfield and downfield shifts is identical to earlier solution NMR studies of KcsA in DPC micelles (Baker et al., 2007b).

As discussed earlier, analysis of the N-terminal helix's ^{1}HN, ^{15}N, $^{13}C_\alpha$, $^{13}C_\beta$, ^{13}CO, and $^{1}H_\alpha$ chemical shifts by TALOS indicates phi and psi angles typical of an alpha-helical fold. The importance here is not simply the preservation of helical content in KcsA's secondary structure, but the ability in this system to utilize backbone correlations, amide connectivities, and sidechain resonances to arrive at this data and these assignments from a single NMR sample.

Of equal note is the similar behavior of the N-terminal helix's properties in a reverse micelle compared to both a traditional aqueous NMR sample and a sample reconstituted in liposomes. Per relaxation studies discussed later in this work, the N-terminal helix of $^{RM}KcsA_{\Delta C35}$ shows a high degree of chemical exchange. This mobility of the N-terminal helix also matches EPR studies of KcsA performed in liposomes. The

Figure 4.12: N-terminal helix ^{15}N-NOESY-HSQC

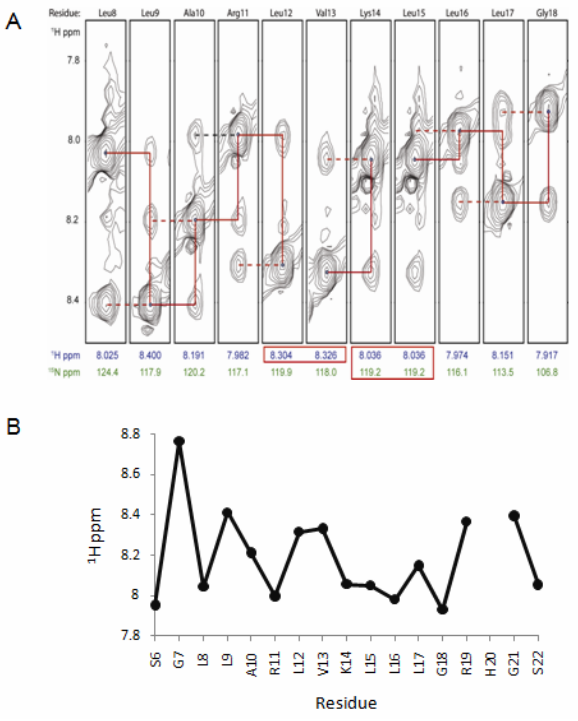

(A) Slices of the ^{15}N NOESY-HSQC spectrum of $KcsA_{\Delta C35}$ in reverse micelles dissolved in pentane showing the connectivities amide HN- amide HN sequential connectivities for N-terminal helix from G18 to. Red boxes indicated spectral overlap in that dimension. A 90 ms mixing time was used. (B) The ^{1}HN shift pattern of the N-terminal helix reveals a wave pattern, indicative of an amphipathic helix. Water exposed amides (S6, L8, R11) generally have upfield shifts, while buried amides (L9, V13, R19) have downfield shifts. As a side note, 'downfield' NMR chemical shifts are greater in value than 'upfield' shifts.

preservation of KcsA's N-terminal helix relative to studies in liposomes is not trivial, and has important implications for the potential to study other membrane proteins in reverse micelles, particularly ones with intra- and/or extracellular domains involved in signaling.

4.9 Discussion

The backbone assignments of $^{RM}KcsA_{\Delta C35}$ are not complete. However, the collection of ~68% of amide assignments and the aggregate total of 78% of residues with at least one chemical shift assignments is an impressive feat for a non-deuterated 54 kDa

membrane protein. From secondary shift and TALOS analysis, it is possible to determine $^{RM}KcsA_{\Delta C35}$'s secondary structure and compare phi and psi angles to the high resolution crystal structure. Secondary structure in helical transmembrane domains is further confirmed by amide-amide connectivities for most of these residues. From ^{15}N-NOESY-HSQC experiments and amide-water NOEs it is possible to determine that the overall tertiary fold of KcsA in the reverse micelle complex is comparable to a membrane protein solubilized in a traditional micelle; intra- and extracellular loops and domains have access to water, while transmembrane residues do not. These findings are reinforced by D_2O-exchange studies discussed in the next section.

The collection of $^{RM}KcsA_{\Delta C35}$ backbone assignments for the selectivity filter also allow for the determination of its fold, which for the most part is comparable to the crystal structure. The extent of collected backbone assignments also allows for the ability to track chemical shift changes in KcsA's selectivity filter as potassium is titrated into reverse micelle samples. The analysis of residue by residue relaxation properties of KcsA in reverse micelles is also possible from the collected backbone assignments. This is discussed in detail later.

Chapter 5: Reverse Micelle KcsA D_2O-Exchanged Sample

5.1 Introduction

The signal-to-noise differences between transmembrane and non-transmembrane domains of $^{RM}KcsA_{\Delta C35}$ leads to the strong possibility that some smaller peaks in the data sets may be lost because of spectral overlap. Given the difficulty of Bax's group (Chill et al., 2006) in back-exchanging deuterium from transmembrane amides in their own studies of KcsA in SDS micelles and their eventual solution of splitting KcsA into two domains for NMR study (D_2O exchangeable versus D_2O non-exchangeable), we adopted this approach for our own purposes. We hypothesized that by exposing KcsA to D_2O-based buffer during its preparation for reverse micelle encapsulation, we could exchange the broad, high signal-to-noise, solvent-exposed loop and N-terminal helix domain amide protons to deuterium, thus silencing their signals, while preserving the non-solvent exposed, lower signal-to-noise transmembrane peaks.

In the solution NMR studies in SDS micelles, the transmembrane regions of KcsA had high protection factors and were essentially non-exchangeable. This is to be expected for the hydrophobic domains of a helical membrane protein, especially given KcsA's overall stability. The typical course of action to exchange deuterium from the amides of a transmembrane region of a deuterated membrane protein is to partake in a regimen of unfolding and refolding in H_2O, a strategy that has proven generally successful for other membrane protein studies by NMR (Oxenoid et al., 2004). This approach is problematic for KcsA, as the channel will only refold in a specific lipid milieu (Valiyaveetil et al., 2002). Given the low, approximately 20% yields of these unfolding and refolding efforts in KcsA, this can make such an approach cost-prohibitive,

even assuming that deuterium to hydrogen exchange of amide protons is successful. Whereas the transmembrane domain amides of KcsA are essentially non-exchangeable, the amides of intra- and extracellular residues had much lower protection factors, and exchanged at rates in the range of 0.001 – 10 sec^{-1} (Chill et al., 2006). For our purposes this would theoretically allow for an exchange of the regions of KcsA that were represented by broad, dominant peaks in the spectra, allowing for an isolation of the weaker peaks of the transmembrane regions of the protein that have been the most difficult to assign.

5.2 Results of D_2O-Exchanged $^{RM}KcsA_{\Delta C35}$

A D_2O-exchanged sample of $^{RM}KcsA_{\Delta C35}$ was prepared using ethane. Many residues did exchange, though somewhat problematic for our purposes, most peaks from KcsA's N-terminal helix did not. A residue by residue summary of reverse micelle KcsA D_2O exchange is shown in Figure 5.1**.** The results here reinforce KcsA's proper tertiary fold in terms of the solubilization of a membrane protein in a traditional detergent micelle. The core residues of TM1 and TM2 have not exchanged, showing that these domains are protected from water and encased in a hydrophobic core – either by the tail regions of surfactants or by alkane solvent. Additionally, these residues have been protected throughout the preparation and encapsulation process of the membrane protein: from buffer exchange to D_2O, to freezing, lyophilization, and final resuspension in a bulk organic solvent. The data here for KcsA's transmembrane domains is consistent with the amide to water NOE presented in Chapter 4 (Figure 4.9).

A

Residue	D_2O Exchange
M1	
A2	
P3	
M4	
L5	
S6	Yes
G7	Yes
L8	No
L9	No
A10	No
R11	No
L12	No
V13	No
K14	No
L15	No
L16	No
L17	No
G18	No
R19	Yes
H20	
G21	
S22	Yes
A23	Yes
L24	No
H25	
W26	
R27	Yes
A28	
A29	
G30	
A31	
A32	No
T33	
V34	No
L35	
L36	
V37	
I38	No
V39	No
L40	No
L41	No
A42	No
G43	No
S44	No
Y45	No
L46	
A47	
V48	No
L49	No
A50	No
E51	
R52	No
G53	
A54	Yes
P55	
G56	Yes
A57	Yes
Q58	Yes
L59	No
I60	
T61	Yes
Y62	Yes
P63	

Residue	D_2O Exchange
R64	
A65	
L66	
W67	No
W68	Yes
S69	Yes
V70	Yes
E71	Yes
T72	Yes
A73	Yes
T74	Yes
T75	Yes
V76	Yes
G77	Yes
Y78	No
G79	
D80	
L81	
Y82	No
P83	
V84	No
T85	No
L86	No
W87	No
G88	
R89	
L90	
V91	
A92	
V93	
V94	
V95	
M96	
V97	
A98	
G99	
I100	
T101	
S102	
F103	
G104	
L105	No
V106	
T107	
A108	
A109	No
L110	
A111	No
T112	
W113	Yes
F114	No
V115	
G116	
R117	
E118	
Q119	
E120	
R121	
R122	
G123	
H124	
F125	

B

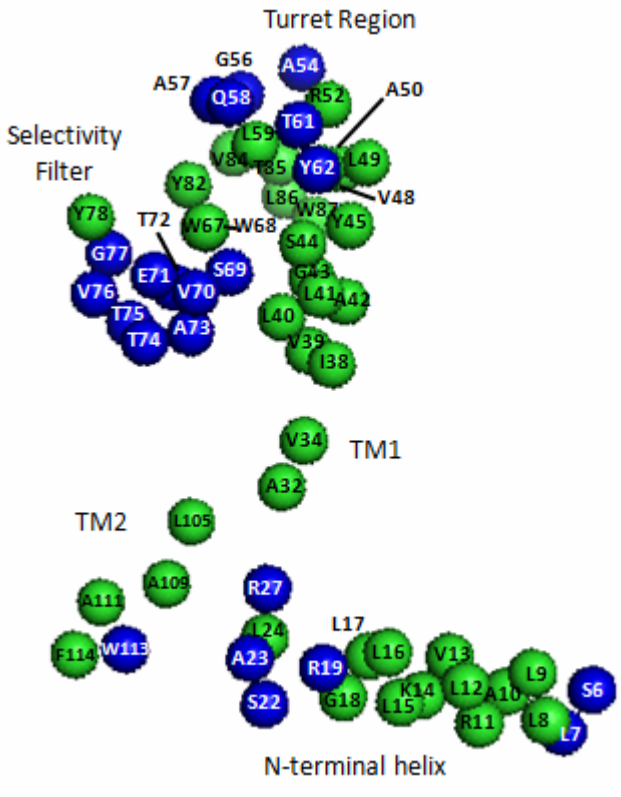

Figure 5.1: D_2O exchange in reverse micelle KcsA

Table (A) of KcsA D_2O-exchange by residue from a sample solubilized in ethane. (B) Structure of KcsA monomer (Cortes et al., 2001) with amide-exchangeable residues colored blue. Non D_2O- exchangeable residues are green.

$^{RM}KcsA_{\Delta C35}$'s N-terminal helix gives conflicting properties. Amide-water NOE data indicates that most of these residues see water, though the amide protons of these residues did not exchange to deuterium despite extensive exposure to D_2O. Thus while KcsA's N-terminal helix is considered mobile – a likelihood given its orientation away from the rest of the protein and the attendant lack of tertiary contacts that come with such isolation - it is nevertheless very well behaved structurally as evidenced by the high signal-to-noise ratios of its peaks both in HSQC and 3D backbone assignment experiments. It is likely that these amide protons are involved in strong hydrogen bonds to backbone carbonyls, resulting in high protection factors for these residues (Cavanaugh et al., 2007). As such, the hydrogen atoms at these amides are unlikely to exchange with the deuterium from free D_2O.

5.3 Discussion

The efforts of this experiment in terms of improving upon the assignment count of $^{RM}KcsA_{\Delta C35}$'s transmembrane regions were not fully realized. This may primarily be due to the lack of exchange of the N-terminal helix residues, which are crowded about the central nitrogen and proton shifts of KcsA's spectra, possibly obscuring other residues of lower signal-to-noise. KcsA's N-terminal helix has been described as mobile, amphipathic helix by EPR studies (Cortes et al., 2001). In terms of the amphipathic, half membrane-embedded character of the N-terminal helix, this has also been shown by solution NMR studies of the channel in foscholine (DPC) micelles (Baker et al., 2007a), and is preserved when KcsA is solubilized in reverse micelles. Additionally, if we define the N-terminal helix as extending from the N-terminus to L24 of the turn leading into

TM1, all but five (K14, L15, L16, L17, R19) of the 18 assigned residues have NOEs to water. Thus, even though this helix is fairly mobile and solvent exposed, the protection factors for G18-L8 are very high. All of these residues have very strong i-1 and i+1 amide-amide NOEs. This strong amide-amide NOE connectivity breaks down at either end of the helix, along with the signal-to-noise in both HSQC and 3D experiments (Figure 4.10 and Figure 4.11). This is where solvent exchange takes place, at R19 and L7 and S6. Additionally there is incidence of multiple conformers for S6 and the residues in the turn leading into TM1: S22, A23, and L24. S22 and A23 both exchange with D_2O.

Solvent exchange also takes place in the turret region of KcsA, at residues A54, G56, A57, and Q58. This exchange extends slightly into the pore helix and residues T61 and Y62. The selectivity filter region of KcsA is also exchangeable with solvent, from S69 in the pore helix to G77 in the filter. These residues may all be exposed to the water molecules escorting potassium into the selectivity filter. Additionally the turn leading into the filter is a generally mobile region, as shown by relaxation studies discussed later and the presence of multiple conformers potentially representative of high- and low-potassium states (Kielec et al., 2009b). All of these residues show amide-water NOEs, as presented in section 4.7 of this work. Y78 also shows an amide-water NOE, though it does not exchange. The amide proton of this residue, along with G79 and the sidechain carboxyl group of D80, are involved in a hydrogen bond network with W67's indole group and the sidechain carboxyl group of E71 from KcsA's pore helix. This hydrogen bond network is hypothesized to be very important for the stability and gating of the selectivity filter (Baker et al., 2007a; Cordero-Morales et al., 2006; Zhou et al., 2001), and in the case here likely prevents exchange of the proton at this residue. This is an

interesting and potentially important result, as it possibly confirms the preservation of this selectivity filter-pore helix hydrogen bond network in reverse micelle KcsA, showing the preservation of this part of the channel in reverse micelles.

Chapter 6: KcsA Reverse Micelle Selectivity Filter Potassium Coordination

6.1 Introduction

The highly conserved potassium channel TVGYG selectivity filter coordinates passage of potassium ions through the channel at near diffusion rates by the backbone carbonyls of ^{75}TVGY and the sidechain hydroxyl of threonine 75 of each of the four KcsA monomers (Zhou et al., 2001) (Figure 6.1). These carbonyls act as surrogates for water in the passage of dehydrated potassium ions as they pass through the filter. This general organization of the potassium channel selectivity mechanism was first envisioned by both Armstrong and Hille (Armstrong, 1975; Hille, 1975), and was later confirmed by the first crystal structure of the KcsA potassium channel (Doyle et al., 1998). The

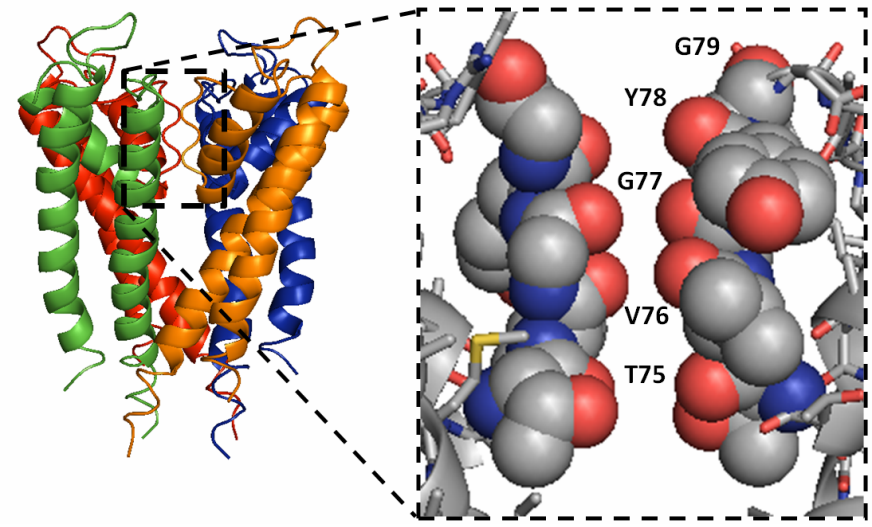

Figure 6.1: KcsA and selectivity filter

The crystal structure of homotetrameric KcsA (Doyle et al., 1998). (Inset) The potassium channel selectivity filter showing the orientation of backbone carbonyls into the filter pore. The furthest and closest monomers have been removed for clarity.

channel architecture was revealed in greater detail by the high resolution structure of KcsA (Zhou et al., 2001), which also showed different conformations of the selectivity filter for structures of low and high concentrations of potassium. In NMR studies such a difference would elicit changing chemical shifts for the residues involved in potassium binding upon the titration of the ion. This was shown by study of KcsA in SDS micelles by Bax's group, and helped confirm not only the channel's functional integrity but the proper quaternary structure, as the selectivity filter is comprised of each of KcsA's four monomers. This approach was utilized here in an attempt to confirm the preservation of both quaternary structure and functionality in reverse micelle KcsA.

6.2 Results of potassium ion titrations in $^{RM}KcsA_{\Delta C35}$

To test for both the proper tetrameric structure of KcsA and its competence in binding potassium in the reverse micelle surfactant system, we titrated potassium ions into a $^{RM}KcsA_{\Delta C35}$ sample prepared without potassium in a background of 50 mM NaCl (Figure 6.2). The increase in potassium concentration was associated with selective chemical shift changes in residues localized to the KcsA selectivity filter, E71, T72, A73, T74, T75, V76, and G77. The chemical shift perturbations show a smooth saturation consistent with specific binding and a corresponding K_D 3.8 +/-1.0 mM for G77 and 2.9 +/-0.5 mM for T72. These calculations assume that all binding sites in the selectivity filter are equal. These results match previous KcsA potassium binding studies by solution NMR in SDS micelles (Chill et al., 2006). Other assigned residues with chemical shift changes upon addition of potassium include L59, a loop region residue which flanks the selectivity filter, and A23, which is in the turn between the N-terminal

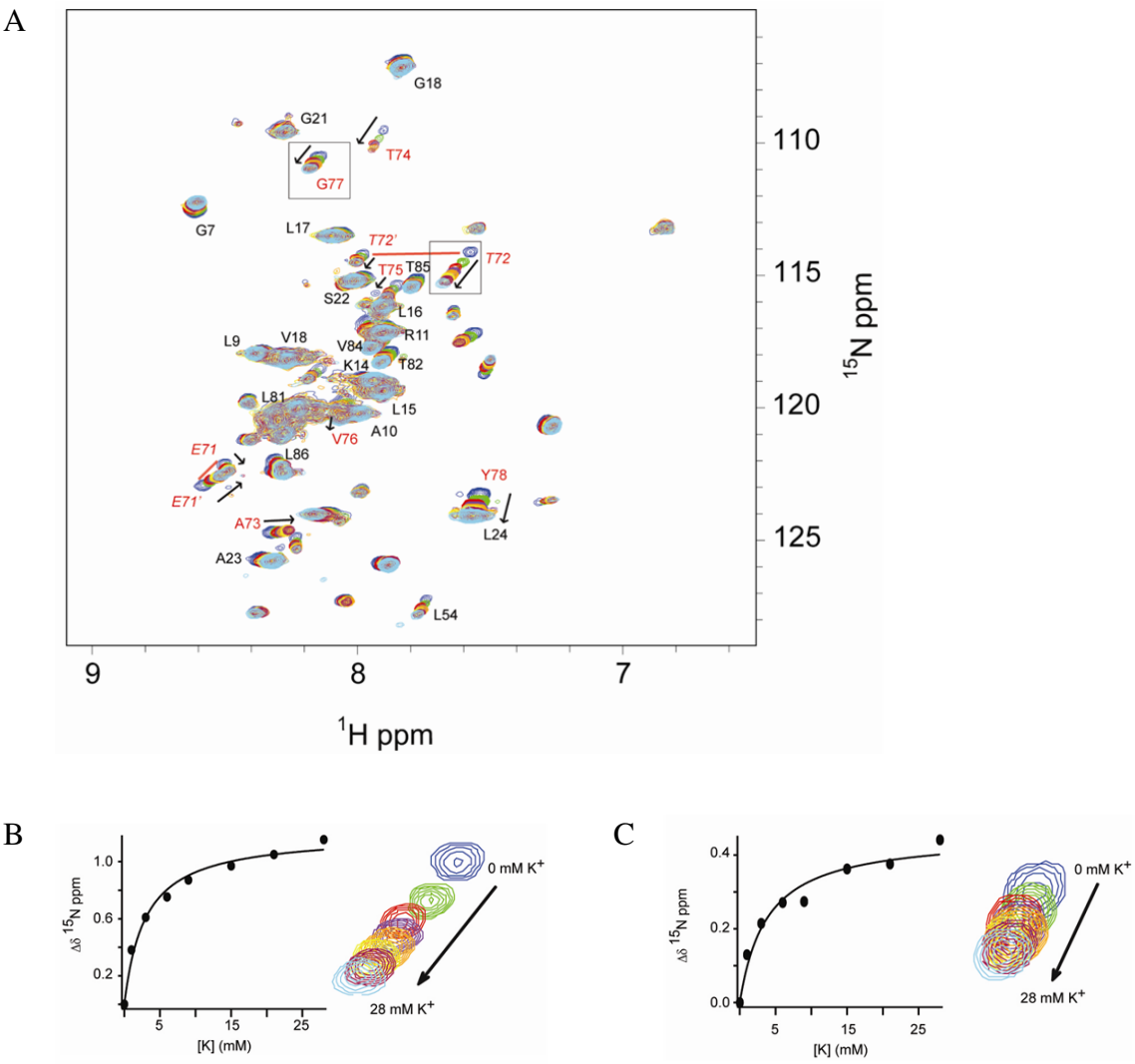

Figure 6.2: KcsA HSQC of Filter K+ titrations

(A) Overlay of eight potassium titration ^{15}N-HSQC spectra, from 0 to 28 mM K^+. Selectivity filter-associated residues are labeled in red, with select other residues assignments labeled black. The presence of multiple conformers in residues T72 and E71 are shown by red lines connecting the two sets of peaks. (B) T72 crosspeak overlays from 0 to 28 mM potassium. The corresponding binding curve was fitted to a simple binding isotherm using the program IGOR Pro 6.0(WaveMetrics, 2007). Similar binding curves are seen for other selectivity filter residues. (C) G77 crosspeak overlays from 0 to 28 mM potassium.

helix and the first transmembrane unit, though these changes are very minor.

6.3 Discussion

The location of chemical shift perturbations are consistent with KcsA's physiological role to conduct potassium and agree with crystallographic studies showing different conformations of the KcsA selectivity filter based on potassium levels (Zhou and MacKinnon, 2004). Thus it appears that the tetrameric structure, essential to the formation of the ion channel, is both preserved and functional in the reverse micelle solubilized protein. Additionally, two residues closely associated with the selectivity filter, E71 and T72, have multiple conformers in slow exchange on the NMR chemical shift timescale. The relative intensity of the conformers does not change as potassium is titrated into the system. It is possible that the distinct conformers of these residues reflects the fluctuation, on a timescale of less than 100 s^{-1}, of the channel as it undergoes the structural transition from low- to high-potassium occupancy states (Zhou et al., 2001). Alternatively, the presence of these conformers may represent a slow exchange between the 1,3 and 2,4 occupancy states of potassium ions in the selectivity filter's four ion-binding sites (Zhou and MacKinnon, 2003), visible here because of the lack of a net flux through the channel in the artificial conditions of presumably identical ionic solutions on both sides of the channel. The existence of such conformers in channel-associated residues is thus expected.

Chapter 7: ^{15}N Relaxation Properties of KcsA in Reverse Micelles

7.1 Introduction

NMR allows for the study of the relaxation properties, or dynamics, of proteins and other macromolecules. The dynamics of a protein in response to ligand binding is becoming an important consideration in the biophysical characterization of macromolecular structures (Wand, 2001). Reverse micelle NMR offers the opportunity to probe both the backbone and sidechain dynamics of protein systems not normally accessible to these suites of experiments due to NMR size restraints. This includes the dynamic characterization of membrane proteins. In the case of potassium channels, a region of great interest is the selectivity filter. As described by Mackinnon and colleagues, potassium is desolvated as it passes from the inner vestibule of the channel, leaving its waters behind while the centrally oriented carbonyl oxygen atoms of the selectivity filter act as surrogates for water (Doyle et al., 1998; Zhou et al., 2001). This confirmed the long-proposed mechanism of ion passage (Armstrong, 1975; Hille, 1975), and reinforced the view that potassium was selected over the similarly charged but 0.38 Angstrom-smaller sodium ion based on the physical dimensions of the channel.

As an alternative to the above hypothesis, Roux has suggested that potassium ion selectivity arises not by the precision of the filter structure matching the size of the ion, but locally from the physical properties of the pore-lining carbonyls that act as surrogate waters (Noskov et al., 2004). Additionally Roux and his colleagues propose that the channel has a high degree of flexibility, (Allen et al., 2004b; Bernache and Roux, 2000; Noskov et al., 2004).

The ultimate answer of whether atoms lining the potassium channel selectivity filter are rigid or dynamic is unlikely to completely resolve the dual hypotheses mentioned, though it may better solidify one of the variables under discussion in the debate. Here we present preliminary data on relaxation properties of KcsA encapsulated in reverse micelles. These results are not conclusive or comprehensive; they describe the relaxation properties of only 23 assigned residues, but establish the ability of the standard relaxation experiments, the T_1, T_2, and the steady state HSQC-NOE, to work for a membrane protein encapsulated in reverse micelles.

7.2 Results

T_2 describes the transverse relaxation – the relaxation of the XY component – of a nuclear spin back to the bulk magnetic field, B_o. This value has been discussed in this work in terms of its importance in NMR data quality: longer T_2 times lead to better transfer efficiency, greater signal-to-noise ratios, and sharper linewidths. Figure 7.1 shows the T_2 times of a pentane $^{RM}KcsA_{\Delta C35}$ sample collected at both 500 and 750 Mhz. The general trend of longer T_2 times at 500 Mhz is due to the effect of chemical shift anisotropy (CSA) at 750 Mhz. This accounts for the shorter T_2 times at 750 Mhz versus 500 Mhz. In terms of running NMR experiments, this faster relaxation is typically overcome at higher fields by the greater signal-to-noise they afford and, particularly for spectrally crowded membrane proteins, their superior resolution. The T_1, measuring longitudinal relaxation – the relaxation of the Z component of a nuclear spin – to B_o, is described as:

$$\frac{1}{T_1} = \left(\frac{\hbar^2 \gamma_I^2 \gamma_S^2}{4 r_{IS}^6} \right) \left[J(\omega_I - \omega_S) + 3J(\omega_S) + 6J(\omega_I + \omega_S) \right] + \frac{\omega_S^2 \Delta\sigma^2}{3} J(\omega_S)$$

(6.1)

The components of this equation are the same ones affecting T_2 relaxation, and are discussed in Chapter 1. T_1 times of $^{RM}KcsA_{\Delta C35}$ are shown in Figure 7.2.

In combination, the evaluation of T_1 and T_2 times – or their inverse values: R_1 and R_2 ($R_1 = 1/T_1$; $R_2 = 1/T_2$) can provide information about the relaxation properties of a spin system. In the analysis here we are specifically interested in chemical exchange, R_{ex}, which describes slower motions on the μs-ms timescale. This is in contrast to analysis of residue order parameters, S^2, which describe motions on the sub-nanosecond timescale. In either case, the bond vector typically observed for backbone relaxation analysis is the amide ^{15}N-^{1}H.

A common approach to study chemical exchange is to look at the R_2/R_1 ratio. However, R_2/R_1 analysis alone can become contaminated by the presence of motional anisotropy – the random tumbling of a protein in solution. As shown by their equations, R_2 transverse relaxation is dominated by the spectral density function J(0), while R_1 longtitudinal relaxation is dominated by the spectral density function $J(\omega)$. The orientation of the aforementioned ^{15}N-^{1}H bond is influenced by the presence of anisotropic motion, meaning that the tumbling motion of the protein can artificially elevate R_2 rates to a greater extent than R_1 rates. As described by Bracken and colleagues (Kneller et al., 2001), the product of R_1 and R_2 can mitigate the influence of anisotropic motion on the interpretation of local chemical exchange.

Figure 7.3 shows the comparison of R_1R_2 versus R_2/R_1 analysis at both 750 Mhz

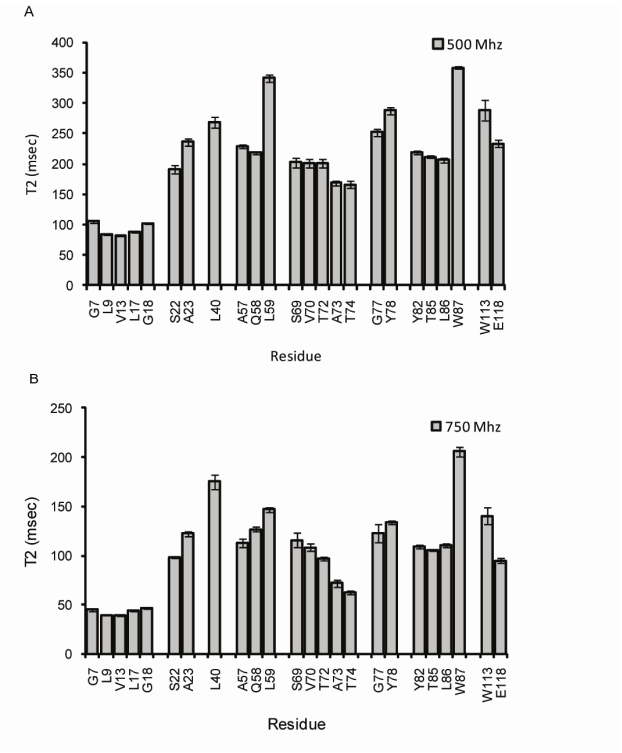

Figure 7.1: $^{RM}KcsA_{\Delta C35}$ T_2 times

T_2 relaxation times by residue at 500 Mhz (A) and 750 Mhz (B) for $^{RM}KcsA_{\Delta C35}$ solubilized in pentane.

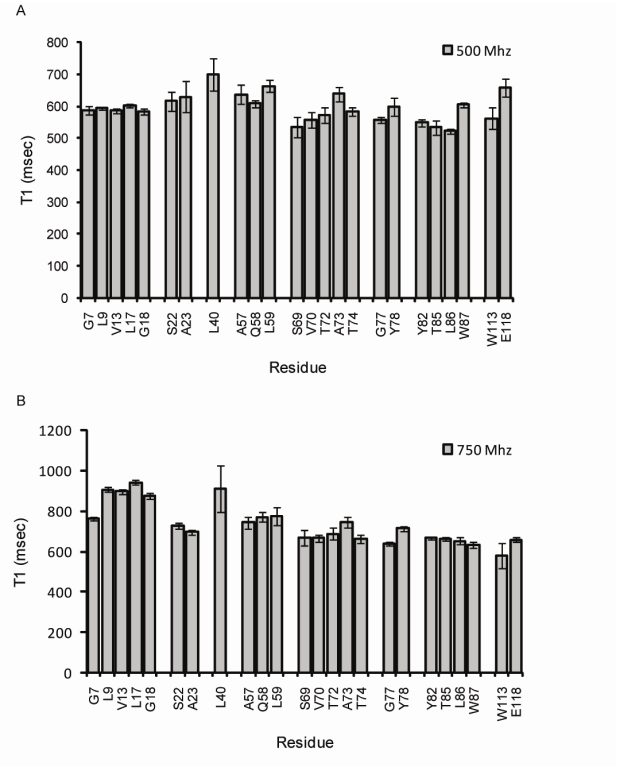

Figure 7.2: $^{RM}KcsA_{\Delta C35}$ T_1 times

T_1 relaxation times by residue at 500 Mhz (A) and 750 Mhz (B) for $^{RM}KcsA_{\Delta C35}$ solubilized in pentane.

(A) and 500 Mhz (B). The values of R_1R_2 and R_2/R_1 for a given residue are not meant to be compared to one another; rather, the comparison is within the same data set. For the most part, the R_1R_2 and R_2/R_1 comparisons are similar across both magnetic fields. A region of discrepancy is the N-terminal helix, where the R_2/R_1 values are much greater relative to the rest of the R_2/R_1 data set at 750 Mhz versus 500 Mhz. This is likely due to the effect of the field-dependent CSA at 750 Mhz on the transverse relaxation (R_2) of these residues.

From analysis of the R_{ex} data presented, the N-terminal helix appears very mobile on this slower μs-ms timescale. This is once again consistent with the EPR investigation of full-length KcsA in liposomes (Cortes et al., 2001). Despite improvements in sample consistency, it was difficult to unambiguously match peaks for transmembrane residues from ^{15}N-KcsA data sets to $^{13}C^{15}N$ samples due to spectral crowding and the close proximity of a many of these peaks. L40, which has a relatively downfield chemical shift in the proton dimension and is thus fairly easy to pick out, can be taken as a representative peak for the middle portion of the TM1 helix. This appears to be a fairly rigid region, albeit one that suffers from poor S/N relative to peaks from other regions.

As we move down KcsA's pore helix (S69, V70, T72, A73) and into the turn at the cusp of the selectivity filter (A73 and T74), there appears to be a slight increase in R_1R_2, culminating in T74 (Figure 7.3.b.). It should be mentioned that this immediate region has multiple conformers as discussed in Chapter 6. This trend of higher R_1R_2 values for this region is stronger at 750 Mhz. The R_1R_2 values drops down from this turn as it goes into the two selectivity filter residues, G77 and Y78. It is possible that the C-terminal end of KcsA's pore helix is fairly mobile, allowing for rapid interconversion

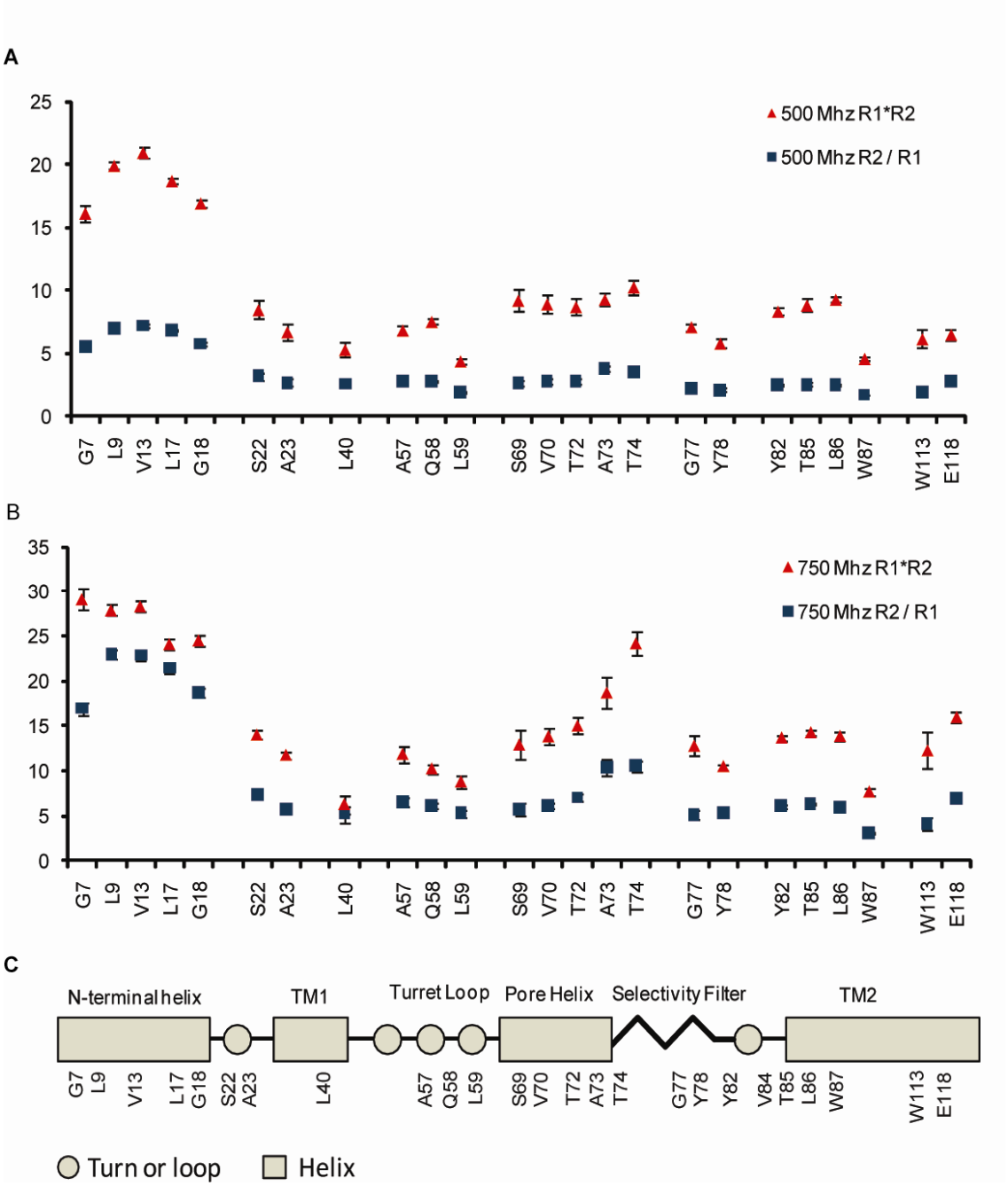

Figure 7.3: $^{RM}KcsA_{\Delta C35}$ R_2/R_1 at 500 and 750 Mhz & R_1R_2 at 500 and 750 Mhz

(A) R_1R_2 and R_2/R_1 at 500 Mhz. (B) R_1R_2 and R_2/R_1 at 750 Mhz. (C) Secondary structure diagram of $KcsA_{\Delta C35}$

between activated and inactivated states of the selectivity filter, while the residues of the filter itself are relatively rigid by comparison.

7.3 Discussion

The amount of data available for ^{15}N relaxation studies of $^{RM}KcsA_{\Delta C35}$ is presently limited in terms of the quantity and distribution of residues. However, the available data validates the use of the relaxation experiments presented here on large membrane proteins in reverse micelles, while at the same time providing a preview of a more exhaustive analysis of $^{RM}KcsA_{\Delta C35}$'s relaxation properties. At issue was the low signal-to-noise ratios of some data sets, as well as the ambiguity for some peaks that prevented a more extensive analysis of residues based on their location in KcsA. This was particularly problematic for residues in TM1. A more complete collection of the residues from this region would have allowed for calculations of τ_m for KcsA in reverse micelles. Future efforts will include the use of a 3D ^{15}N-NOESY-HSQC for the pattern of sidechain protons to match resonances, which will assist greatly increasing the number of resonances that can be matched to their assignments, particularly for peaks from crowded regions of the spectra. The use of experimental sets from no-potassium and high-potassium samples will also be used, to examine whether the relaxation properties of the selectivity filter differ in these two conditions.

In terms of the present data in hand, the N-terminal helix is floppy, comparable to results from EPR studies. The turn leading into the selectivity filter is also flexible, perhaps to facilitate the rapid transition between a potassium occupied to a potassium

unoccupied state. The actual filter itself is more relatively rigid compared to the turn, with R_1R_2 values in line with the rest of the protein save the N-terminal helix.

S^2 order parameters that would describe motions on a subnanosecond timescale are not available for this data set. An aqueous study of ^{15}N KcsA relaxation in SDS micelles by Bax's group using a modified TROSY-HNCO experiment generated S^2 values consist with a relatively rigid selectivity filter, or at least values consistent with the transmembrane residues of the rest of the protein (Chill et al., 2006). This study was hampered by the use of only two timepoints due to the poorer signal-to-noise of the HNCO-based experiment. The rigid results of this work were contradictory to ^{15}N relaxation studies of a water soluble-engineered KcsA construct, WSK3 (Ma et al., 2008), which suggested that the selectivity filter was much more flexible. It should be noted that due to the introduction of the solubilizing mutations in WSK3 and the disruptions to wildtype intersubunit contacts that this introduced caused a high degree of flexibility throughout the protein. Thus, amide relaxation data from WSK3's selectivity filter may be more of a reflection of the surrounding dynamics of the protein than the filter itself.

Chapter 8: Conclusions

In this work we have shown the validation of reverse micelles for the structural investigation of large membrane proteins by solution NMR using the KcsA potassium channel as a model system. At this writing ~68% of 125 backbone amide resonances for the 54 kDa homotetrameric $KcsA_{\Delta C35}$ construct, and nearly 80% of the residues have chemical shift information for at least one atom. Due to the improved transverse relaxation properties of the channel's residues in both pentane and pressurized ethane, none of the samples on which data was collected were deuterated. This removed the necessity of back-exchanging amide protons, and allowed for the collection of 3D backbone correlation, NOESY, and TOCSY experiments on a single type of sample preparation. The bulk of assignments and most of the data discussed in this work are drawn from preparations in pressurized ethane, supplemented with data from pentane for some regions of the protein that are better resolved in that solvent. We have shown that there are no major heavy atom chemical shift differences between pentane and ethane samples of $^{RM}KcsA_{\Delta C35}$.

Based on comparisons to other structural studies (Baker et al., 2007a; Chill et al., 2006; Cortes et al., 2001; Doyle et al., 1998; Schneider et al., 2008; Zhou et al., 2001), we have confirmed the secondary, tertiary, and quaternary structure of $KcsA_{\Delta C35}$ in reverse micelles, as well as the specific coordination of potassium ions by the selectivity filter. Secondary chemical shifts of C_α and C_β atoms suggest helical content that is consistent with the above studies for the N-terminal helix, TM1, and TM2. The utilization of additional chemical shifts from residues and their comparison to a database of existing structures using the program TALOS+ allowed for estimation of phi and psi

backbone torsion angles for $^{RM}KcsA_{\Delta C35}$. The calculated backbone torsion angles are consistent with secondary structure elements for KcsA, and compare favorably to the high resolution crystal structure of KcsA except for a few differences in turn and loop regions.

Through the use of a D_2O-exchanged sample and amide-to-water NOEs from a 3D ^{15}N-NOESY-HSQC experiment, we have been able to show that the solvation characteristics of $^{RM}KcsA_{\Delta C35}$ are analogous to that of a membrane protein solubilized by a traditional aqueous micelle. The intra- and extracelluar residues of $KcsA_{\Delta C35}$ are either exposed to water through NOEs or exchanged with D_2O, while the transmembrane residues are not. The results from the D_2O-exchange experiment also show that KcsA's structure is preserved throughout the reverse micelle preparation and encapsulation process; transmembrane domain residues are either protected from D_2O or are kept well-ordered, preventing their exchange.

Based on ^1HN shift patterns, the N-terminal helix of KcsA has amphipathic character in reverse micelles. This character of laying along the interfacial region of a lipid or detergent is consistent with solution NMR studies of the channel showing the same shift pattern (Baker et al., 2007a), as well as EPR studies of the channel in liposomes (Cortes et al., 2001). The amide-water NOE connectivity of N-terminal helix residues supports this characteristic. However, the core region of this helix does not exchange with D_2O, suggesting that it is well-ordered with high protection factors for these individual amides. Also consistent with EPR studies of KcsA is the apparent mobility of the N-terminal helix, which shows a high degree of chemical exchange on the μs-ms timescale compared to other residues based on R_1R_2 relaxation analysis.

These relaxation studies have revealed domain-specific dynamics for the rest of KcsA, showing apparent rigidity in for both transmembrane regions and, in general, the selectivity filter, while the turn bridging the selectivity filter to the pore helix shows a greater degree of motion. Although a more rigorous experimental data set is required for further analysis, the data in hand validate this approach and lay the foundation for additional relaxation studies on KcsA in reverse micelles.

As a validation for both $^{RM}KcsA_{\Delta C35}$ quaternary structure and functionality, we have shown specific selectivity filter chemical shifts showing saturation in response to titration of potassium ions into the reverse micelle, consistent with results demonstrated by aqueous NMR studies (Chill et al., 2006), and demonstrating structural changes shown by high and low-potassium concentrations from high resolution x-ray crystallography structures of KcsA (Zhou et al., 2001).

The screen utilized for the selection of detergents and optimization of NMR conditions described here did not require any prior knowledge of KcsA's structure, though previous characterizations of the channel in a variety of milieu, including x-ray crystallography (Doyle et al., 1998), aqueous NMR studies in micelles (Baker et al., 2007a; Chill et al., 2006), solid state NMR studies in bicelles (Schneider et al., 2008), and EPR studies in liposomes (Cortes et al., 2001), allowed for the validation of our approach by comparison to these studies.

The efforts here lay the foundation not only for additional structural and dynamic studies of KcsA, but for the encapsulation of other membrane proteins as well. The success of the latter will ultimately define the importance of this technique, since the present adoption of reverse micelle NMR for the investigation of membrane proteins

based on results from KcsA alone is not likely; validation of a single example will not elicit a paradigm shift in the field. The task is simply too risky compared to traditional, established methodologies of for working with membrane proteins in solution NMR, such as deuteratation and other labeling techniques, despite their shortcomings.

However, the roadmap is in place for the exploration of additional membrane protein systems, building upon the foundation of knowledge already in place. Through efforts to encapsulate other proteins, one expects the discovery of additional hybrid surfactants, expanding the current library. It is unlikely that the number of surfactants with dual aqueous-organic properties will rival the assortment of detergents available for aqueous NMR studies, but there is certainly room for expansion. The potential to draw on a larger variety of surfactants will only increase the likelihood for success of encapsulating other integral or peripherally-associated membrane proteins in reverse micelles.

Chapter 9: Materials and Methods

9.1 KcsA growth and purification

Full length $^{13}C^{15}N$-KcsA was grown using a pQE-60 plasmid vector in M15 cells in M9 minimal media. Cell cultures were grown to an OD_{600} of 0.7 at 37 ^{o}C, allowed to cool to room temperature, and induced with IPTG to a final concentration of 1 mM overnight at 27 ^{o}C (Chill et al., 2006). Cells pellets were resuspended in 150 mM KCl, 50 mM Tris, pH 7.5 buffer, sonicated, and then solublized with n-decyl-β-D-maltopyranoside (DM, Anatrace) at a concentration of 40 mM and incubated for 3 hours. Following centrifugation at 35,000 g for 45 min, the supernatant containing the His-tagged full length KcsA was bound to TALON resin (Clontech) and washed first with 500 mM KCl, 50 mM Tris, pH 7.5, 10 mM DM high salt buffer and then with 150 mM KCl, 50 mM Tris, 50 mM imidazole, pH 7.5, 10 mM DM buffer. Transfer from the cell extraction detergent DM to a different detergent was accomplished by exchanging the detergent in place on the TALON resin with the protein still bound. Initial extraction with DM and then exchange to another detergent yielded better overall yields than extracting directly with another detergent. For KcsA, after the aforementioned high salt and low imidazole washes, a solution of 10 mM CTAB, 150 mM KCl, 50 mM Tris, pH 7.5 was run over the column at a volume of 10-fold greater volume than the resin. The resin was then placed with a 10-fold excess of fresh CTAB buffer and allowed to mix overnight on a rotisserie at room temperature. The resin was repacked and washed with an additional 20-fold volume of 10 mM CTAB buffer, then with 30-fold volume of 2.5 mM CTAB buffer. The switch from a higher concentration of CTAB to a lower concentration helps avoid accumulation of excessive amounts of CTAB detergent. In the

case of using a different detergent such as LDAO, it would simply be substituted for CTAB. When evaluating different detergents in the case of screening for optimal conditions, the TALON resin can be split into equal portions after protein loading and high salt and low imidazole wash steps, and rinsed and eluted with different detergent solutions in parallel.

Protein was eluted from the column with a solution of 2 mM CTAB, 150 mM KCl, 50 mM Tris, 500 mM imidazole, pH 7.5. Imidazole was removed by repetitive ultrafiltration or by overnight dialysis. The C-terminal cytoplasmic domain and His-tag were cleaved with α–chymotrypsin and purified by gel exclusion chromatography (Superdex-200) in 3 mM CTAB, 150 mM KCl and 50 mM Tris, pH 7.0, concentrated, and subsequently dialyzed against water containing 5 mM CTAB. Samples were frozen and lyophilized overnight in a small glass tube to reduce the water content to that required for optimal encapsulation. A more detailed overview of this protocol can be found in the Appendix of this work.

9.2 Reverse micelle sample preparation (Pentane)

For $KcsA_{\Delta C35}$, typical optimized reverse micelle conditions utilized a mixture of 1:1 CTAB:DHAB with a total surfactant concentration of 200-250 mM, and a molar ratio of water to surfactant ("water loading" or w_0) of 6 to 8. The aqueous buffer of a typical sample consisted of 50 mM KCl, 50 mM Bis-Tris, pH 7.0, and 50 mM sodium 3-(trimethylsilyl)-1-propanesulfonate (DSS) for chemical shift referencing. The bulk solvent consisted of 94% volume d-Pentane. Hexanol at a volume of 6%, or about a 5:1 molar ratio of hexanol to CTAB surfactant, was added as a co-surfactant. Typically a co-

surfactant such as DHAB is added to the lyophilized protein-hybrid detergent mixture, followed by the bulk solvent (i.e. pentane), hexanol, and finally aqueous buffer. Initial preparations of reverse micelles from lyophilized KcsA-detergent mixtures used the addition of aqueous buffer as the first step, allowing the buffer to 'dissolve' some of the lyophilized mixture. However, the addition of the bulk solvent first proved to provide comparable, if not superior, results to this method. Samples were typically stored and run in screw-cap NMR tubes (Wilmad Labglass)

9.3 High pressure reverse micelle sample preparation

The philosophy behind ethane encapsulation is the same as that of pentane, only a high pressure cell is utilized (Peterson and Wand, 2005). At this writing, the current generation high pressure cell has a volume of 1.82 mL, necessitating the obvious need for more protein per sample than a pentane sample to obtain a suitable signal. Additionally the setup is such that all of the components (lyophilized protein and detergent, additional detergent, hexanol, and pentane (if necessary)), must be added into the cell at the same time. Once the cell is sealed, the bulk solvent is added. Thus it is important to add in these components in a rapid, but safe manner. For high pressure samples, 10% v/v of hexanol as an additional co-surfactant is typically employed. This is more than what may be required for pentane samples but this generally helps with encapsulation of the protein (Ron Peterson, personal communication). Additionally, a volume of pentane in the range of 5-20% v/v may also be employed, as this is believed to assist in sample longevity (Ron Peterson, personal communication). Adding pentane will be deleterious to the overall viscosity of the sample, though the effects are obviously more apparent at higher

percentages of pentane and higher pressures. A graph of this relationship is shown in Figure 9.1. Both the high pressure tube and mixing cell are commercially available (Daedalus Innovations, LLC).

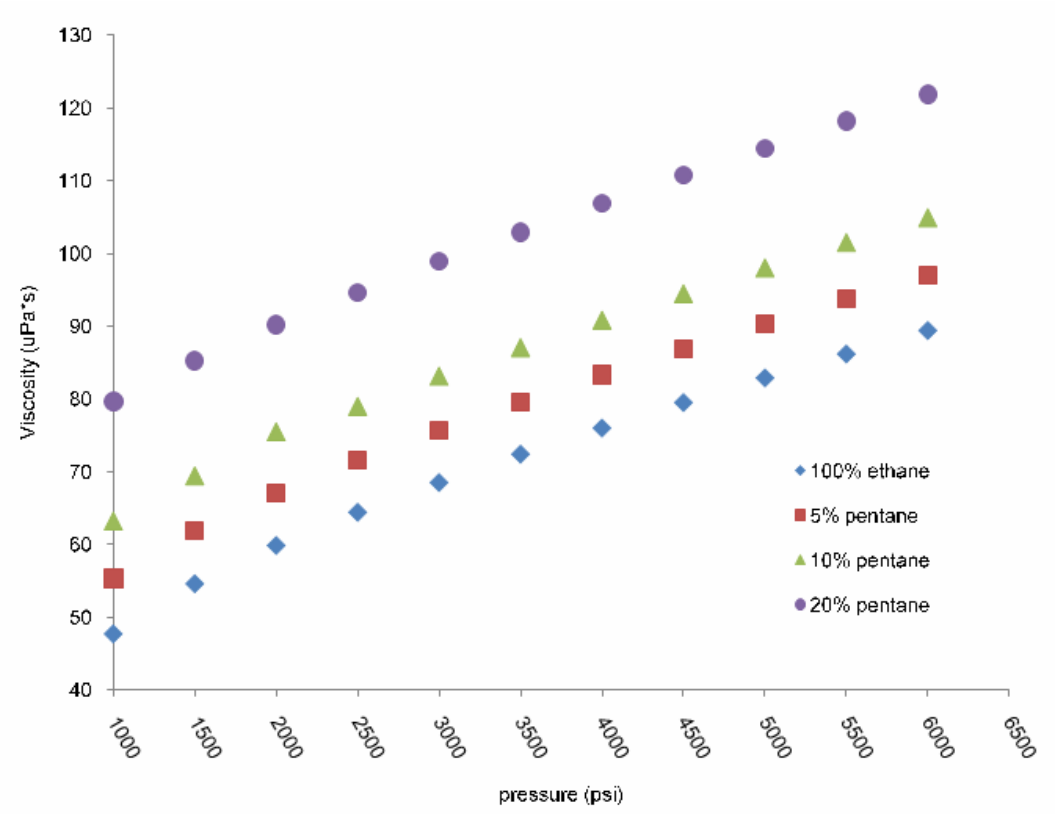

Figure 9.1: Viscosity of ethane and ethane/pentane mixtures by pressure

Values for the ethane/pentane mixtures are calculated from the molar fractions of the two solvents at the given pressure, taking the compressibility of pentane from its initial volume and density at surface pressure (15 psi) into account. Values for all calculations are from the NIST Chemistry WebBook (NIST, 2009).

9.4 Circular dichroism

An Aviv Biomedical, Inc. Circular Dichroism Spectrometer Model 202 was used for all measurements. Typical protein preparations had a concentration of 10-20 uM. All samples were run at 25° C. The pathlength of the cuvette used was 0.1 cm.

Mean residue ellipticity (MRE) was calculated from the equation:

$$\text{M.R.E.}=\theta[\text{deg cm}^2\text{dmol}^{-1}] = \frac{\text{md}}{C \times N \times l \times 10} \tag{8.1}$$

M.R.E. = θ [deg cm^2 $dmol^{-1}$] = md / (C x N x l x 10)

md = machine reading (CD signal)

N = number of amino acids in the protein

C = molar concentration of the protein (M)

l = path length of cuvette in cm

Helical content was calculated by the equation:

$$\%\ \text{helix} = \frac{\frac{\text{md} \times 100}{c \times N \times l}}{39.5 + \frac{2.57 \times H}{N}} \tag{8.2}$$

% helix = ((md x 100) / (c * l * N)) / (39.5 + ((2.57 x H) / N))

md = machine reading (CD signal)

c = protein concentration (μM)

l = path length of cuvette in cm

N = number of amino acids in the protein

H = number of distinct helices in protein

9.5 Preparation of D_2O-exchanged KcsA sample

The preparation of a D_2O-exchanged reverse micelle KcsA sample follows the same principles as the preparation of a traditional reverse micelle same, with the addition of dialysis steps in D_2O and the use of D_2O in the aqueous buffer:

1) Prep KcsA by TALON resin and exchange to CTAB on column.

2) Overnight α-chymotrypsin cleavage, inhibition of protease by PMSF, then use Superdex-200 column to separate cut from uncut KcsA. Concentrate volume down to ~1 mL by using Amicon 50kDa filter spin concentrator.

3) For ethane cell volumes, use two 0.1-0.5 mL dialysis cassettes. Dialyze each cassette overnight in 1 L of H_2O with 5 mM CTAB.

4) Dialyze the two cassettes in 250-300 mL volume of D_2O with 5 mM CTAB (pH checked: 9.3) for 5 hours.

5) Combine samples into a glass vial. Weigh. Freeze on a dry ice bath and place overnight on lyophilizer.

6) Prepare reverse micelle sample normally, save for the buffer. Take 500 uL of traditional KcsA NMR Buffer (50 mM BIS-TRIS, 50 mM KCl, 50 mM DSS, pH 7.0), freeze, and lyophilize. Bring the sample back up in 99.9% D_2O, and pH to 7.4 (the

equivalent pD is ~7.0) using stocks of HCl and KOH (i.e. high concentration) that have been diluted with D_2O.

9.6 KcsA relaxation experiments

All ^{15}N T_1 and T_2 relaxation values reported in this work were measure using the pulse sequence of Farrow et. al. (Farrow et al., 1994). All relaxation experiment data was processed using NMRPipe (Delaglio et al., 1995) and analyzed with Sparky (Goddard and Kneller, 2004).

9.6.1 Effects of Temperature on the NMR relaxation properties of $^{RM}KcsA_{\Delta C35}$

Delay times for 15^o were 7.8, 15.5, 31.0, 46.5, 69.8, and 93.0 milliseconds. Delay times for 25^o were 7.8, 15.5, 38.8, 63, 85.3, and 116.3 milliseconds. Delay times for 35^o were 7.8, 23.2, 31.0, 69.8, 93.0, and 124 milliseconds. In all data sets the 7.8 millisecond delay time was repeated. Spectra were collected at 500 Mhz (^1H) with a Varian Inova NMR spectrometer.

9.6.2 Distribution of T_2 times for ethane and pentane KcsA samples

The pentane sample contained 150 mM total surfactant of a 1:1 molar ratio of CTAB:DHAB and 400 mM hexanol, and had delay times of 7.8, 23.3, 46.7, 70.0, 101, and 140 milliseconds. The 7.8 millisecond delay value was repeated. The ethane sample contained 268 mM total surfactant of a 1:1 molar ratio of CTAB:DHAB and 800 mM hexanol, and had delay times of 17, 34, 68, 102, 136, and 204 milliseconds. The 17 and 134 millisecond values were repeated. Spectra were collected at 600 Mhz (^1H) with a Varian Inova NMR spectrometer.

9.6.3 Effect of surfactant concentration on the NMR relaxation properties of $^{RM}KcsA_{\Delta C35}$

All samples were solubilized in pentane as the bulk solvent and run at 25° C. The High Detergent sample contained 390 mM total surfactant of a 1:1 molar ratio of CTAB:DHAB, and 560 mM hexanol. The Low Detergent sample contained 150 mM total surfactant of a 1:1 molar ratio of CTAB:DHAB and 400 mM hexanol. Delay times for the High Detergent sample were 7.8, 15.6, 23.3, 38.9, 54.5, 77.7, and 93.3 milliseconds. The 7.8 millisecond delay value was repeated. Delay times for the Low Detergent sample were 7.8, 23.3, 46.6, 70.0, 101.0, and 140.0 milliseconds. The 7.8 millisecond delay value was repeated. Spectra were collected at 600 Mhz (^1H) with a Varian Inova NMR spectrometer.

9.6.4 T_1 and T_2 Relaxation Experiment Set

Samples were solubilized in pentane as the bulk solvent and run at 25° C. The sample contained 270 mM total surfactant of a 1:1 molar ration of CTAB:DHAB and 555 mM hexanol. T_1 relaxation delay times at 750 Mhz were 26, 73, 135, 207, 290, 381, 480, 587, and 700 milliseconds. The 73, 207, and 587 millisecond spectra were repeated. T_1 relaxation delay times at 750 Mhz were 10.1, 30.1, 50.1, 90.1, 135.1, 207.1, 380.1, 290.1, and 480.1 milliseconds. The 30.1, 90.1, and 380.1 millisecond spectra were repeated. T_2 relaxation delay times at 750 Mhz were 10, 20, 30, 40, 60, 80, 100, 130, and 160 milliseconds. The 10, 40, and 130 millisecond spectra were repeated. T_2 relaxation delay

times at 500 Mhz were 17, 33, 66, 82, 99, 131, 164, and 197 milliseconds. The 17, 66, and 197 millisecond spectra were repeated.

9.7 KcsA potassium titration experiments

Encapsulated $^{RM}KcsA_{\Delta C35}$ was prepared as described above except using 50 mM NaCl in place of 50 mM KCl for all post-TALON resin buffers, to an initial w_0 of 7.0. ^{15}N-HSQC spectra were collected between sample titrations with 50 mM BIS-TRIS, pH 7.0, with differing amounts of KCl in 0.5 mL volumes that resulted in small 0.2 increases in water loading while raising the K^+ levels in increments of 1 to 7 mM. This ultimately resulted in an overall water loading increase of 2 during a full titration as measured by integration of one dimensional ^1H NMR spectra, which is not enough to appreciably affect the spectra or particle tumbling time.

9.8 NMR data collection

All samples were prepared in liquid D-pentane or D-ethane (Isotec or Cambridge Isotope Laboratories). The majority of data was collected at 600 Mhz (^1H) with a Varian Inova NMR spectrometer equipped with an early-generation triple-resonance cryogenic probe (EB S/N 3600:1) or at 750 Mhz (^1H) with a Bruker Avance III current-generation triple-resonance cryogenic probe (EB S/N 9500:1). Experiments are described in detail in section 4.3. DSS in the aqueous buffer was used as an internal reference (0.0 ppm). Data was processed using both FELIX and NMRPipe. SPARKY was used for data analysis.

Appendix A: Circular Dichroism Survey of Buffer and Detergent Conditions

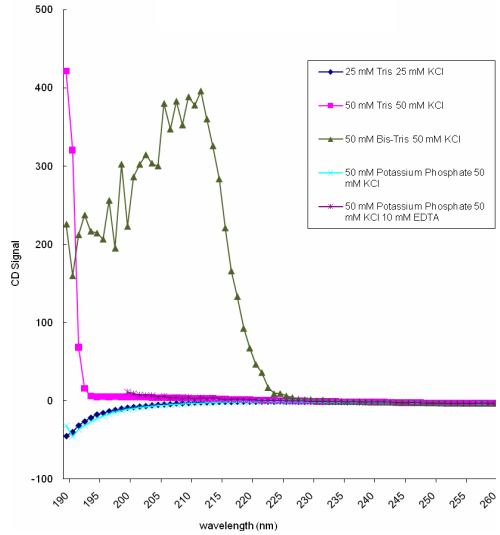

Figure A.1: Circular dichroism buffer evaluations

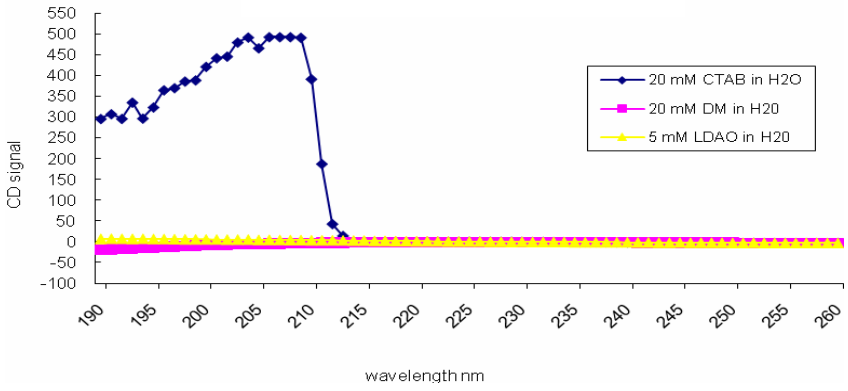

Figure A.2: Circular dichroism of select detergents

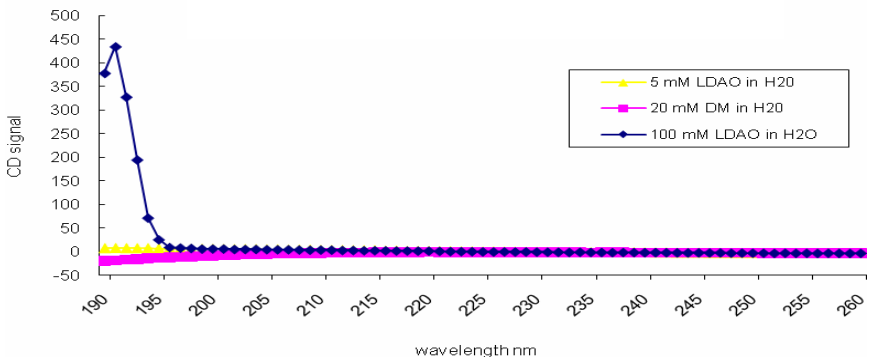

Figure A.3: Circular dichroism of LDAO at different concentrations

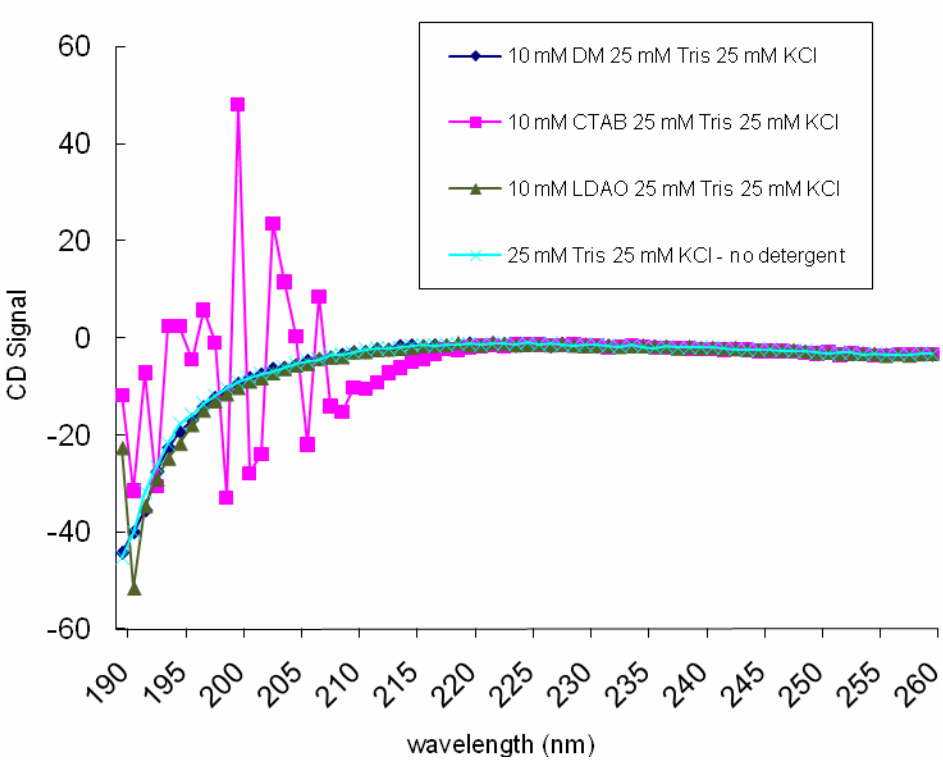

Figure A.4: Circular dichroism of both buffers and detergents

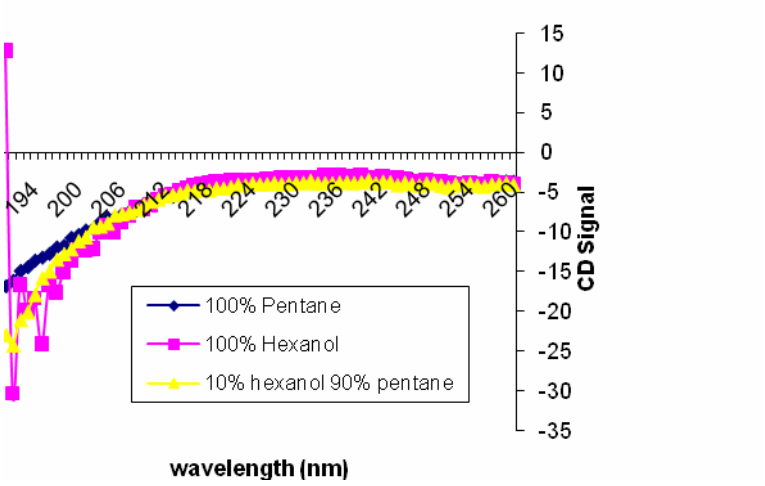

Figure A.5: Circular dichroism of reverse micelle components

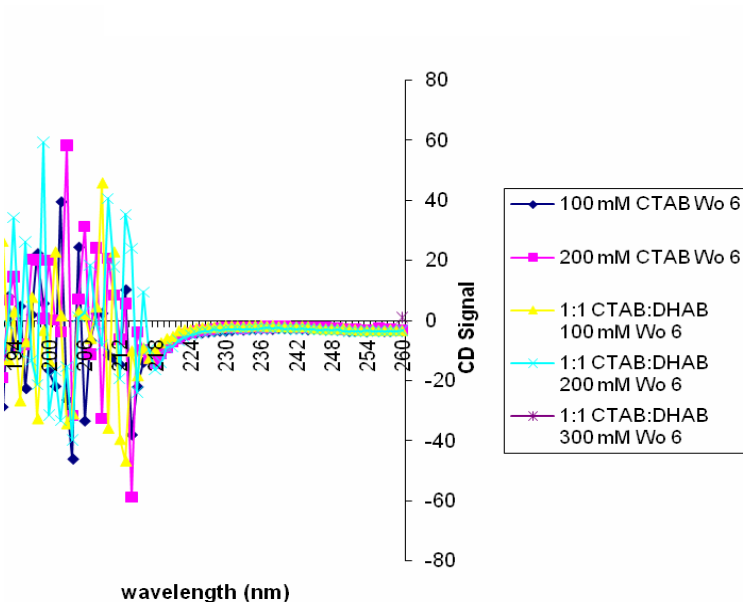

Figure A.6: Circular dichroism of CTAB and CTAB/DHAB reverse micelles

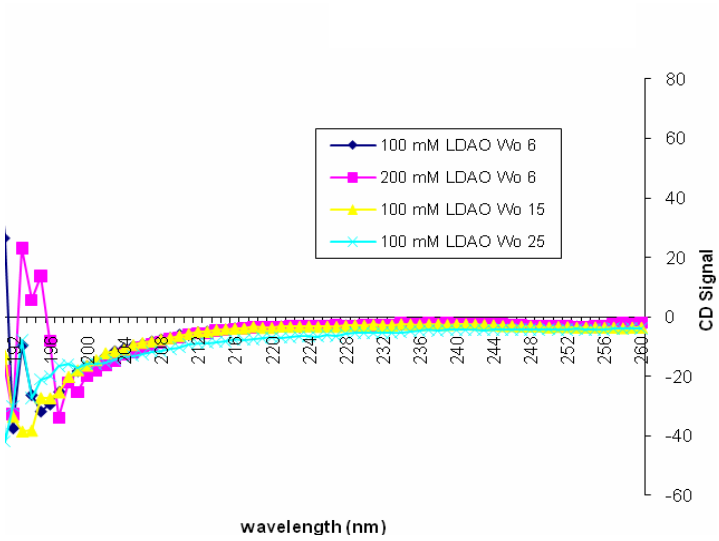

Figure A.7: Circular Dichroism of LDAO reverse micelles

Appendix B: Step-by-Step Growth and Preparation of KcsA for NMR

Version 3.0 Updated 1/8/09

The core of this prep is based upon the prep used by the MacKinnon group's original crystal structure of KcsA(Doyle et al., 1998). All stages should be completed as quickly as possible to prevent proteolysis of the protein or its inclusion into bacertial protein aggregates (i.e. do NOT leave unlysed OR lysed cells out all day at RT. Also, elute protein off the column the SAME day it is loaded on the column, if possible). Additionally, yields have been best if the protein prep is begun the same day that cells are harvested (i.e. do not freeze the pelleted cells to do the prep at a later date). If you are unsure about a step or procedure, feel free to ask for help.

A note about the construct: Full-length KcsA (160 a.a. from *Streptomyces lividans*) is in a pQE-60 vector. The chymotrypsin cleavage site cuts off the his-tag as well as the 35 C-terminal residues (the entire cytoplasmic domain of the protein).

For best yields, cells are grown to an optical density (OD) of 0.7 at 37^{o}C. Protein expression should then be induced overnight at 27^{o}C with a final concentration of 1 mM IPTG.

Part I: Preparation of N15-Labeled 1.5x M9 Media (Use ^{13}C Glucose for double-labeled protein)

Based on the Wand Lab M9 Salts/Minimal Media recipe (http://192.168.13.200/mediawiki-1.4.7/index.php/Minimal_Media)

1) If instructions are followed rapidly and the prep is completed in a rapid time period to minimize protein degradation, prep yields can yield about 15-20 mg/Liter for $^{15}N^{13}C$-labeled protein.

2) Prepare M9 Media as follows:

Table B.1: Growth 1.5x M9 Culture Preparation

1 L Amount / Ingredient	**2 L**	**4 L**	**8 L**
12.8 g Na_2HPO_4-$7H_20$	38.4 g	76.8 g	153.6 g
3.0 g KH_2PO_4	9.0 g	18.0 g	36.0 g
Add H_20 to: **1000 mL**	**2,000 ml**	**4,000 mL**	**8,000 mL**

3) pH the media to 7.4 with NaOH and place into 4 L Erlenmeyer flasks.

4) For each liter of media prepared, remove 25 ml to use as a starter culture and place in a smaller Erlenmeyer flask.

5) Autoclave all of the media on liquid cycle for 45'.

6) Prepare the M9 Media Supplement to add to each flask:

Table B.2: M9 minimal media preparation

	2 L	**4 L**	**8 L**
1 M $MgSO_4$	2 mL	9 mL	18 mL
1 M $CaCl_2$	100 ul	450 ul	900 ul
1 M Thiamine stock	1.0 mL	4.5 mL	9 mL
1 M $FeSO_4$	1.0 mL	4.5 mL	9 mL
1.0 g ^{15}N-labled NH_4CL	2.0 g	4.0 g	8.0 g
5 g/L D-Glucose (0.5% final)	10 g	20 g	40 g
Total Volume	100 mL	200 ml	400 mL

*For ^{13}C labeled media, use 4 g/Liter of glucose in place of unlabeled glucose.

Filter the M9 Media Supplement and store at 4^{o}C until use (Do not store for too long).

-Add 50 ml of supplement per 1000 ml of M9 media prior to incubation (**growth cultures**).

-Add 2.5 ml of supplement to 50 ml of M9 media prior to incubation (**starter cultures**).

Part II: Growth and Induction of Cultures

*** Antibiotics: M15 Cells (Qiagen) : [100 ug/mL] ampicillin & [25 ug/mL]**

Kanamycin

****Check your stock antibiotics concentrations****

*****Use yeast extract at a final concentration at 0.02% for both starter and growth cultures**

7) Inoculate each M9 starter culture with KcsA glycerol stock. Use ~ 25 ul of glycerol stock per 50 ml of starter culture. The glycerol stocks are good for about a year. After that, re-plate some onto a petri dish (LB media is fine, with appropriate antibiotics), and grow up a new batch of glycerol stocks.

8) Grow the starter cultures overnight in an incubator at 37^{o}C.

9) Inoculate the 1 liter growth cultures with the overnight starter culture. Don't forget your antibiotics, M9 media supplement, and yeast extract. Grow the growth cultures in an incubator at 37^{o}C.

10) Track the A_{600} OD closely until it reaches 0.7. Set the incubator at 27^{o}C.

11) Remove the growth cultures from the incubator and let them sit at room temperature for about 10', swirling occasionally. This allows the media to cool somewhat before addition of IPTG.

12) Add IPTG to 1 mM concentration (1 ml per liter of culture for a 1 M IPTG stock). Let the cells incubate overnight at 27^{o}C.

13) Pellet down the cells for 15' @ 4^{o}C @ 5,700 g. Do not fill the centrifuge bottles all the way to the top or they will leak.

14) Resuspend the pellets in 150 mM KCl and 50 mM Tris pH 7.5 (this is Buffer 1). Use 25 ml per liter of culture. Keep the cells on ice while resuspending. Also be sure that all large and small clumps of cells are removed when resuspending.

Part III: KcsA Purification

***Part III, from cell lysis to elution off the cobalt column, should be completed in two days or less (including detergent exchange); this allows for less exposure to proteases and the aggregation of bacterial proteins. If you are keeping the KcsA in the DM prep detergent, there is no excuse to leave the protein on the column overnight. Ever.**

16) Sonicate the cells. Divide cells up into smaller volumes (50 – 75 mL). Run each volume twice at 50% Duty Cycle, 9 Output Control, for 5' (Branson Sonifier 450). Place the cells on ice for five minutes between each round of sonication.

17) After lysis, add n-DECYL-B-MALTOPYRANOSIDE (DM, Anatrace #D322) to a final concentration of 40 mM (1.9 g per 100 ml of lysate solution). Place on a stirrer @ 4^{o}C for 2-3 hours.

18) Pellet down unlysed cells and membrane @34,600 g for 45' and remove the supernatant.

34,600 g	=	21,030 RPM in Ti-45 rotor (ultracentrifuge)
	=	~17,000 RPM in SA-600 (Wand Sorval will not go this fast)
	=	17,100 RPM in SS-34

19) Make a cobalt column with slurry (2.5 ml matrix for 1 L of culture) and wash with 10x volume of Buffer 1. It is best to freshly charge the column with cobalt before each step. ***Read the Amersham catalog on TALON resin for proper maintenance of the column.**

20) Add the supernatant to the column at a rate of 2 mL/min. Save this flow-through. Also save the flow-through of all subsequent wash steps.

21) Wash with High Salt Concentration Buffer (500 mM KCl, 50 mM Tris pH 7.5, and 10 mM DM @ pH 7.5) @ 2 mL/min. Use ~ 25 ml per 2 liters of culture or until the absorbance reaches baseline.

22) Wash with Low Concentration Imidazole Buffer (150 mM KCl, 50 mM Tris pH 7.5, 50 mM Imidazole, and 10 mM DM @ pH 7.5) @ 2 mL/min. Wash until A_{280} reaches baseline for about 10'.

**Before proceeding to the next step: Many detergents that are suitable for NMR studies are not suitable for protein electrophoresis. If you are using a detergent that is cationic (i.e. CTAB or DTAB) or zwitterionic (LDAO), you may have trouble. To ensure that your protein growth was pure, take a small fraction of TALON resin still in DM and pack onto a column, then elute with the high imidazole (500 mM) buffer with DM. Run this on a gel. Alternatively, in many cases, the his-tag attachment of a protein to a cobalt or talon resin will be disrupted by boiling a small amount for 5' – similar to the preparation undertaken anyway to run a protein sample on an SDS-PAGE gel, for example.

23) Detergent Exchange: This step tries to ensure a complete exchange from the mild extraction/solubilization detergent of DM to one that is more suitable for your experiments (i.e. LDAO, CTAB) for more consistent, reproducible results. It works best

with detergents that are not too expensive. Wash the column with 100 ml 10 mM CTAB, 150 mM KCl, 50 mM Tris, pH 7.5 buffer (use ~10x TALON column volume) @ flow rate of 2-3 mL/min Remove the TALON resin from the column and break into equal slurry volumes, placing about 5 ml of slurry into a single 50 ml conical (i.e. if you have a 10 ml TALON resin column, use two 50 ml conical tubes). Add 10 mM CTAB buffer (same as earlier) to each conical to bring the total volume to 45 mL.

24) Let the conical with the slurry in them rotate overnight at room temperature.

25) Load the slurries back onto the column, letting all of the excess buffer drain through as the slurry settles back down.

26) Wash the column with 200 ml (or 20x column volume) with 10 mM CTAB buffer.

27) Wash the column with 300 ml of **2.5 mM** CTAB buffer. In the case of CTAB, since the aggregation number is quite large and the resultant micelle is of significant size (~60 kDa), the detergent has a tendency to reach untenable concentrations that are not easily removed as the prep continues. The best way to deal with this without losing protein (i.e. BioBeads) is to simply use a minimal amount of the detergent throughout the prep process.

28) Set the flow rate to ~1.0 mL/min and collect the elutions in 1 ml fractions in eppendorf tubes. Elute with High Concentration Imidazole Buffer (150 mM KCl, 50 mM Tris pH 7.5, 500 mM Imidazole, and 2 mM CTAB, pH 7.5).

29) Proceed to Part IV soon; it is generally not a good idea to leave protein sitting around in Imidazole for too long (a weekend at the absolute most).

Part IV: Buffer Replacement

30) Use a 50 ml capacity Amicon concentrator with a 30,000 MW filter for buffer replacement.

a) After pooling elution fractions, bring the volume down to 5-10 ml @ 1 mL/min rate.

b) Bring the volume back up to 50 ml with KcsA Dialysis Buffer (150 mM KCl, 50 mM Tris, 0.01 mM sodium azide, 10 mM EDTA, and 0.5 MM CTAB, pH 7.5).

c) Concentrate down to ~20-30 ml. This should lower the imidazole enough.

31) Measure the concentration and determine the amount of protein.

a. determine the concentration of the protein by reading the absorbance at 280 nm. (Usually use a 1/50 dilution of the protein to do this.)

Absorbance: $A = E \times L \times C$

$E_{\text{Full-length KcsA}} = 33{,}570$ units

L = 1 cm

A = from spectrophotometer

C = X (in Molar)

b. Convert the concentration to M and determine the total moles of protein present.

moles of protein / volume (liters) = protein concentration (C) in M

c. Convert from moles to grams.

(moles of protein) x (17,607.5 g/mol) = amount of protein in grams

*17,607.5 is the molecular weight of full-length monomer KcsA

Part V: Chymotrypsin Cleavage

***Optional. Do not use for full-length KcsA; step cuts off his-tag and cytoplasmic domain of protein.**

32) To cut the chymotrypsin site, use 1 mg of chymotrypsin for every 15 mg of protein:

(KcsA in mg / 15) / ([25 mg/mL] chymotrypsin stock) = amount of stock to use in mL

33) Allow the cleavage to proceed overnight at room temperature, then add PMSF (a protease inhibitor) to 0.5 mM.

34) Concentrate the sample down to 0.5-1 mL and run over a Superdex-200 column equilibrated with 150 mM KCl, 50 mL Tris, 3 mM CTAB, pH 7.5. The column will separate cut KcsA tetramer from any uncut tetramer, and remove any additional chymotrypsin (MW of chymotrypsin ~ 27,000, and should be removed somewhat by the use of 30 kDa concentration filters). The natural tetrameric state of KcsA protein as well as the associated weight of the detergent micelle surrounding it should provide for safe filtration up to and including 50,000 MW cutoffs.

Part VI: Protein Concentration

***Be sure to do the prerinsing step for all concentrators to remove trace amounts of glycerin from the filter. See instruction manuals for more information.**

35) Use Amicon Centricon 30,000 MW centrifuge filters to concentrate protein down to a suitable concentration (0.5 – 1 mM).

**Save your flow-through: If the filter ever breaks – and they do – your protein will go through

***A smaller MW cutoff may be used for the filter if the chymotrypsin cleavage step was not used.

36) At smaller volumes it may be necessary to switch to Amicon Microfilters.

37) Checking protein concentration:

Absorbance: $A = E \times L \times C$

$E_{\Delta C35}$ = 32,290 units

L = 1 cm

A = from spectrophotometer

C = X

b. Convert the concentration to M and determine the total moles of protein present.

x moles / volume (liters) = M

c. Convert from moles to grams.

(moles) x (13,295.7 g/mol) = amount of protein in grams

*13,295.7 g is the molecular weight of KcsA with the 35 C-terminal residues cleaved off.

Appendix C: Step-by-Step Protocol for Encapsulation of KcsA in Reverse Micelles

Preparation of the Membrane Protein KcsA for Reverse Micelles

Introduction

This technique uses the dialysis-lyophilization to prepare KcsA for reverse micelles. KcsA-micelle complexes are not soluble enough for the injection method and the phase transfer method does not allow for sufficient control of water loading. Since low water loadings (i.e. 6-10) seem to be optimal for reverse micelles (Binks et al., 1989; Kielec et al., 2009a) and, given the difficulty in concentrating aqueous membrane protein preparations to the multi-millimolar range typically afforded to soluble proteins such as flavodoxin, the dialysis-lyophilization method or some as-yet-discovered variant may be the best way to encapsulate membrane proteins. It allows control over protein concentration, buffer amount, and buffer composition.

Procedure

1) KcsA-micelles are dialyzed against water containing detergent. It should be noted that this dialysis is not sufficient to exchange detergents, but is sufficient to remove the KcsA prep buffer. The dialysis step should not take longer than overnight, as the protein may begin to crash out of solution. Additionally it may be necessary to heat the water when first making the detergent-water preparation due to the lack of counterions for anionic or cationic detergents, to get the detergent to go into solution cleanly. Usually 5 mM or 10 mM is a sufficient amount; generally you should use 2-3x the detergents critical micelle concentration (the concentration in solution at which a detergent will begin to exist as aggregate micelles).

2) Pierce Slide-A-Lyzers work best, as you are generally working with smaller, single-NMR-sample sizes of protein and solution. I prefer 0.1-0.5 mL sizes, as this prevents excess water and detergent from getting into your sample. Generally I will concentrate the protein down to this volume at a concentration that will be suitable for NMR. If I am going to want a 650 ul pentane reverse micelle NMR sample with 250 uM of protein, I will make sure a 500 ul sample that I place in a Slide-A-Lyzer has a concentration of at least 325 uM (650 ul / 500 ul = 1.3. 1.3 x 250 uM = 325 uM). Keep in mind that some protein will invariably be lost in this dialysis step, so make sure you are generous here.

3) After Dialysis, check the concentration of your protein to make sure you have enough. Do not assume that your volume is the same as well you first put your sample in the Slide-A-Lyzer; it has probably increased. Then place your sample into a small screw thread glass vial (12 x 35 mM, Fisher # 03-338A). This size is typically suitable for a single pentane sample. If you require a larger sample volume to accommodate a high pressure sample mixing chamber, a larger glass vial may be used.

   Important: Weigh the glass vial with a balance before you add your protein.

   weighing the glass vial allows you to later determine the approximate amount of detergent in your sample. This is essential information for calculating your water loadings and the correct ratios of any co-surfactants (either lipid or detergent) that you may use.

4) Use a dry-ice ethanol bath (liquid N_2 works as well) to freeze your protein. Place on a trusted lyophilizer that will not suck your protein into oblivion, as has happened more than once on to me on the old Wand Lab lyophilizer. Overnight is usually sufficient.

5) Remove the sample from the lyophilizer. Because of the detergents the sample will likely take up the same volume it did in aqueous form. Weigh the sample/glass vial, using the same balance as before. Since all of the water is removed from the system due to lyophilization, and the salts and buffers were removed in the dialysis step, the only contributors to mass are the glass vial, the protein, and the detergent. Since we know the first two items, we can subtract them out from the total mass to determine the amount of protein.
6) With the detergent concentration in the sample in hand, calculate your water loading from the equation: w_o = water in sample (mM) / detergent in sample (mM).
7) To the sample: add your D-pentane (use at least 30%) and pentane, then hexanol (if necessary), and your buffer. Seal with Teflon tape and parafilm, and mix by hand, then by rotisserie (for about 30' to overnight), then place in your NMR tube.

<u>An Actual Example: Preparation of Sample U1: ^{15}N KcsA wt Reverse Micelles in Ethane</u>

*Note: This amount of protein and detergent discussed here are for a 1.82 mL sample to be made in a high pressure mixing chamber. A pentane sample can be scaled down to preparation for a sample volume of only 0.65 – 0.7 mL.

This protocol begins after the protein has come off the Superdex-200 column. For KcsA concentration and weights, the extinction coefficient of 32,290 and MW of 13,295.7 of $KcsA_{\Delta C35}$ are used, respectively.

1) Pool fractions 10-25.

2) 1/50 A_{280} = 0.018 → 27.8 uM KcsA in 21 mL →7.77 mg KcsA

   Concentration Calculations: ((0.018 x 50) x 1 cm pathlength) / 32,290 = 2.78 $x10^{-5}$ M

   Protein Weight Calculations: 2.78 $x10^{-5}$ M x 0.021 L x 13,295.6 kDa = 0.00778 g

3) Concentrate the sample down to ~ 1 mL using a 15 mL Amicon 30 kDa MW spin filter.

   1/50 A_{280} = 0.282 → 437 uM KcsA in 1 mL →5.797 mg KcsA

4) Split the sample into equal 500 uL portions and place each in a 0.1-0.5 mL 3 kDa Pierce Slide-A-Lyzer.

5) Place each sample (in Slide-A-Lyzer) into 1 L of H_20 with 5 mM CTAB for overnight dialysis. The dialysis buffer was prepared by dissolving 1.82 mg of CTAB into water, and heated slightly until the detergent dissolved in solution.

6) Dialyze overnight.

7) Post-dialysis, remove samples from Slide-A-Lyzer and place in a threaded glass tube (used a larger one here).

   Weight of empty glass tube (no cap): 4.5947 g

   Post-Dialysis sample volume (total): ~1.55 mL

   1/50 A_{280} = 0.176 → 275 uM KcsA in 1.55 mL →5.6 mg KcsA

   *Note how much the Slide-A-Lyzer volume swelled here.

8) Freeze and lyophilize sample.

9) Preparation for reverse micelles. Remove sample from lyophilizer and weigh to determine detergent amount.

Tube + protein + detergent	4.6611 g
Tube	4.5947 g
Protein	- 0.0056 g
Detergent (CTAB)	0.0608 g

0.0608 g / 364.46 (MW of CTAB) = 1.668×10^{-4} moles CTAB

The current generation high pressure mixing chamber has a volume of 1.82 mL (0.0182 L).

1.668×10^{-4} moles CTAB / 0.0182 L = 0.00917 M CTAB in 1.82 mL

At this volume, theoretical (100% encapsulation efficiency) concentration of KcsA is ~234 uM

Keeping this amount of CTAB (i.e. not adding extra), we will add an equal molar amount of DHAB to arrive at a final detergent concentration of 183.4 mM of 1:1 CTAB:DHAB. This works out to a 784:1 protein:detergent ratio

For the sample detergents we have:

a) 91.7 mM CTAB: 0.0917 M x 364.46 (MW of CTAB) x 0.00182 L = 0.0608 g CTAB
b) 91.7 mM DHAB: 0.0917 M x 574.87 g (MW of DHAB) x 0.00182 L = 0.0959 g DHAB

As the carrier / hybrid detergent, CTAB is already present in the sample. Add dry powdered DHAB carefully, using a good balance (the Wand lab balance is shit – be friends with the Black lab or Vanderkoi lab and use theirs).

10) Calculate water loading. Use w_o of 6.

    183.4 mM total detergent x 6 = 1100.4 mM H_20

    1100.4 mM H_20 x 18 g x 0.00182 L = 36.049 ul of buffer

    In this case, the buffer consists of 50 mM BIS-TRIS, 50 mM KCl, and 50 mM DSS, pH 7.0

11) Use 10% hexanol for the sample: 10% x 1.82 mL = 0.182 mL

12) Use 5% pentane for the sample: 5% x 1.82 mL = 0.091 mL

13) Add sample, buffer, hexanol, and pentane to mixing chamber. Seal mixing chamber and add D-ethane. Begin encapsulation.

Appendix D: Average Secondary Chemical Shift Values for C_α and C_β atoms

*All values are from Zhang and co-workers (Zhang et al., 2003).

Table D.1: Random coil shift values

Residue		Average	Std. Dev.	S.D. Min	S.D. Max	2xS.D.Min	2xS.D.Max
Ala (A)	**Cα**	**52.84**	1.64	51.2	54.48	**49.56**	**56.12**
	Cβ	**19.06**	1.26	17.8	20.32	**16.54**	**21.58**
Arg (R	**Cα**	**56.42**	1.94	54.48	58.36	**52.54**	**60.3**
	Cβ	**30.66**	1.67	28.99	32.33	**27.32**	**34**
Asn (N)	**Cα**	**53.23**	1.51	51.72	54.74	**50.21**	**56.25**
	Cβ	**38.55**	1.41	37.14	39.96	**35.73**	**41.37**
Asp (D)	**Cα**	**54.18**	1.6	52.58	55.78	**50.98**	**57.38**
	Cβ	**40.85**	1.32	39.53	42.17	**38.21**	**43.49**
Cys (C	**Cα**	**57.53**	3.05	54.48	60.58	**51.43**	**63.63**
(reduced)	**Cβ**	**29.35**	2.52	26.83	31.87	**24.31**	**34.39**
Gln (Q)	**Cα**	**56.12**	1.72	54.4	57.84	**52.68**	**59.56**
	Cβ	**29.14**	1.69	27.45	30.83	**25.76**	**32.52**
Glu (E)	**Cα**	**56.87**	1.82	55.05	58.69	**53.23**	**60.51**
	Cβ	**30.2**	1.55	28.65	31.75	**27.1**	**33.3**
Gly (G)	**Cα**	**45.51**	1.05	44.46	46.56	**43.41**	**47.61**
His (H)	**Cα**	**55.86**	1.96	53.9	57.82	**51.94**	**59.78**
	Cβ	**29.97**	2.42	27.55	32.39	**25.13**	**34.81**
Ile (I)	**Cα**	**61.03**	1.9	59.13	62.93	**57.23**	**64.83**
	Cβ	**38.65**	1.69	36.96	40.34	**35.27**	**42.03**
Leu (L)	**Cα**	**54.92**	1.7	53.22	56.62	**51.52**	**58.32**
	Cβ	**42.38**	1.64	40.74	44.02	**39.1**	**45.66**
Lys (K)	**Cα**	**56.59**	1.78	54.81	58.37	**53.03**	**60.15**
	Cβ	**32.79**	1.67	31.12	34.46	**29.45**	**36.13**
Met (M)	**Cα**	**55.67**	1.54	54.13	57.21	**52.59**	**58.75**
	Cβ	**33.36**	2.26	31.1	35.62	**28.84**	**37.88**
Phe (F)	**Cα**	**57.98**	2.02	55.96	60	**53.94**	**62.02**
	Cβ	**39.45**	1.98	37.47	41.43	**35.49**	**43.41**
Pro (P)	**Cα**	**63.47**	1.26	62.21	64.73	**60.95**	**65.99**
	Cβ	**31.94**	0.95	30.99	32.89	**30.04**	**33.84**
Ser (S)	**Cα**	**58.38**	1.69	56.69	60.07	**55**	**61.76**
	Cβ	**64.03**	1.27	62.76	65.3	**61.49**	**66.57**
Thr (T)	**Cα**	**61.64**	2.07	59.57	63.71	**57.5**	**65.78**
	Cβ	**70.12**	1.33	68.79	71.45	**67.46**	**72.78**
Trp (W)	**Cα**	**57.78**	1.71	56.07	59.49	**54.36**	**61.2**
	Cβ	**29.67**	1.74	27.93	31.41	**26.19**	**33.15**
Tyr (Y)	**Cα**	**57.97**	2.17	55.8	60.14	**53.63**	**62.31**
	Cβ	**38.95**	1.84	37.11	40.79	**35.27**	**42.63**
Val (V)	**Cα**	**62.06**	2.16	59.9	64.22	**57.74**	**66.38**
	Cβ	**32.71**	1.37	31.34	34.08	**29.97**	**35.45**

Table D.2: Helical chemical shift values

Residue		Average	Std. Dev.	S.D. Min	S.D. Max	2xS.D.Min	2xS.D.Max
Ala (A)	**Cα**	**54.83**	1.05	53.78	55.88	**52.73**	**56.93**
	Cβ	**18.26**	0.88	17.38	19.14	**16.5**	**20.02**
Arg (R	**Cα**	**58.93**	1.55	57.38	60.48	**55.83**	**62.03**
	Cβ	**30.14**	1.14	29	31.28	**27.86**	**32.42**
Asn (N)	**Cα**	**55.45**	1.42	54.03	56.87	**52.61**	**58.29**
	Cβ	**38.61**	1.31	37.3	39.92	**35.99**	**41.23**
Asp (D)	**Cα**	**56.7**	1.61	55.09	58.31	**53.48**	**59.92**
	Cβ	**40.51**	1.33	39.18	41.84	**37.85**	**43.17**
Cys (C	**Cα**	**61.31**	3.5	57.81	64.81	**54.31**	**68.31**
(reduced)	**Cβ**	**27.75**	2.07	25.68	29.82	**23.61**	**31.89**
Gln (Q)	**Cα**	**58.47**	1.19	57.28	59.66	**56.09**	**60.85**
	Cβ	**28.51**	0.92	27.59	29.43	**26.67**	**30.35**
Glu (E)	**Cα**	**59.11**	1.16	57.95	60.27	**56.79**	**61.43**
	Cβ	**29.37**	0.99	28.38	30.36	**27.39**	**31.35**
Gly (G)	**Cα**	**46.91**	1.1	45.81	48.01	**44.71**	**49.11**
His (H)	**Cα**	**59.04**	1.74	57.3	60.78	**55.56**	**62.52**
	Cβ	**29.54**	1.46	28.08	31	**26.62**	**32.46**
Ile (I)	**Cα**	**64.57**	1.74	62.83	66.31	**61.09**	**68.05**
	Cβ	**37.6**	1.15	36.45	38.75	**35.3**	**39.9**
Leu (L)	**Cα**	**57.52**	1.23	56.29	58.75	**55.06**	**59.98**
	Cβ	**41.65**	1.05	40.6	42.7	**39.55**	**43.75**
Lys (K)	**Cα**	**58.93**	1.44	57.49	60.37	**56.05**	**61.81**
	Cβ	**32.27**	0.88	31.39	33.15	**30.51**	**34.03**
Met (M)	**Cα**	**58.09**	1.81	56.28	59.9	**54.47**	**61.71**
	Cβ	**32.37**	1.66	30.71	34.03	**29.05**	**35.69**
Phe (F)	**Cα**	**60.81**	1.9	58.91	62.71	**57.01**	**64.61**
	Cβ	**38.78**	1.31	37.47	40.09	**36.16**	**41.4**
Pro (P)	**Cα**	**65.49**	1.08	64.41	66.57	**63.33**	**67.65**
	Cβ	**31.46**	0.95	30.51	32.41	**29.56**	**33.36**
Ser (S)	**Cα**	**60.88**	1.61	59.27	62.49	**57.66**	**64.1**
	Cβ	**63.08**	1.12	61.96	64.2	**60.84**	**65.32**
Thr (T)	**Cα**	**65.61**	2.39	63.22	68	**60.83**	**70.39**
	Cβ	**68.88**	1.17	67.71	70.05	**66.54**	**71.22**
Trp (W)	**Cα**	**60.01**	1.77	58.24	61.78	**56.47**	**63.55**
	Cβ	**29.3**	1.4	27.9	30.7	**26.5**	**32.1**
Tyr (Y)	**Cα**	**60.98**	1.76	59.22	62.74	**57.46**	**64.5**
	Cβ	**38.25**	1.11	37.14	39.36	**36.03**	**40.47**
Val (V)	**Cα**	**66.16**	1.55	64.61	67.71	**63.06**	**69.26**
	Cβ	**31.49**	0.72	30.77	32.21	**30.05**	**32.93**

Table D.3: Beta strand chemical shift values

Residue		Average	Std. Dev.	S.D. Min	S.D. Max	2xS.D.Min	2xS.D.Max
Ala (A)	**Cα**	**51.53**	1.48	50.05	53.01	**48.57**	**54.49**
	Cβ	**21.14**	2.05	19.09	23.19	**17.04**	**25.24**
Arg (R	**Cα**	**55.14**	1.64	53.5	56.78	**51.86**	**58.42**
	Cβ	**32.19**	1.8	30.39	33.99	**28.59**	**35.79**
Asn (N)	**Cα**	**52.74**	1.47	51.27	54.21	**49.8**	**55.68**
	Cβ	**40.12**	2.07	38.05	42.19	**35.98**	**44.26**
Asp (D)	**Cα**	**53.87**	1.64	52.23	55.51	**50.59**	**57.15**
	Cβ	**42.3**	1.62	40.68	43.92	**39.06**	**45.54**
Cys (C	**Cα**	**56.88**	2.02	54.86	58.9	**52.84**	**60.92**
(reduced)	**Cβ**	**30.16**	1.97	28.19	32.13	**26.22**	**34.1**
Gln (Q)	**Cα**	**54.83**	1.41	53.42	56.24	**52.01**	**57.65**
	Cβ	**31.28**	1.93	29.35	33.21	**27.42**	**35.14**
Glu (E)	**Cα**	**55.52**	1.67	53.85	57.19	**52.18**	**58.86**
	Cβ	**32.01**	1.98	30.03	33.99	**28.05**	**35.97**
Gly (G)	**Cα**	**45.22**	1.17	44.05	46.39	**42.88**	**47.56**
His (H)	**Cα**	**55.09**	1.78	53.31	56.87	**51.53**	**58.65**
	Cβ	**31.85**	2.22	29.63	34.07	**27.41**	**36.29**
Ile (I)	**Cα**	**60.05**	1.57	58.48	61.62	**56.91**	**63.19**
	Cβ	**39.86**	1.98	37.88	41.84	**35.9**	**43.82**
Leu (L)	**Cα**	**54.08**	1.31	52.77	55.39	**51.46**	**56.7**
	Cβ	**43.79**	2	41.79	45.79	**39.79**	**47.79**
Lys (K)	**Cα**	**55.4**	1.34	54.06	56.74	**52.72**	**58.08**
	Cβ	**34.65**	1.78	32.87	36.43	**31.09**	**38.21**
Met (M)	**Cα**	**54.58**	1.24	53.34	55.82	**52.1**	**57.06**
	Cβ	**35.05**	2.29	32.76	37.34	**30.47**	**39.63**
Phe (F)	**Cα**	**56.65**	1.59	55.06	58.24	**53.47**	**59.83**
	Cβ	**41.54**	1.74	39.8	43.28	**38.06**	**45.02**
Pro (P)	**Cα**	**62.64**	1.03	61.61	63.67	**60.58**	**64.7**
	Cβ	**32.27**	1.2	31.07	33.47	**29.87**	**34.67**
Ser (S)	**Cα**	**57.54**	1.4	56.14	58.94	**54.74**	**60.34**
	Cβ	**65.16**	1.51	63.65	66.67	**62.14**	**68.18**
Thr (T)	**Cα**	**61.06**	1.59	59.47	62.65	**57.88**	**64.24**
	Cβ	**70.75**	1.51	69.24	72.26	**67.73**	**73.77**
Trp (W)	**Cα**	**56.41**	1.87	54.54	58.28	**52.67**	**60.15**
	Cβ	**31.5**	1.7	29.8	33.2	**28.1**	**34.9**
Tyr (Y)	**Cα**	**56.83**	1.71	55.12	58.54	**53.41**	**60.25**
	Cβ	**40.97**	1.85	39.12	42.82	**37.27**	**44.67**
Val (V)	**Cα**	**60.83**	1.64	59.19	62.47	**57.55**	**64.11**
	Cβ	**33.91**	1.61	32.3	35.52	**30.69**	**37.13**

Table D.4: Average chemical shift values

Residue		Average	Std. Dev.	S.D. Min	S.D. Max	2xS.D.Min	2xS.D.Max
Ala (A)	**Cα**	**53.44**	1.91	51.53	55.35	**49.62**	**57.26**
	Cβ	**19.22**	1.78	17.44	21	**15.66**	**22.78**
Arg (R	**Cα**	**57.11**	2.29	54.82	59.4	**52.53**	**61.69**
	Cβ	**30.83**	1.68	29.15	32.51	**27.47**	**34.19**
Asn (N)	**Cα**	**53.69**	1.82	51.87	55.51	**50.05**	**57.33**
	Cβ	**38.93**	1.66	37.27	40.59	**35.61**	**42.25**
Asp (D)	**Cα**	**54.9**	2.01	52.89	56.91	**50.88**	**58.92**
	Cβ	**41.03**	1.5	39.53	42.53	**38.03**	**44.03**
Cys (C	**Cα**	**58.4**	3.32	55.08	61.72	**51.76**	**65.04**
(reduced)	**Cβ**	**29.14**	2.33	26.81	31.47	**24.48**	**33.8**
Gln (Q)	**Cα**	**56.77**	2.05	54.72	58.82	**52.67**	**60.87**
	Cβ	**29.39**	1.8	27.59	31.19	**25.79**	**32.99**
Glu (E)	**Cα**	**57.66**	2.09	55.57	59.75	**53.48**	**61.84**
	Cβ	**30.19**	1.74	28.45	31.93	**26.71**	**33.67**
Gly (G)	**Cα**	**45.63**	1.18	44.45	46.81	**43.27**	**47.99**
His (H)	**Cα**	**56.65**	2.44	54.21	59.09	**51.77**	**61.53**
	Cβ	**30.29**	2.23	28.06	32.52	**25.83**	**34.75**
Ile (I)	**Cα**	**61.89**	2.65	59.24	64.54	**56.59**	**67.19**
	Cβ	**38.81**	1.93	36.88	40.74	**34.95**	**42.67**
Leu (L)	**Cα**	**55.78**	2.06	53.72	57.84	**51.66**	**59.9**
	Cβ	**42.52**	1.8	40.72	44.32	**38.92**	**46.12**
Lys (K)	**Cα**	**57.12**	2.11	55.01	59.23	**52.9**	**61.34**
	Cβ	**33.09**	1.72	31.37	34.81	**29.65**	**36.53**
Met (M)	**Cα**	**56.58**	2.2	54.38	58.78	**52.18**	**60.98**
	Cβ	**33.25**	2.28	30.97	35.53	**28.69**	**37.81**
Phe (F)	**Cα**	**58.43**	2.57	55.86	61	**53.29**	**63.57**
	Cβ	**40.08**	2.09	37.99	42.17	**35.9**	**44.26**
Pro (P)	**Cα**	**63.61**	1.46	62.15	65.07	**60.69**	**66.53**
	Cβ	**31.94**	1.02	30.92	32.96	**29.9**	**33.98**
Ser (S)	**Cα**	**58.74**	2.01	56.73	60.75	**54.72**	**62.76**
	Cβ	**64.15**	1.5	62.65	65.65	**61.15**	**67.15**
Thr (T)	**Cα**	**62.31**	2.65	59.66	64.96	**57.01**	**67.61**
	Cβ	**70.07**	1.54	68.53	71.61	**66.99**	**73.15**
Trp (W)	**Cα**	**58.05**	2.34	55.71	60.39	**53.37**	**62.73**
	Cβ	**30.23**	1.88	28.35	32.11	**26.47**	**33.99**
Tyr (Y)	**Cα**	**58.21**	2.52	55.69	60.73	**53.17**	**63.25**
	Cβ	**39.71**	2.02	37.69	41.73	**35.67**	**43.75**
Val (V)	**Cα**	**62.82**	2.9	59.92	65.72	**57.02**	**68.62**
	Cβ	**32.87**	1.68	31.19	34.55	**29.51**	**36.23**

REFERENCES

Allen, S.J., Curran, A.R., Templer, R.H., Meijberg, W., and Booth, P.J. (2004a). Controlling the Folding Efficiency of an Integral Membrane Protein. J Mol Biol *342*, 1293-1304.

Allen, T.W., Anderson, O.S., and Roux, B. (2004b). On the importance of atomic fluctuations, protein flexibility, and solvent in ion permeation. J Gen Physiol *124*, 679-690.

Armstrong, C.M. (1975). Potassium pores of nerve and muscle membranes. Membranes *3*, 325-358.

Arora, A., Abildgaard, F., Bushweller, J.H., and Tamm, L.K. (2001). Structure of outer membrane protein A transmembrane domain by NMR spectroscopy. Nat Struct Biol *8*, 334-338.

Babu, C.R., Flynn, P.F., and Wand, A.J. (2001). Validation of protein structure from preparations of encapsulated proteins dissolved in low viscosity fluids. J Am Chem Soc *123*, 2691-2692.

Babu, C.R., Flynn, P.F., and Wand, A.J. (2003). Preparation, characterization, and NMR spectroscopy of encapsulated proteins dissolved in low viscosity fluids. J Biomol NMR *25*, 313-323.

Baker, K.A., Tzitzilonis, C., Kwiatkowski, W., Choe, S., and Riek, R. (2007a). Conformational dynamics of the KcsA potassium channel governs gating properties. Nat Struct Mol Biol *14*, 1089-1095.

Barrera, F.N., Renart, M.L., Molina, M.L., Poveda, J.A., Encinar, J.A., Fernandez, A.M., Neira, J.L., and Gonzalez-Ros, J.M. (2005). Unfolding and refolding in vitro of a

tetrameric, alpha-helical membrane protein: the prokaryotic potassium channel KcsA. Biochemistry *44*, 14344-14352

Bernache, S., and Roux, B. (2000). Molecular dynamics of the KcsA K(+) channel in a bilayer membrane. Biophysical journal *78*, 2900-2917.

Binks, B.P., Chatenay, D., Nicot, C., Urbach, W., and Waks, M. (1989). Structural parameters of the myelin transmembrane proteolipid in reverse micelles. Biophysical journal *55*, 949-955.

Blois, T.M., and Bowie, J.U. (2009). G-protein-coupled receptors were not built in a day Prot Sci *18*, 1335-1342.

Carlomagno, T., Maurer, M., Sattler, M., Schwendinger, M.G., Glaser, S.J., and Griesinger, C. (1996). PLUSH TACSY: Homonuclear planar TACSY with two-band selective shaped pulses applied to Cα,C′ transfer and Cβ,Caromatic correlations. J Biol NMR *8*, 161-170.

Cavanaugh, J., Fairbrother, W.J., Palmer, A.G., Rance, M., and Skelton, N.J. (2007). Protein NMR Spectroscopy, 2nd Edition (Burlington, MA, Elsevier Academic Press).

Chill, J.H., Louis, J.M., Baber, J.L., and Bax, A. (2006). Measurement of 15N relaxation in the detergent-solubilized tetramertic KcsA potassium channel. J Biol NMR *36* 123-136.

Clowes, R.T., Boucher, W., Hardman, C.H., Domaille, P.J., and Laue, E.D. (1993). A 4D HCC(CO)NNH experiment for the correlation of aliphatic side-chain and backbone resonances in 13C/15N-labelled proteins. J Biol NMR *3*, 349-354.

Columbus, L., Lipfert, J., Jambunathan, K., Fox, D.A., Sim, A.Y., Doniach, S., and Lesley, S.A. (2009). Mixing and Matching Detergents for Membrane Protein NMR Structure Determination. J Am Chem Soc *131*, 7320-7326.

Cordero-Morales, J.F., Cuello, L.G., Zhao, Y., Jogini, V., Cortes, D.M., Roux, B., and Perozo, E. (2006). Molecular determinants of gating at the potassium-channel selectivity filter. Nat Struct Mol Biol *13*, 311-318

Cornilescu, G., Delaglio, F., and Bax, A. (1999). Protein backbone angle restraints from searching a database for chemical shift and sequence homology. J Biomol NMR *13*, 289-302.

Cortes, D.M., Cuello, L.G., and Perozo, E. (2001). Molecular architecture of full-length KcsA: role of cytoplasmic domains in ion permeation and activation gating. The Journal of general physiology *117*, 165-180.

Darszon, A., Strasser, R.J., and Montal, M. (1979). Rhodopsin--phospholipid complexes in apolar environments: photochemical characterization. Biochemistry *18*, 5205-5213.

Delaglio, F., Grzesiek, S., Vuister, G.W., Zhu, G., Pfeifer, J., and Bax, A. (1995). NMRPipe: a multidimensional spectral processing system based on UNIX pipes. J Biomol NMR *6*, 277-293.

Derst, C., and Karschin, A. (1998). Evolutionary link between prokaryotic and eukaryotic K+ channels. The Journal of experimental biology *201*, 2791-2799.

Doyle, D.A., Cabral, J.M., Pfuetzner, R.A., Kuo, A.L., Gulbis, J.M., Cohen, S.L., Chait, B.T., and MacKinnon, R. (1998). The structure of the potassium channel: Molecular basis of K+ conduction and selectivity. Science *280*, 69-77.

Ekwall, P., Mandell, L., and Fontell, K. (1969). The cetyltrimethylammonium bromide-hexanol-water system. J Colloid Interface Sci *29*, 639-646.

Farrow, N.A., Muhandiram, R., Singer, A.U., Pascal, S.M., Kay, C.M., Gish, G., Shoelson, S.E., Pawson, T., Formankay, J.D., and Kay, L.E. (1994). Backbone dynamics of a free and a phosphopeptide-complexed Src homology-2 domain studied by N-15 NMR relaxation. Biochemistry *33*, 5984-6003.

Fernandez, C., Hilty, C., Wider, G., Guntert, P., and Wuthrich, K. (2004). NMR structure of the integral membrane protein OmpX. J Mol Biol *336*, 1211-1221.

Flynn, P.F., Mattiello, D.L., Hill, H.D.W., and Wand, A.J. (2000). Optimal use of cryogenic probe technology in NMR studies of proteins. J Am Chem Soc *122*, 4823-4824.

Geux, N., and Peitsch, M.C. (1997). SWISS-MODEL and the Swiss-Pdb viewer: an environment for comparative protein modeling. Electrophoresis *18*, 2714-2723. Goddard, T.D., and Kneller, D.G. (2004). SPARKY 3 (University of California, San Fransisco).

Grzesiek, S., Anglister, J., and Bax, A. (1993). Correlation of Backbone Amide and Aliphatic Side-Chain Resonances in 13C/15N-Enriched Proteins by Isotropic Mixing of 13C Magnetization. J Magn Reson, Ser B *101*, 114-119.

Grzesiek, S., and Bax, A. (1992). Improved 3D triple-resonance NMR techniques applied to a 31 kDa protein. J Magn Reson *96*, 432-440.

Grzesiek, S., and Bax, A. (1993). Amino acid type determination in the sequential assignment procedure of uniformly 13C/15N-enriched proteins. J Biomol NMR *3*, 185-204.

Heginbotham, L., Abramson, T., and MacKinnon, R. (1992). A functional connection between the pores of distantly related ion channels as revealed by mutant K+ channels. Science *258*, 1152-1155.

Hille, B. (1975). Ionic selectivity of Na and K channels of nerve membranes. Membranes *3*, 256-323.

Hiller, S., Garces, R.G., Malia, T.J., Orekhov, V.Y., Colombini, M., and Wagner, G. (2008). Solution structure of the integral human membrane protein VDAC-1 in detergent micelles. Science *321*, 1206-1210.

Hong, H., and Tamm, L.K. (2003). Elastic coupling of integral membrane protein stability to lipid bilayer forces. Proc Natl Acad Sci USA *101*, 4065-4070.

Kainosho, M., Torizawa, T., Iwashita, Y., Terauchi, T., Mei Ono, A., and Guntert, P. (2006). Optimal isotope labelling for NMR protein structure determinations. Nature *440*, 52-57.

Kay, L.E., Keifer, P., and Saarinen, T. (1992). Pure absorption gradient enhanced heteronuclear single quantum correlation spectroscopy with improved sensitivity. J Am Chem Soc *114*, 10663-10665.

Kay, L.E., Xu, G.Y., and Yamazaki, T. (1994). Enhanced-Sensitivity Triple-Resonance Spectroscopy with Minimal H2O Saturation. J Magn Reson, Ser A *109*, 129-133.

Kielec, J.M., Valentine, K.G., and Wand, A. (2009a). A method for solution NMR structural studies of large integral membrane proteins: reverse micelle encapsulation. Biochim Biophys Acta *doi:10.1016/j.bbamem.2009.07.027*.

Kielec, J.M., Valentine, K.G., and Wand, A.J. (2009b). Reverse micelles in integral membrane protein structural biology by solution NMR spectroscopy. Structure *17*, 345-351.

Kneller, J.M., Lu, M., and Bracken, C. (2001). An effective method for the discrimination of motional anisotropy and chemical exchange. J Am Chem Soc *124*, 1852-1853.

Knight, E.J., and Hardy, R.W. (1967). Flavodoxin. Chemical and biological properties. J Biol Chem *242*, 13370-13374.

Krueger-Koplin, R.D., Sorgen, P.L., Krueger-Koplin, S.T., Rivera-Torres, A.O., Cahill, S.M., Hicks, D.B., Grinius, L., Krulwich, T.A., and Girvin, M.E. (2004). An evaluation of detergents for NMR structural studies of membrane proteins. J Biomol NMR *28*, 43-57.

Lau, F.W., Nauli, S., Zhou, Y., and Bowie, J.U. (1999). Changing single side-chains can greatly enhance the resistance of a membrane protein to irreversible inactivation. J Mol Biol *290*, 559-564.

Lefebvre, B.G., Liu, W., Peterson, R.W., Valentine, K.G., and Wand, A.J. (2005). NMR spectroscopy of proteins encapsulated in a positively charged surfactant. J Magn Reson *175*, 158-162.

LeMasurier, M., Heginbotham, L., and Miller, C. (2001). KcsA: It's a potassium channel. J Gen Physiol *118*, 303-314.

Levitt, M.H. (2001). Spin Dynamics (Chichester, West Sussex, John Wiley & Sons).

Lipari, G., and Szabo, A. (1982a). Model-free approach to the interpretation of nuclear magnetic resonance relaxation in macromolecules. 1. Theory and range of validity. J Am Chem Soc *104*, 4546-4559.

Lipari, G., and Szabo, A. (1982b). Model-free approach to the interpretation of nuclear magnetic resonance relaxation in macromolecules. 2. Analysis of experimental results. J Am Chem Soc *104*, 4559-4570

Logan, T.M., Olejniczak, E.T., Xu, R.X., and Fesik, S.W. (1993). A general method for assigning NMR spectra of denatured proteins using 3D HC(CO)NH-TOCSY triple resonance experiments. J Biomol NMR *3*, 225-231.

Lyons, B.A., and Montelione, G.T. (1993). An HCCNH Triple-Resonance Experiment Using Carbon-13 Isotropic Mixing for Correlating Backbone Amide and Side-Chain Aliphatic Resonances in Isotopically Enriched Proteins. J Magn Reson *101*, 206-209.

Ma, D., Tillman, T.S., Tang, P., Meirovitch, E., Eckenhoff, R., Carnini, A., and Xu, Y. (2008). NMR studies of a channel protein without membranes: structure and dynamics of water-solubilized KcsA Proc Natl Acad Sci USA *105*, 16537-16542.

MacKinnon, R., Cohen, S.L., Kuo, A.L., Lee, A., and Chait, B.T. (1998). Structural conservation in prokaryotic and eukaryotic potassium channels. Science *280*, 106-109.

Montelione, G.T., Lyons, B.A., Emerson, S.D., and Tashiro, M. (1992). An efficient triple resonance experiment using carbon-13 isotropic mixing for determining sequence-specific resonance assignments of isotopically-enriched proteins. J Am Chem Soc *114*, 10974-10975.

Neal, S., Nip, A.M., Zhang, H.Y., and Wishart, D.S. (2003). Rapid and accurate calculation of protein H-1, C-13, and N-15 chemical shifts. J Biomol NMR *26*, 215-240.

NIST, C.W. (2009). National Institute of Standards and Technology (NIST) Chemistry WebBook.

Noskov, S.Y., Bernache, S., and Roux, B. (2004). Control of ion selectivity in potassium channels by electrostatic and dynamic properties of carbonyl ligands. Nature *431*, 830-834.

Oxenoid, K., and Chou, J.J. (2005). The structure of phospholamban pentamer reveals a channel-like architecture in membranes. Proc Natl Acad Sci USA *102*, 10870-10875.

Oxenoid, K., Kim, H.J., Jacob, J., Sonnichsen, F.D., and Sanders, C.R. (2004). NMR Assignments for a Helical 40 kDa Membrane Protein. J Am Chem Soc *126*, 5048-5049.

Palmer, A.G., Cavanaugh, J., Wright, P.E., and Rance, M. (1991). Sensitivity improvement in proton-detected 2-dimensional heteronuclear correlation NMR-spectroscopy. J Magn Reson, 151-170.

Perozo, E., Cortes, D.M., and Cuello, L.G. (1998). Three-dimensional architecture and gating mechanism of a K+ channel studied by EPR spectroscopy. Nat Struct Biol *5*, 459-569.

Perozo, E., Cortes, D.M., and Cuello, L.G. (1999). Structural rearrangements underlying K1-channel activation gating. Science *285*, 73-78.

Pervushin, K., Riek, R., Wider, G., and Wuthrich, K. (1997). Attenuated T2 relaxation by mutual cancellation of dipole-dipole coupling and chemical shift anisotropy indicates an avenue to NMR structures of very large biological macromolecules in solution. Proc Natl Acad Sci U S A *94*, 12366-12371.

Peterson, R.W., Anbalagan, K., Tommos, C., and Wand, A.J. (2004). Forced folding and structural analysis of metastable proteins. J Am Chem Soc *126*, 9498-9499.

Peterson, R.W., Lefebvre, B.G., and Wand, A.J. (2005a). High-resolution NMR studies of encapsulated proteins in liquid ethane. J Am Chem Soc *127*, 10176-10177.

Peterson, R.W., Pometun, M.S., Shi, Z., and Wand, A.J. (2005b). Novel surfactant mixtures for NMR spectroscopy of encapsulated proteins dissolved in low-viscosity fluids. Prot Sci *14*, 2919-2921.

Peterson, R.W., and Wand, A.J. (2005). Self contained high pressure cell, apparatus and procedure for the preparation of encapsulated proteins dissolved in low viscosity fluids for NMR spectroscopy. Rev Sci Instrum *76*, 1-7.

Pometun, M.S., Peterson, R.W., Babu, C.R., and Wand, A.J. (2006). Cold denaturation of encapsulated ubiquitin. J Am Chem Soc *128*, 9498-9499.

Ramakrishnan, V.R., Darszon, A., and Montal, M. (1983). A small angle x-ray scattering study of a rhodopsin-lipid complex in hexane. The Journal of biological chemistry *258*, 4857-4860.

Roosild, T.P., Greenwald, J., Vega, M., Castronovo, S., Riek, R., and Choe, S. (2005). NMR structure of Mistic, a membrane-integrating protein for membrane protein expression. Science *307*, 1317-1321.

Ruta, V., Jiang, Y., Lee, A., Chen, J., and MacKinnon, R. (2003). Functional analysis of an archaebacterial voltage-dependent K+ channel. Nature *422*, 180-185.

Sanders, C.R., and Oxenoid, K. (2000). Customizing model membranes and samples for NMR spectroscopic studies of complex membrane proteins. BBA *1508*, 129-145.

Schleucher, J., Sattler, M., and Griesinger, C. (1993). Coherence selection by gradients without signal attenuation: application to three-dimensional HNCO experiments. Angew Chem Int Ed Engl *32*, 1489-1491.

Schleucher, J., Schwendinger, M., Sattler, M., Schmidt, O., Schedletzky, O., Glaser, S.J., Sorensen, O.W., and Griesinger, C. (1994). A general enhancement scheme in heteronuclear multidimensional NMR employing pulsed field gradients. J Biomol NMR *4*, 301-306.

Schneider, R., Ader, C., Lange, A., Giller, K., Hornig, S., Pongs, O., Becker, S., and Baldus, M. (2008). Solid-State NMR Spectroscopy Applied to a Chimeric
Potassium Channel in Lipid Bilayers. J Am Chem Soc *130*, 7427-7435.

Schnell, J.R., and Chou, J.J. (2008). Structure and mechanism of the M2 proton channel of influenza A virus. Nature *451*, 591-595.

Schrempf, H., Schmidt, O., Kummerlen, R., Hinnah, S., Muller, D., Betzler, M., Steinkamp, T., and Wagner, R. (1995). A prokaryotic potassium ion channel with two predicted transmembrane segments from Streptomyces lividans. The EMBO journal *14*, 5170-5178.

Seigneuret, M., Neumann, J.M., and Rigaud, J.L. (1991). Detergent delipidation and solubilization strategies for high-resolution NMR of the membrane protein bacteriorhodopsin. J Biol Chem *266*, 10066-10069.

Shen, Y., Delaglio, F., Cornilescu, G., and Bax, A. (2009). TALOS+: a hybrid method for predicting protein backbone torsion angles from NMR chemical shifts. J Biomol NMR *44*, 213-223.

Slovic, A.M., Kono, H., Lear, J.D., Saven, J.G., and DeGrado, W.F. (2004). Computational design of water-soluble analogues of the potassium channel KcsA. Proc Natl Acad Sci USA *101*, 1828-1833.

Spera, S., and Bax, A. (1991). Empirical Correlation between Protein Backbone

Conformation and Ca and Cb 13C Nuclear Magnetic Resonance Chemical Shifts. J Am Chem Soc *113*, 5490-5492.

Takeuchi, K., Takahashi, H., Kawano, S., and Shimada, I. (2007). Identification and characterization of the slowly exchanging pH-dependent conformational rearrangement in KcsA. J Biol Chem *282* 15179-15186.

Tiburu, E.K., Bowman, A.L., Struppe, J.O., Janero, D.R., Avraham, H.K., and Makriyannis, A. (2009). Solid-state NMR and molecular dynamics characterization of cannabinoid receptor-1 (CB1) helix 7 conformational plasticity in model membranes. Biochim Biophys Acta *1788*, 1159-1167.

Valentine, K.G., Pometun, M.S., Kielec, J.M., Baigelman, R.E., Staub, J.K., Owens, K.L., and Wand, A.J. (2006). Magnetic susceptibility-induced alignment of proteins in reverse micelles. J Am Chem Soc *128*, 15930-15931.

Valiyaveetil, F.I., Zhou, Y., and MacKinnon, R. (2002). Lipids in the structure, folding, and function of the KcsA K+ channel. Biochemistry *41*, 10771-10777.

van den Brink-van der Laan, E., Chupin, V., and de Kruijff, B. (2004). Small alcohols destabilize the KcsA tetramer via their effect on the membrane lateral pressure Biochemistry *43*, 5937-5942.

Van Horn, W.D., Kim, H.J., Ellis, C.D., Hadziselimovic, A., Sulistijo, E.S., Karra, M.D., Tian, C., Sonnichsen, F.D., and Sanders, C.R. (2009). Solution nuclear magnetic resonance structure of membrane-integral diacylglycerol kinase. Science *324*, 1726-1729.

Van Horn, W.D., Ogilvie, M.E., and Flynn, P.F. (2008). Use of reverse micelles in membrane protein structural biology. Journal of biomolecular NMR *40*, 203-211.

Wand, A.J. (2001). Dynamic activation of protein function: a view emerging from NMR spectroscopy. Nat Struct Biol *8*, 926-931.

Wand, A.J., Ehrhardt, M.R., and Flynn, P.F. (1998). High-resolution NMR of encapsulated proteins dissolved in low-viscosity fluids. Proc Natl Acad Sci USA *95*, 15299-15302.

Wand, A.J., and Nelson, S.J. (1991). Refinement of the main chain directed assignment strategy for the analysis of 1H NMR spectra of proteins. Biophys J *59*, 1101-1112.

Watts, A. (2005). Solid-State NMR in drug design and discovery for membrane-embedded targets. Nat Rev Drug Discovery *4*, 555-568.

WaveMetrics (2007). IGOR Pro 6.0 (Portland, OR, WaveMetrics).

White, S.H. (2009). Membrane proteins of known 3D structure (http://blanco.biomol.uci.edu/Membrane_Proteins_xtal.html).

Wittekind, M., and Mueller, L. (1993). HNCACB, a High-Sensitivity 3D NMR Experiment to Correlate Amide-Proton and Nitrogen Resonances with the Alpha- and Beta-Carbon Resonances in Proteins. J Magn Reson, Ser B *101*, 201-205.

Xu, Y., Zheng, Y., Fan, J., and Yang, D. (2006). A new strategy for structure determination of large proteins in solution without deuteration. Nat Methods *3*, 931-937.

Zhang, H., Neal, S., and Wishart, D. (2003). RefDB: A database of uniformly referenced protein chemical shifts. J Biomol NMR *25*, 173-195.

Zhang, O., Kay, L.E., Olivier, J.P., and Forman-Kay, J.D. (1994). Backbone 1H and 15N resonance assignments of the N-terminal SH3 domain of drk in folded and unfolded states using enhanced-sensitivity pulsed field gradient NMR techniques. Journal of biomolecular NMR *4*, 845-858.

Zhou, Y., Cierpicki, T., Flores-Jimenez, R.H., Lukasik, S.M., Ellena, J.F., Cafisco, D.S., Kadokura, H., Beckwith, J., and Bushweller, J.H. (2008). NMR solution structure of the integral membrane enzyme DsbB: functional insights into DsbB-catalyzed disulfide bond formation. Mol Cell *31*, 896-908.

Zhou, Y., and MacKinnon, R. (2003). The occupancy of ions in the K+ selectivity filter: charge balance and coupling of ion binding to a protein conformational change underlie high conduction rates. J Mol Biol *333*, 965-975.

Zhou, Y., and MacKinnon, R. (2004). Ion binding affinity in the cavity of the KcsA potassium channel. Biochemistry *43*, 4978-4982.

Zhou, Y., Morais-Cabral, J.H., Kaufman, A., and MacKinnon, R. (2001). Chemistry of ion coordination and hydration revealed by a K+ channel-Fab complex
at 2.0 A resolution. Nature *414*, 43-48.